UNIVERSITY OF CAPE TOWN
IYUNIVESITHI YASEKAPA • UNIVERSITEIT VAN KAAPSTAD

Cross-shore exchange in the northern Benguela and the related role of upwelling filaments

Dissertation presented for the degree of
Doctor of Philosophy
in the department of Oceanography
Faculty of Science

University of Cape Town

Author:
Annethea Auguste MULLER

Main Supervisor:
Prof. Chris J.C. REASON

Co-Supervisors:
Dr. Volker MOHRHOLZ
Dr. Martin SCHMIDT

February 2013

Abstract

The purpose of this research is to quantify where, how much and by what mechanisms water leaves or comes on to the Namibian shelf and secondly to gain a better understanding into the circulation associated with upwelling filaments in the northern Benguela region and quantify their contribution to the exchange across the shelf edge. For the analyses results from a MOM-4 regional ecosystem model are combined with remote sensing and cruise data. Great temporal and spatial variability exists in the transport across and along the 300 m deep shelf next to the coast of Namibia and the results show that it is feasible to divide the northern Benguela system into four regions with distinct cross-shore dynamics. The strong annual offshore transport associated with the region surrounding the Lüderitz upwelling cell seems to be seasonally shaped by a distinct interchange between the meridional currents. During summer (DJF) a strong poleward flux, associated with the poleward undercurrent, promotes offshore transport whereas during winter (JJA) a northward flux driven by the coastal branch of the Benguela current exhibit the same effect. The region off Cape Frio is highly complex and a unique interplay exists in transport across the shelf edge between year round offshore transport in what appears to be narrow jets or filaments and strong subsurface transport onto the shelf. The central regions are dominated by strong subsurface compensatory transport onto the shelf between 19°S and 25°S. The results thus highlight the unique interaction between the meridional currents in shaping the seasonal and geographic variability in transport across the shelf edge. In addition to the complex large scale regional circulation, this work further shows that mesoscale features like upwelling filaments are extremely dynamic with the potential to dramatically shape local ecosystem dynamics on the shelf as well as across the shelf edge and into the open ocean. Observations from an upwelling filament sampled during 2010 show that multifaceted mesoscale flow fields are associated with these features and complex exchanges of on- and offshore transport, linked with subsurface dipole eddies, are observed in and around the structure. Furthermore, the offshore transport associated with the filament, found to be in the order of magnitude of 3 Sv, was substantially larger than the integrated Ekman transport across the study area.

Plagiarism declaration

This thesis is a presentation of my original research work. Wherever contributions of others are involved, every effort is made to indicate this clearly, with due reference to the literature. Aside from guidance from my supervisors, I have received no assistance, except as acknowledged.

Annethea A. Muller

Publication based on this work:

Muller,A.A., Mohrholz,V. and Schmidt,M., 2013. The circulation dynamics associated with a northern Benguela upwelling filament during October 2010, *Continental Shelf Research*, http://dx.doi.org/10.1016/j.csr.2013.04.037

Acknowledgements

Normally a document like this is attributed to one person, yet in reality numerous people contribute to it in many distinct ways. I would like to acknowledge, to the best of my ability, all those who assisted me in realizing this goal:

My supervisor, **Prof. Chris Reason**. It was truly an honor to have had the opportunity to work with you again. Thank you for being willing to supervise this project.

My co-supervisors, **Dr. Volker Mohrholz and Dr. Martin Schmidt**. Thank you for the faith you put in me to work on this project. I am extremely grateful for the support and assistance you gave me.

The **German Federal Ministry of Education and Research** supported this work as part of the Geochemistry and Ecology of the Namibian upwelling system (GENUS) project.

GENUS working group. Working on a multidisciplinary project like this is a huge honor, and I learned a great deal from all of you. Thanks for all the special onboard memories.

Thank you to the **captain and crew of the R.R.S. Discovery** for their assistance during September and October 2010.

Staff and students at the IOW. I owe a great deal of gratitude to many of you.

Toralf Heene. The amount of assistance you provided both onboard during research cruises as well as during data analysis was invaluable. Thank you.

Anja Eggert. You gave my work its second wind, so to speak, with your incredible positivity and enthusiastic support. There is no way I could have finished without our co-operative work. Thank you also for your input during the final editing.

Thank you also to my **FeG Rostock** family, **family Sismey** and my dear friends **Tanya**,

Corlia, **Engela** and **Vuyi**.

My German family: **Marcus**, **Maria**, **Anna-Lena**, **Markus**, **Neli**, **Andrea**, **Johannes**, **Tabbi** and **Thomas**. There are no words to describe how much your encouragement, support and prayers have meant to me during these last 3 years.

lAtEx Richter and reader Matthias. Thank you both from the bottom of my heart!

Pamela McGinty. Your part came right at the end. It was, however, invaluable. Thank you.

Mom, Dad and the rest of families Muller and Cloete. Distance in kilometer does not lessen the extent to which you continue to carry me with your love and support.

And my dear **Mr. M. Grohmann**. Time will tell if the house is big enough for two PhDs!

"The valleys of the sea were exposed and the foundations of the earth laid bare at the rebuke of the LORD, at the blast of breath from his nostrils. He reached down from on high and took hold of me; he drew me out of deep waters." Ps. 18:15-16

Contents

1 Introduction **2**

1.1 Background to the study 2

1.1.1 Shelf edge exchange processes 2

1.1.2 The Benguela current system 4

1.1.3 Upwelling filaments (in the northern Benguela) 16

1.2 Summary and research motivation 21

2 Research design and methodology **23**

2.1 Introduction to the coupled ecosystem model adjusted for the Benguela region 23

2.1.1 Description of the model setup 23

2.1.2 The physical circulation model component 26

2.1.3 The 3D biogeochemical ecosystem model 27

2.2 Calculating volume transport fluxes 27

2.3 Sampling an upwelling filament during October 2010 29

2.4 Data description 34

2.4.1 SST satellite data 34

2.4.2 World Ocean Atlas 2009 (WOA09) 34

2.4.3 CTD cruise data from BENEFIT programme 35

2.4.4 Software tools 35

3 Validation of ecosystem model adjusted for the Benguela **36**

3.1 Surface patterns: Temperature and salinity 36

3.2 Vertical structures: temperature, salinity, oxygen and density 38

3.3 General regional features 42
3.4 Section summary 47

4 Advection associated with the northern Benguela shelf 49

4.1 Variability in longshore and cross-shore current flow in the northern Benguela 49
4.1.1 Regional transport 49
4.1.2 Meridional and zonal current flow through the mixed layer and below 50
4.1.3 Seasonal and geographic variation in circulation through the water column 59
4.2 Quantifying transport flux budgets for the northern Benguela shelf 67
4.2.1 Annual budgets 67
4.2.2 Summer (DJF) and winter (JJA) budgets 72
4.3 Section summary 72

5 Northern Benguela upwelling filament 78

5.1 Surface structure of the upwelling filament 78
5.2 Vertical structure of the upwelling filament 79
5.3 Circulation and transport associated with the upwelling filament 87
5.4 Frontal mixing in the upwelling filament 88
5.5 Filament development over time 89
5.6 Section summary 90

6 Conclusions, limitations and recommendations 94

6.1 Evaluating MOM-4 ecosystem model 95
6.2 Large scale circulation in the northern Benguela and transport across the shelf edge 96
6.3 Northern Benguela upwelling filaments 97
6.4 Future research 98

List of Figures

1.1 Geometry of the shelf and shelf break 4
1.2 Pressure systems and wind regime across the Benguela 6
1.3 Wind-stress curl across the Benguela 7
1.4 Upwelling 9
1.5 SST showing mesoscale features across the Benguela. 9
1.6 Benguela features 10
1.7 Watermasses of the Benguela upwelling system 11
1.8 Benguela bathymetry 13
1.9 Watermasses and oxygen 15
1.10 Surface geostrophic EKE in Benguela 17
1.11 Dipole eddies associated with an upwelling filament 19
1.12 Upwelling filaments across the Benguela. 20

2.1 Rectangular model grid in geophysical coordinates and ETOPO-5 topography 24
2.2 Arakawa B-grid layout in model 25
2.3 The conceptual cycling of nitrogen through the ecosystem in the model. . . . 28
2.4 U,V components for cross-shore budget calculation 29
2.5 Defining four geographic regions along the Namibian shelf 30
2.6 SST image with station locations and transect tracks 32
2.7 Hourly averaged winds during filament sampling 32
2.8 Scanfish track showing resolution of data 33

3.1 Annual SST comparison between model and satellite data 37

3.2 Annual mean SST model bias 38
3.3 Seasonal SST model bias 39
3.4 Annual mean SSS: WOA vs model 39
3.5 Annual mean temperature at 23°S: WOA vs model 41
3.6 Annual mean oxygen at 23°S: WOA vs model 42
3.7 Model temperature, salinity and density bias at 23°S 43
3.8 CTD vs model vertical depth profiles of temperature and salinity 44
3.9 Relationship between CTD measurements and model output values 44
3.10 Regional oxygen profile across the northern Benguela: mixed layer and below 45
3.11 Current measurements: ADCP data from mooring vs model output 46
3.12 Regional annual meridional and zonal flow off Namibia presented by model . 46

4.1 Seasonal current vectors through the mixed layer in northern Benguela . . . 51
4.2 Seasonal current vectors through depths 40-300 m in northern Benguela . . . 52
4.3 Seasonal meridional current through mixed layer (0-40 m) 54
4.4 Seasonal meridional current through 40-300 m 55
4.5 Seasonal zonal current through 40-300 m 56
4.6 Seasonal zonal current through the mixed layer (0-40 m) 57
4.7 Seasonal density integrated vertical velocity through 0-300 m 58
4.8 DJF (a) meridional current, (b) zonal current and (c) density weighted vertical current through 5 transects 62
4.9 JJA (a) meridional current, (b) zonal current and (c) density weighted vertical current through 5 transects 63
4.10 Zonal and meridional currents through a transect along the 300 m deep shelf break for summer (DJF) and winter (JJA) 64
4.11 Density weighted vertical current through a transect along the 300 m deep shelf-break for summer (DJF) and winter (JJA) 66
4.12 Hovmöller diagrams of integrated transport through transects at 16°S, 19°S, 25°S and 28°S 66
4.13 Hovmöller diagram of integrated zonal transport through a transect along the 300 m deep shelf-break 67

4.14 Mean annual volume transport fluxes (Sv) across four regions of the northern Benguela . . . 68
4.15 Mean summer volume transport fluxes (Sv) across four regions of the northern Benguela . . . 70
4.16 Mean winter volume transport fluxes (Sv) across four regions of the northern Benguela . . . 71
4.17 Volume transport flux budgets across the northern Benguela shelf . . . 74
4.18 Oxygen transport along and across the Namibian shelf through the mixed layer. 76
4.19 Oxygen transport along and across the Namibian shelf through 40-300 m . . 77

5.1 SST image for 2 October 2010 . . . 80
5.2 Filament development and decay . . . 80
5.3 Surface temperature and salinity profiles along transect 1 . . . 81
5.4 Surface temperature and salinity profiles along transect 2 . . . 81
5.5 Temperature, salinity, density and Chl-a profiles along transects 1 and 2 through filament . . . 82
5.6 Zonal and meridional currents from ADCP along transects 1 and 2 . . . 84
5.7 Horizontal latitude vs temperature profiles of transects 1 and 2 . . . 86
5.8 Horizontal latitude vs salinity profiles of transects 1 and 2 . . . 86
5.9 MOM-4 depiction of temperature profile of filament and associate current vectors . . . 88
5.10 TKE dissipation along transect 1 . . . 89
5.11 Short term spatial changes in temperature across a filament transect . . . 90
5.12 Hovmöller diagram showing change in zonal transport related to filament development . . . 91
5.13 Hovmöller diagram of temperature, salinity and density showing subsurface filament development . . . 92

List of Tables

3.1 Correlation statistics for model vs measured data 42

Chapter 1

Introduction

1.1 Background to the study

Literature on past research is reviewed here in order to provide a background context and motivation for the present study. Despite making mention of certain aspects of the greater East South Atlantic area, the main focus will be on the northern Benguela upwelling region. The Benguela system however consists of both the nearshore upwelling area as well as the large scale Benguela Current. In this work, the northern Benguela upwelling regime is defined as the cool coastal region lying between the Lüderitz upwelling cell and the Angola-Benguela frontal zone (ABFZ), with the defined geographic area investigated being: 16 to 28°S, 10.5 to 15.5°E. Therefore, after an extensive literature review, the project aims and motivation are summarized in section 1.2.

1.1.1 Shelf edge exchange processes

The shelf edge, where the shelf-sea meets the deep ocean, can often be observed from satellite images due to the distinctive water masses which make up the two ocean bodies on either side. Driven by an interest in global fluxes and budgets, and in particular their response to climate change and human activities, there has been an ever increasing focus on the exchanges happening at the ocean-shelf boundary following the initial shelf edge exchange program (SEEP) in the 1980s [Huthnance, 1981, 1995; Walsh et al., 1988; Biscaye et al., 1994]. Physical processes have been recognized as an important control of large-scale movement and irreversible small-scale mixing of water and its constituents at the shelf edge [Armi, 1978; Huthnance, 1981, 1995; Knauer, 1987; Mackenzie, 1991]. Some of these physical processes and related features present at the shelf edge include: coastal and shelf edge upwelling, barotropic tides and currents, kelvin and edge waves, internal waves, inertial motions, mixing, eddies, meanders, topographic Rossby waves, fronts, and filaments. Cross-shore transport

mechanisms also include the Ekman transport as well as the effects of topography and instabilities of the alongshore coastal jets [Marchesiello et al., 2003]. In addition, Rossby wave dynamics have been related to offshore transport in eastern boundary currents as their offshore progression affects the vertical structure of coastal currents resulting in instability and their separation from the coast as filaments [McCreary and Kundu, 1985]. [Shannon and Nelson, 1996] observed an almost persistent upward displacement of isopycnals at the shelf break in the Benguela, which at times is independent of upwelling. They argue that this bulge may be largely sustained through vertical advection due to bottom friction and flow acceleration. The acceleration can be produced by either the semi-diurnal internal tide, or strong currents generated at the shelf edge by transient long-shore wind [Shannon and Nelson, 1996]. [Johnson and Nurser, 1983] suggest a weak link between on- and off-shelf circulation, which may be spatially complex. For example, they mention that while upwelling events over the shelf may change on a scale of a few days and currents tend to change rapidly in response to wind stress variation, offshore from the shelf break the circulation features tend to change more slowly on a time scale of months (seasonal). In a model study by [Heaps, 1980], which treats each side of the shelf-break differently it was suggested that close to or at the shelf edge the onshore and offshore circulation would need to be joined resulting in a region of shearing motion. The dynamics of this region is very complicated [Johnson and Nurser, 1983]. The study of [Johnson and Nurser, 1983] did however show that as the shelf break becomes sharper, the magnitude of the secondary upwelling will increase within this shear layer as a result of the way in which the velocity onshore of the shelf break is reduced in magnitude. Figure 1.1 from [Johnson and Nurser, 1983] shows the geometry of the shelf. Here αL and αR is offshore and onshore of the shelf break respectively, and the difference between αR and αL defines the sharpness of the shelf break. The break would be absent if the slopes are equal and then unsteady flow would be observed [Johnson and Manja, 1980].

[Huthnance, 1995] recommended that more work be done on defining and clarifying basic processes which determine the quantities, transformation and fate of materials between the shelf and the open ocean, and this remains the case for many ecosystems. [Huthnance, 1995] further recommended that these exchange processes should be measured and models should be developed in consideration with the challenges resulting from the combination of steep bathymetry and stratification at the shelf edge.

In the northern Benguela, observations of cross-shelf transports have been very patchy and often site specific and thus of low spatial resolution. Examples include [Giraudeau et al., 1993] using coccolithophores and planktonic foraminifera fluxes as "tracers" and [Monteiro et al., 2006, 2008; Mohrholz et al., 2008] observing low oxygen water (LOW) on the Namibian shelf. However, numerous studies carried out in the South Atlantic and in particular next to the coasts of Namibia, Angola and South Africa, have provided great insight into the dynamics of the unique Benguela ecosystem and thus provide a basis for a study like this

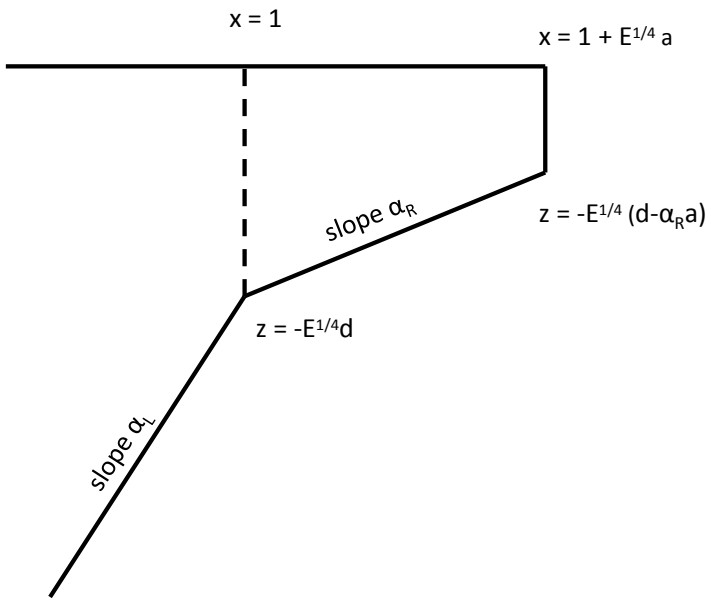

Fig. 1.1: Geometry of the shelf and shelf break from [Johnson and Nurser, 1983]. $E^{1/4}a$ is the dimensionless width of the shelf and $E^{1/4}d$ is the dimensionless depth of the shelf break, where E is an Ekman number with a typical numerical value of $6.25 \cdot 10^{-6}$.

which looks at the exchange of water across the shelf edge in the northern part of the (eco)system.

1.1.2 The Benguela current system

Wind and upwelling cells

The basin-scale ocean-atmosphere interactions across the South Atlantic, largely determines the oceanographic conditions of the Benguela region [Hardman-Mountford et al., 2003]. Next to the coasts of South Africa and Namibia (16-34°S) coastal upwelling is caused by offshore Ekman transport in the near surface layers which in turn is driven by the equatorward component of the southeast trade winds. These prevailing upwelling favorable winds are controlled by three pressure systems: 1) the South Atlantic anticyclone high pressure; 2) the pressure field over the continent and 3) the eastward moving cyclones, generated by perturbations in the subtropical jet stream, to the south [Nelson and Hutchings, 1983; Tyson, 1986; Shannon, 1995]. It has long been known that the oceanic response to a band of constant meridional wind would be concentrated near the coast with a downwind, equatorward coastal

jet flowing above a poleward undercurrent, and a signal increase toward the southern edge of the wind band [Fennel, 1988]. [Fennel et al., 2012b] showed that if the wind maxima is close to the coast than the ocean will respond similar as to a band of constant wind. If however, the wind maxima is shifted seaward, the undercurrent will reach the surface and the equatorward coastal jet will weaken. Figure 1.2 summarizes some of these drivers and processes. The South Atlantic anticyclone shifts by approximately 6° of latitude in a yearly cycle, with a southernmost position in February and a northernmost position in May-July [Tyson and Preston-Whyte, 2000]. When this regional wind field is combined with local wind forcing, topography, bathymetry as well as factors like dynamic instabilities in the flow of currents and other remotely forced processes, the distinct cold upwelling cells found along the west coast of southern Africa can be produced. At these cells cool, nutrient rich water comes to the surface along the coastal edge of the continental shelf [Cole, 1997]. There are however differences in the seasonal wind regimes between the northern and southern Benguela regions [Hart and Currie, 1960; Shannon and Nelson, 1996], driven by variation in the pressure systems mentioned above. Two centres where upwelling favourable winds tend to persist have been identified, near Lüderitz (27°S) and near Cape Frio (18°S). These two zones are located just south of coastal cyclonic wind-stress curl maxima [Bakun and Nelson, 1991] as can be seen in Figure 1.3. Despite upwelling winds being nearly perennial here, a spring-summer (Nov-Feb) maximum and winter minimum have been observed between 25 and 30°S, and a winter maximum near Cape Frio [Boyd, 1987]. Off central Namibia the wind speeds are lower and there is little seasonality (see Figure 1.3). The southern Benguela is effected more by the northward shift of the South Atlantic high pressure cells and there is thus a greater seasonality in upwelling here, with upwelling favorable winds reaching a maximum during spring and summer (Sept-Mar) [Shannon, 1966; Andrews and Hutchings, 1980]. The Lüderitz upwelling cell (∼27°S) mentioned above is not only the strongest and most persistent locally wind-driven upwelling cell in the Benguela but most possibly all eastern boundary currents [Hardman-Mountford et al., 2003]. Shelf waters here tend to be well mixed year round due to the intense perennial windstress at the centre of the upwelling cell [Parrish et al., 1983; Bakun, 1993]. See Figure 1.4 for a conceptual view of the circulation associated with both active and quiescent upwelling phases. The Lüderitz upwelling cell also forms a physical and biological boundary between the southern and northern parts of the Benguela system [Shannon, 1985; Pitcher et al., 1992]. The Cape Frio or Cunene cell mentioned above is the other strong upwelling cell in the northern Benguela [Copenhagen, 1953; Shannon et al., 1981; Nelson and Hutchings, 1983]. Two weaker upwelling cells have also been observed at 20 and 23°S, the latter being near Walvis Bay. [Shannon and Nelson, 1996] estimated the extent of offshore influence through the upwelling to be between 150-250 km. These values exclude the influence of upwelling filaments.

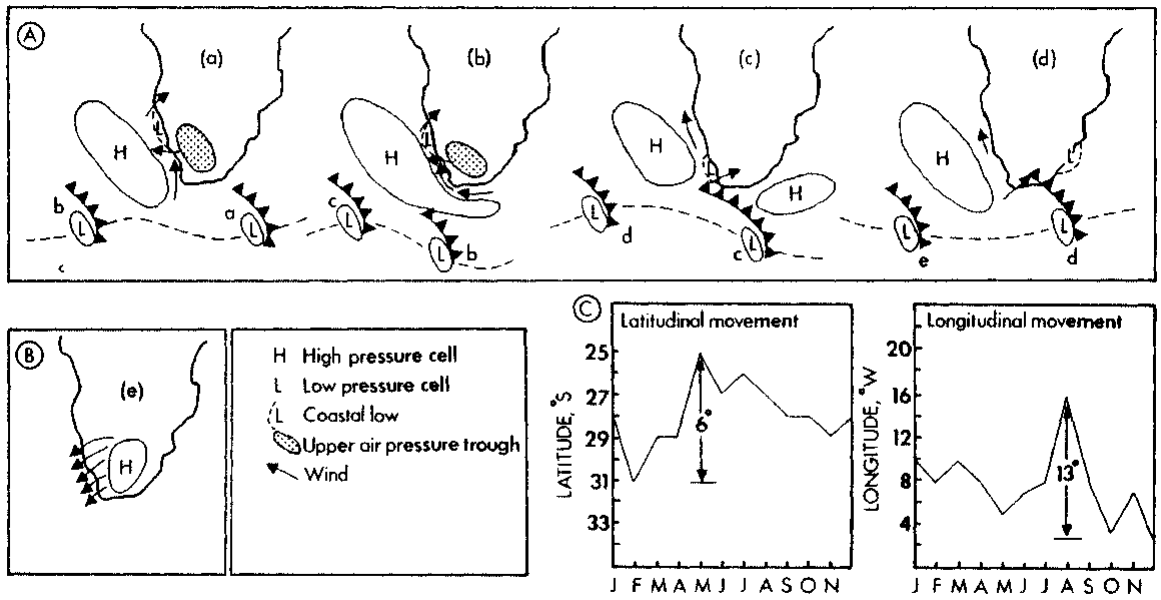

Fig. 1.2: A) Typical summer weather pattern across the Benguela, with the establishment of the South Atlantic high, and a coastal low near Lüderitz (a), followed by southward migration of the low as the high pressure ridges around the continent (b). The high pressure cell than splits as the coastal low migrates to Cape Town (c), followed by the strengthening of the high pressure cell (d). B) With a high pressure over the land, Berg wind conditions result. C) The annual migration of the South Atlantic anticyclone. Figure from [Shannon and Nelson, 1996].

Borders and features

The Benguela is also unique among eastern boundary current systems (EBCS) due to it being bordered by warm water regimes at either end, the Angola current system to the north and the Agulhas current system to the south [Hart and Currie, 1960; Nelson and Hutchings, 1983; Shannon, 1985, 1995]. At the northern boundary, between 14 and 16°S, therefore lies the Angola-Benguela surface frontal zone (ABFZ). The ABFZ is most marked in the upper 50 m but can be identified by both its temperature and salinity signal [Shannon et al., 1987], up to a depth of 200 m or more [Shannon and Nelson, 1996]. The presence of the different water masses in such close proximity within this zone [Mohrholz et al., 2001] means that it is also a region of great variability in biological distribution and abundance [John et al., 2004]. The ABF has a general west east orientation [Meeuwis and Lutjeharms, 1990] and migrates seasonally by more than 2° latitude with a northerly extent in winter (August) and a southerly extent in late summer (March) [Boyd et al., 1987]. This shift coincides with maximum poleward flow of the Angolan current [Shannon et al., 1987] and a minimum in upwelling favorable winds at Cape Frio mentioned above [Boyd, 1987]. The Angola-Benguela front (ABF) also varies in seaward extent, temperature and strength. A tendency has been observed for the southward intrusion of warm water from the Angola current into the northern Benguela region during autumn (Feb-Mar), resulting in a southward

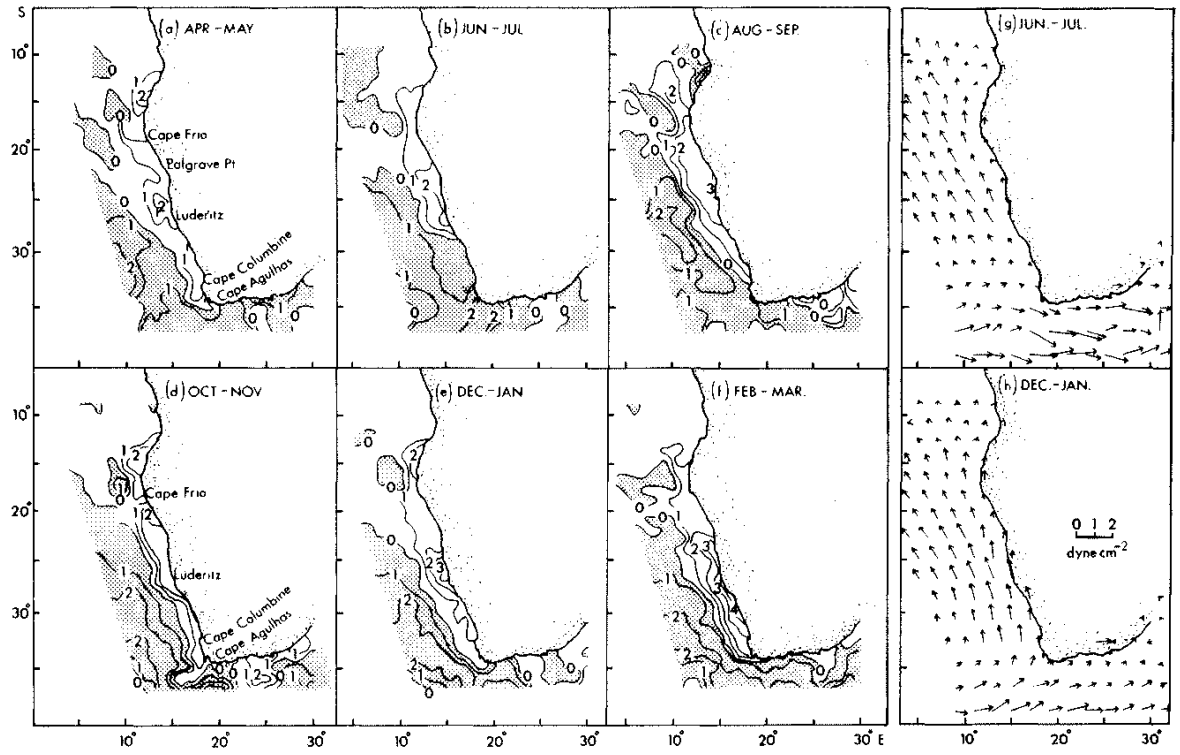

Fig. 1.3: Wind-stress curl (10^{-8}dyn·cm^{-3}) in the Benguela region (a-f) and surface winds (dyn·cm^{-2}) (g-h). Regions of anticyclonic wind-stress curl are shaded. Figure from [Shannon and Nelson, 1996] modified from [Bakun and Nelson, 1991].

migration of the ABF and warming along the northern Namibian coast [Hart and Currie, 1960; Stander, 1964; O'Toole, 1980; Badenhorst and Boyd, 1980; Hardman-Mountford et al., 2003]. This deepens the thermocline [Salat et al., 1992], so even if upwelling is taking place in the northern Benguela, it may not be cool water which comes to the surface. [Salat et al., 1992] further found that despite the lack of a surface signal, water being upwelled from 50-100 m depth next to Walvis Bay was actually Angolan current water. In addition to the northern and southern warm system boundaries, a strong thermal front tends to define the outer seaward boundary of the Benguela system [Currie, 1953; Jury et al., 1985; Jury, 1988; Shannon, 1985; Shillington et al., 1992]. [Shannon, 1985] also suggests that the baroclinic frontal zone off Namibia is relatively diffused compared to that of the southern Benguela. In addition to the equatorward and poleward boundaries, zonally oriented fronts also tend to develop equatorward of the major upwelling cells. One example is the front near 25°S just north of the Lüderitz cell [Shannon and Nelson, 1996]. This zone has important biological consequences for the system [Agenbag and Shannon, 1988].

Another common feature in the Benguela is the presence of quasi-permanent shallow (50 m deep) upwelling filaments which tends to transport freshly upwelled water offshore and into the south Atlantic [Van Foreest et al., 1984; Lutjeharms and Stockton, 1987; Lutjeharms et al., 1991; Shillington et al., 1992]. [Ikeda and Emery, 1984] propose that filament generation in the region is largely related with irregularities in the alongshore windstress, coastal geometry and the bathymetry of the continental shelf. Dispersed between these filaments are zones with minimum windstress and onshore Ekman transport and thus relatively undisturbed coastal dynamics, such as Palgrave Point (20.5°S) [Parrish et al., 1983]. Due to low wind mixing intensity during winter (Jul-Sept), the water column tends to be largely stabilized here [Bakun, 1993]. The exact quantitative cross-shelf contribution of these features within the Benguela system however remains unresolved.

Finally, the oceanography of the southern Benguela is also influenced by Agulhas rings from the south, which inject heat and salt into the region [Shannon and Nelson, 1996]. These rings, however, play a minor role in the northern Benguela. Many of the features described in this and the next subsection are summarized in Figures 1.5 and 1.6.

Currents, water masses and transport

The Benguela is thus an equatorward flowing, cool system, that is composed predominantly of an Indian and a south Atlantic subtropical thermocline mix, with added contributions of saline, low oxygen tropical Atlantic and cooler, fresher subantarctic water [Garzoli et al., 1996]. See Figure 1.7 for water masses from the Benguela region. Between 24 and 30°S the oceanic component of the current separates from the coast and flows northwest into the

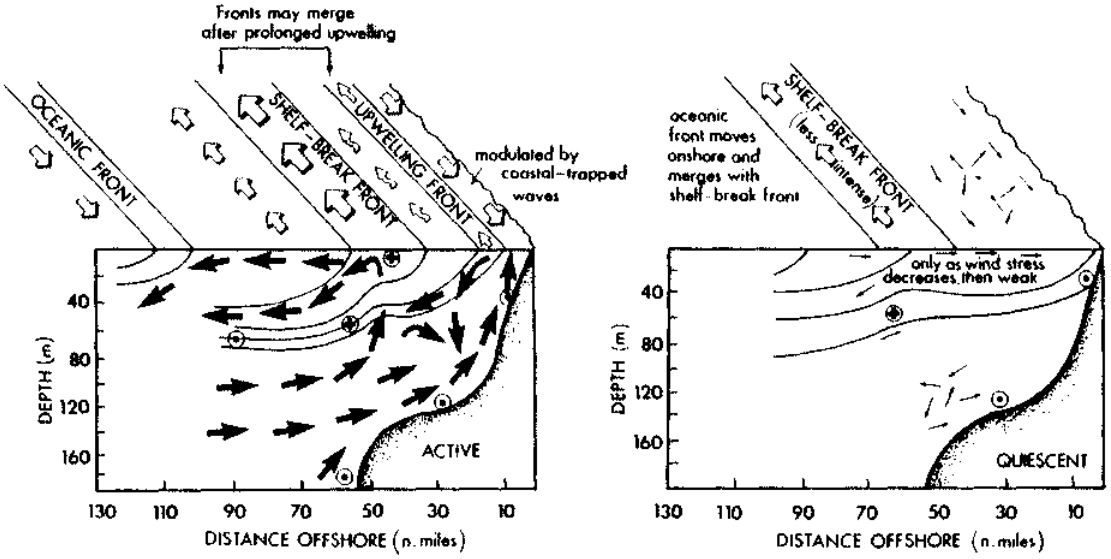

Fig. 1.4: A conceptual 3D model of cross-shelf circulation for periods of active (left) and quiescent (right) upwelling in the northern Benguela region. Poleward current presented by encircled dots, and equatorward current by encircled crosses. Figure from [Shannon and Nelson, 1996] after [Barange and Pillar, 1992].

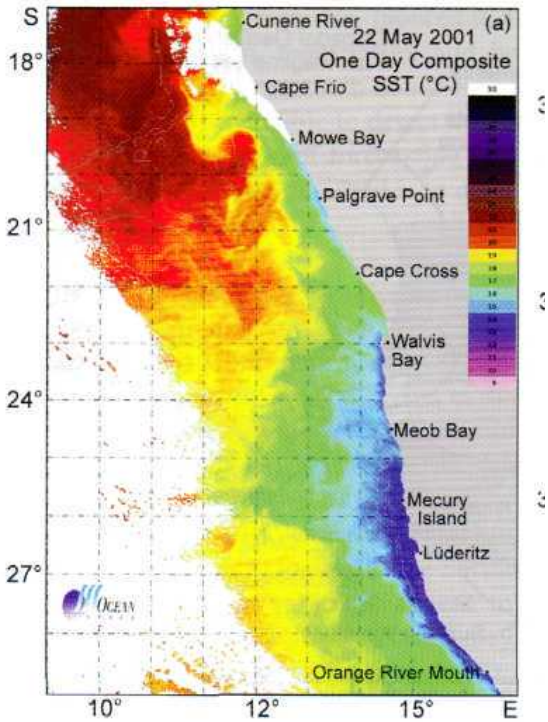

Fig. 1.5: The dynamics of the Benguela system. Mesoscale features like plumes, fronts, eddies and filaments can be seen across the Benguela in this SST image from [van der Lingen et al., 2006].

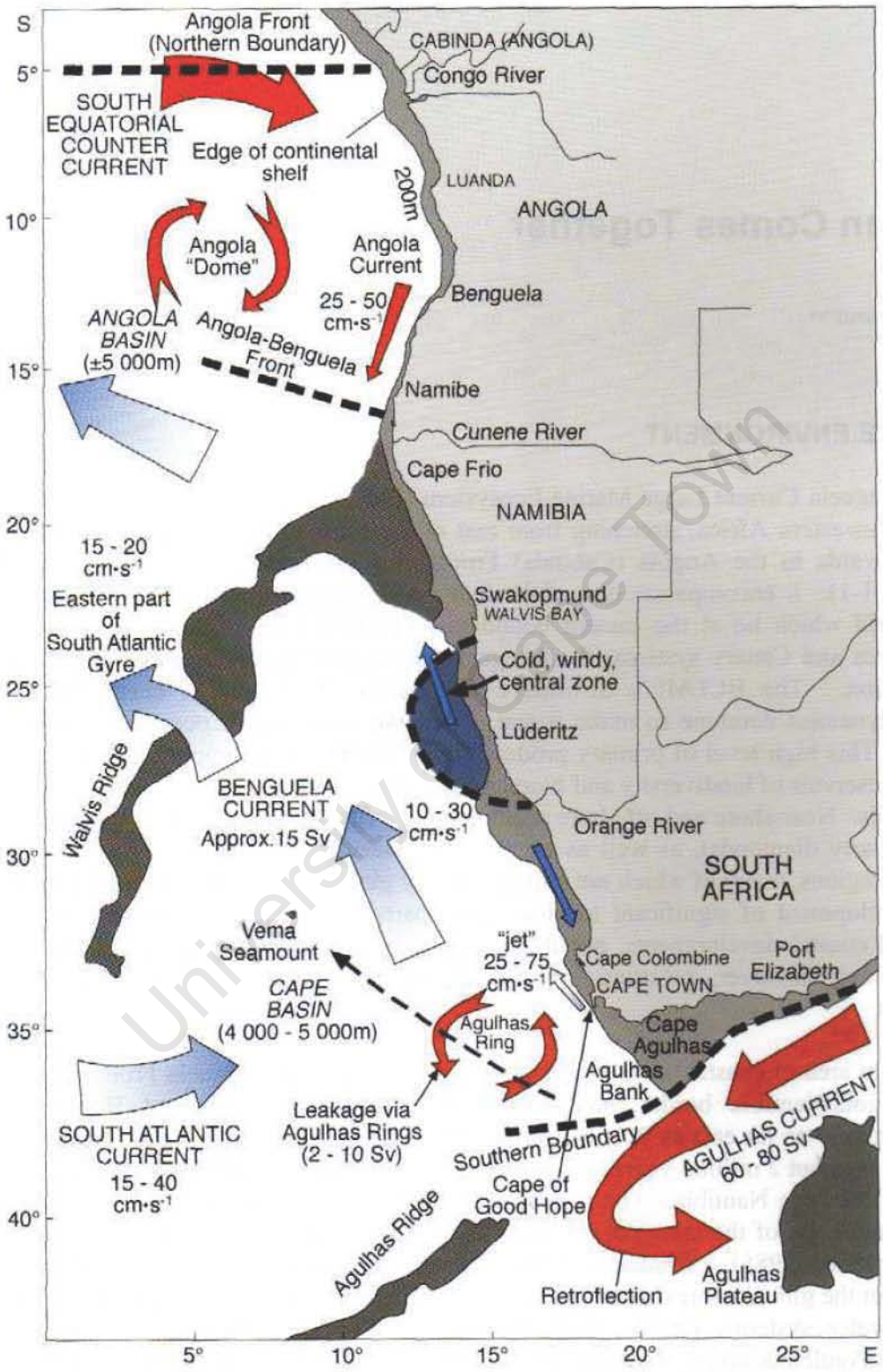

Fig. 1.6: The large- and small-scale circulation features of the Benguela upwelling system showing mainly currents and boundaries. Figure from [Shannon, 2006].

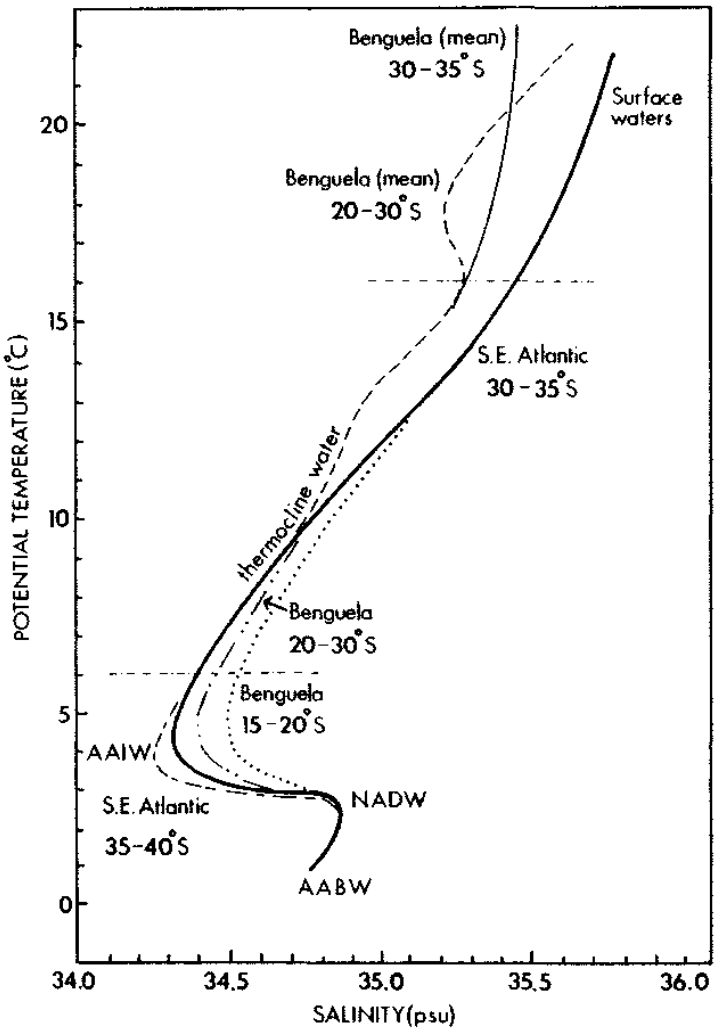

Fig. 1.7: Principal water masses and potential temperature-salinity characteristics of the South East Atlantic and the Benguela upwelling system. AABW is the Antarctic Bottom Water, AAIW is the Antarctic Intermediate Water and NADW is the North Atlantic Deep Water. Figure from [Shannon and Nelson, 1996].

South Equatorial Current, while several branches continue along the coast and eventually meet up with the Angola current near 16°S (ABFZ) [Moroshkin et al., 1970; Wedepohl et al., 2000] (see Fig. 1.6). Between these branches and across the continental slope lies an offshore divergence zone [Hardman-Mountford et al., 2003]. Following the seasonal trade wind migration, the Benguela current is strongest in the south during austral summer, while in the north the strongest flow can be observed during winter. It is also suggested that the current has a width of 200 km in the south which increases rapidly to 750 km in the north [Wedepohl et al., 2000].

Another key feature of the Benguela is the subsurface poleward transport of low oxygen water (LOW) along the entire coast of southern Africa, regularly spilling onto the shelf

or off the shelf and continuously being modified by localized depletion of the shelf waters [Nelson, 1989; Shannon, 1995; Monteiro and van der Plas, 2006; Mohrholz et al., 2008; Monteiro et al., 2008]. Water from the tropical Atlantic is in fact advected poleward at least as far south as 27°S [Gordon et al., 1995; Stander, 1964; De Dekker, 1969; Chapman and Shannon, 1985; Boyd et al., 1987]. In fact [Shannon and Nelson, 1996] suggest that the net flow through the water column tends to be poleward, despite the wind driven surface flow being equatorwards or the water transported north via the shelf edge jet. The presence of the undercurrent in upwelling regions had been suggested by [Hart and Currie, 1960] and subsequently verified in the Benguela by measurements [Nelson, 1989]. A correlation between the onset of the poleward flow and the onset of seasonal upwelling winds have been shown by coastal moorings in the region [Shannon and Nelson, 1996]. Processes which may account for the PUC (poleward undercurrent) in the Benguela are: tidal rectification, forcing by boundary mean density fields and wind stress [Shannon and Nelson, 1996; Clarke, 1989] or wind stress curl [Colberg and Reason, 2006]. T/S water mass analysis in the Benguela also revealed that upwelled water seems to move alongshore in the PUC rather than across the shelf [Shannon and Nelson, 1996]. There is however also a great variability in the bathymetry of the continental margin off southern Africa as can be seen in Figure 1.8, with a narrow shelf off southern Angola (20 km), off Lüderitz (75 km), and off Cape Peninsula (40 km). The shelf is wider off the Orange River (180 km) and near the Agulhas Bank in the south (230 km) [Shannon and Nelson, 1996], while double breaks are also present near Walvis Bay for example [Siesser et al., 1974]. One can therefore also expect great variability in the influence of the poleward undercurrent (PUC) as well as the surface Benguela current on the shelf condition.

Two sources of biogeochemically different water types have therefore been identified as coming onto the shelf of the Benguela upwelling system. One comes from the Cape Basin South Atlantic Central Water (termed Eastern South Atlantic Central Water, ESACW) and the other from the Angola Basin Central Water (termed South Atlantic Central Water, SACW) [Mohrholz et al., 2001; Duncombe Rae, 2005; Mohrholz et al., 2008]. The former is relatively fresh and well-oxygenated while the latter is more saline, nutrient rich and oxygen poor. SACW is transported into the Benguela upwelling system by the PUC mentioned above, which is an extension of the Angolan current below the thermocline [De Dekker, 1969; Shannon and Agenbag, 1987; Nelson, 1989; John et al., 2000]. ESACW is transported north by the Benguela current. While these two distinct water masses form a geochemically distinct boundary at the slope, they tend to mix on the shelf following upwelling and longshore wind stress driven cross-shore circulation [Monteiro et al., 2006; Brüchert et al., 2003, 2006] resulting in a smooth transition area between the ABFZ and the Lüderitz upwelling cell [Mohrholz et al., 2008]. Deeper water masses reaching the shelf edge can include both the Antarctic Intermediate Water (AAIW) as well as the North Atlantic Deep Water (NADW). [Brüchert et al., 2003, 2006] therefore suggest that the mixing proportion of the water masses

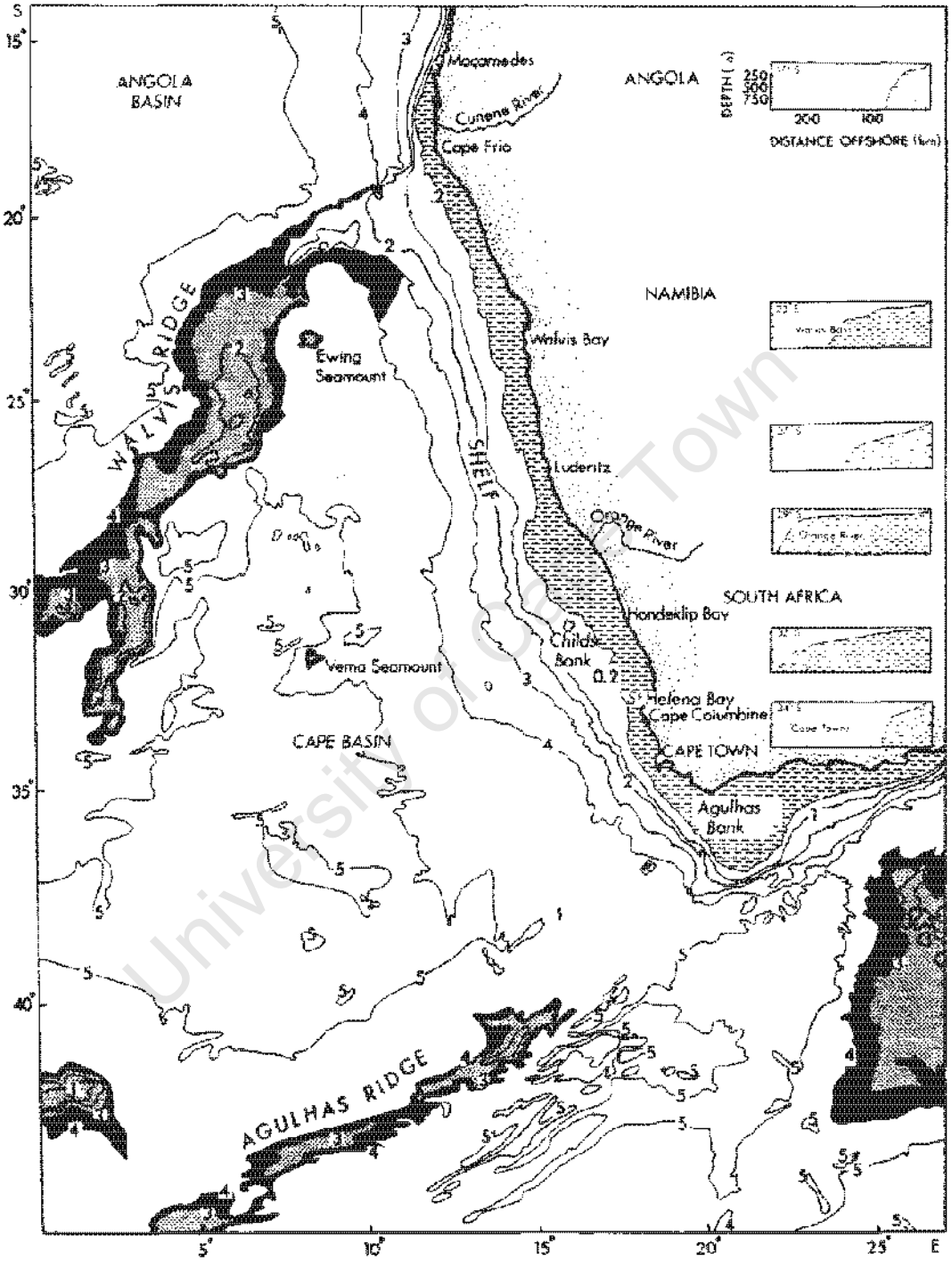

Fig. 1.8: Bathymetry of the South East Atlantic Ocean. The coastal shelf is indicated along the coast of Namibia and South Africa. Profiles of the shelf at selected latitudes are shown. Figure from [Shannon and Nelson, 1996].

found on the shelf may depend on strength and persistence of the PUC, carrying the SACW southwards, as well as the advection of ESACW onto the shelf below the thermocline. They go on to conclude that central water composition thus depends on distance from the ABFZ, distance from the shelf edge and wind field variations, because a weakening of the trade winds will reduce oxygen rich ESACW from being advected onto the shelf. Similarly the wind field across the ABFZ may very well control the extend of the PUC.

Oxygen and nutrient budgets on the shelf

It has long been known that oxygen-deficient water is a common feature in the bottom layers of the shelf region of central Namibia. Also known is that this condition is prominently driven by both the poleward advection of hypoxic water from the Angolan region [Nelson, 1989], as well as in situ production through plankton blooms or bacterial activity [Chapman and Shannon, 1985; Bailey, 1991]. A by-product of an intensification of this bacterial activity across the carbon rich sediments found on the shelf is hydrogen sulphide. When the hydrogen sulphide erupts from the sediments localized hypoxia and mass mortalities tend to occur. Figure 1.9 and the text below describe the formation and transport of low oxygen water on the Benguela shelf.

[Brüchert et al., 2006] mention that the contribution of advected oxygen to the oxygen budget on the shelf is implied by the zonal oxygen gradient and the cross-shelf circulation. They suggest for example that due to a higher fraction of SACW the near shore region is likely to have a lower oxygen concentration than the area west of the shelf break, where ESACW dominates. Additional measurements from them further suggested that the intermediate layer may be ventilated by ESACW while nutrient rich, oxygen poor water is supplied to the region at greater depth through the PUC. In the absence of strong meridional transport water will tend to remain stationary on the shelf and will become oxygen and nutrient depleted.

[Monteiro et al., 2006] linked four dynamically acting factors as being behind the seasonal and interannual variability of the hypoxia associated with the subsurface shelf waters in the central Benguela: 1) differential shelf boundary conditions (i.t.o. T,S,O characteristics) of the two central water types (Equatorial and South Atlantic) at Cape Frio and Lüderitz; 2) advection of the equatorial hypoxic boundary conditions by a poleward flow from Cape Frio along the central Benguela shelf in late summer; 3) the ventilation phase with an equatorward flow from Lüderitz in spring-early summer from the Cape Basin onto the shelf and 4) the winter peaked biogeochemical sediment flux of reduced metabolites. Work from both [Monteiro et al., 2006] as well as [Brüchert et al., 2006] further showed that the north-south shelf flows are seasonally phased and that there are large fluctuations in the oxygen concentrations of the bottom waters, particularly offshore of Walvis Bay. In their paper, [Pollock and Shannon, 1987] suggested an expansion in LOW distribution along the Namibian

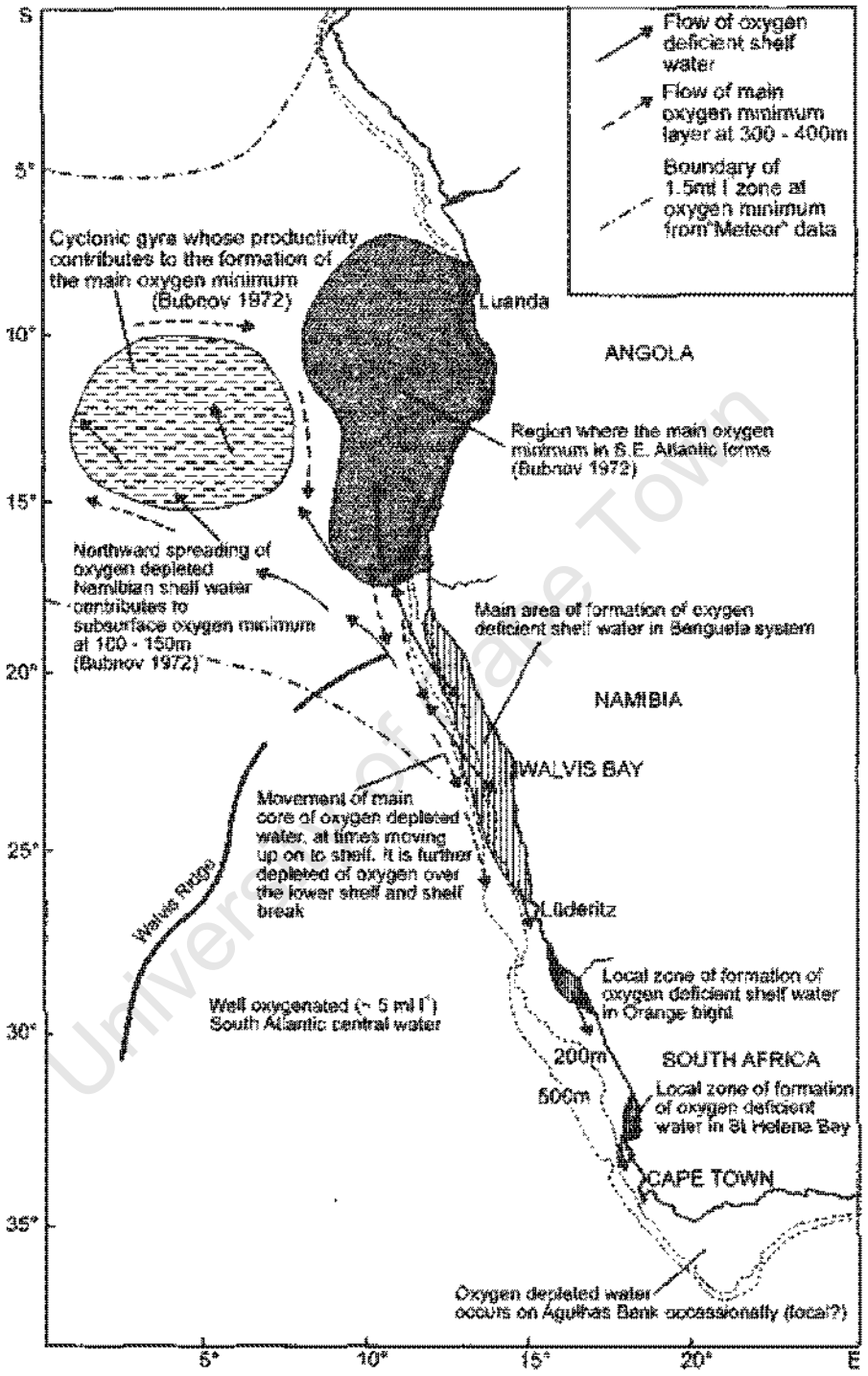

Fig. 1.9: Conceptual model showing areas where low oxygen water is formed in the South East Atlantic and how it is transported along the coasts of Namibia and South Africa. Figure from [Shannon and Nelson, 1996] after [Chapman and Shannon, 1987].

shelf since the late 1960s. A suggested reason for this trend was either an increase in phytoplankton production or reduction in stocks, and thus grazing, of clupeoid fish.

Understanding the drivers behind the anoxic water on the shelf is important because the distribution of many species is limited by the extend of the anoxic water on the shelf [Tomalin, 1993; Grobler and Noli-Peard, 1997]. In addition, nutrient availability and distribution plays a crucial role in the dimensions and speed of primary production [Giraudeau et al., 1993]. Thus, variability in both the biochemical properties as well as the physical processes which drives these properties needs to be considered due to the importance of these aspects for the countries bordering the Benguela upwelling system, which are greatly dependent on the prosperous industrial fisheries yielded from the region.

Mesoscale processes and dynamics

Similar to other eastern boundary upwelling systems, the shelf region of the Benguela is characterized by intense mesoscale activity [Shannon and Nelson, 1996; Field and Shillington, 2006; Shillington et al., 2006]. Mesoscale processes are those which have a spatial extend of hundred of meters to a few hundred kilometers and a time scale of between hours to several months. Major forcing factors for these mesoscale processes include the wind induced coastal upwelling and its interaction with the topography and open ocean circulation features [van der Lingen et al., 2006]. Mesoscale processes include the plumes, fronts, eddies and filaments already mentioned. These mesoscale structures strongly modulate surface flow as well as vertical motion on the continental shelf [Barange and Pillar, 1992]. Figure 1.10 provides a view on the difference in mesoscale structure which exist between the northern and southern Benguela as observed by both [Veitch, 2009] and [Capet et al., 2008]. Here low EKEs are observed at the coast and over the shelf and extremely high EKEs offshore in the southern Benguela, due to the presence of Agulhas rings and eddies [Veitch, 2009]. In the northern Benguela this increase in EKE offshore is less intense. Close to the ABF the EKE increase offshore is again more intense. Note that a log-scale is necessary to capture both the high offshore EKEs as well as the very low nearshore EKEs. Of great interest in the current study is the mesoscale dynamics of upwelling filaments within the northern Benguela.

1.1.3 Upwelling filaments (in the northern Benguela)

Upwelling filaments, previously also referred to as tongues, plumes or squirts, are narrow jets which tend to originate on the shelf, specifically in eastern boundary current systems (EBCS), and then advect upwelled water offshore [Brink, 1983; Flament et al., 1985; Brink and Cowles, 1991]. In addition, the ageostrophic divergence, resulting from the current flow within the filament, likely also produces in-situ upwelling [Haynes et al., 1993]. There are a

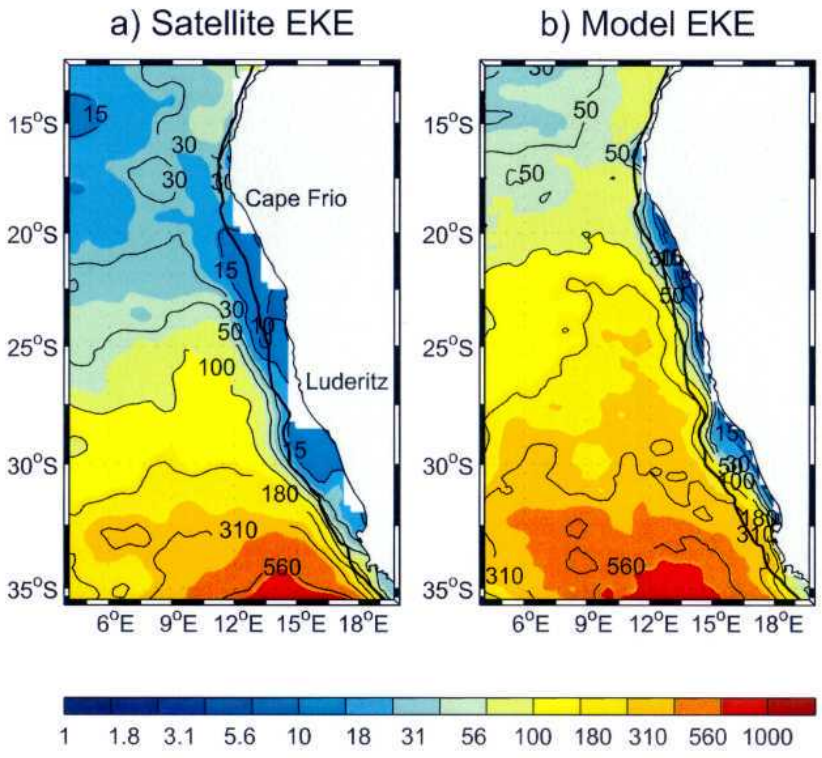

Fig. 1.10: Satellite and model-derived surface geostrophic EKE in the Benguela system. The 500 m isobath is shown. Figure from [Veitch, 2009].

number of theoretical possibilities for the formation of filaments, which are probably not mutually exclusive. Three common theories also presented by [Brink and Cowles, 1991] are: 1) dynamic instability, where inherent baroclinic instabilities in the upwelling associated flows of the equatorward surface and the poleward undercurrent can lead to filament formation, 2) topographic forcing, where irregularities of the coastline or shelf induced wind stress variations could lead to filament formation, or 3) geostrophic disturbance, where the interaction of eddies with the coastal upwelling zone may lead to filament formation. Results from a high resolution model (3.5 km) from [Marchesiello et al., 2003] revealed a large number of small-scale eddies (<20 km) which they attributed to short-wavelength ageostrophic frontal instability (see Fig. 1.11). As frontal instabilities form along the coastal current they seem to roll up into cyclonic vortices as can be seen in Figure 1.11. In their results [Marchesiello et al., 2003] found further evidence for [Mied et al., 1991]'s suggestion that counterrotating dipole eddies cause hammerheads or mushroom-shaped SST patterns. Large dipole eddies (200 km) at the surface were found to consist of strong low pressure cyclonic and weak high pressure anticyclonic vortices. At greater depths they found that the situation reversed and strong anticyclonic and weak cyclonic vortices persisted [Marchesiello et al., 2003]. These dipoles most likely result from instabilities in both the coastal and subsurface currents. [Chereskin et al., 2000] additionally observed that these flow structures systematically propogate westward and thus that offshore transport and mixing of materials can take place.

These filaments are therefore believed to make a significant contribution to the exchange between the coastal waters and the open ocean [Pillar et al., 1998; Barton et al., 2001], as they provide an effective mechanism to transport not only nutrients and plankton biomass [Lutjeharms and Stockton, 1987; Lutjeharms et al., 1991; Kostianoy and Zatsepin, 1996], but also suspended matter [Sivkov, 1994] offshore. Previous research has shown that filaments from EBCS tend to have strong lateral gradients as well as a strong offshore flow [Davis, 1985; Brink et al., 1991; Huyer et al., 1991], often interacting with and terminating in eddy-like structures [Mooers and Robinson, 1984; Kosro and Huyer, 1986]. In addition, filament waters are often nutrient rich and high in chlorophyll [Traganza et al., 1980, 1981; Navarro-Perez and Barton, 1998; Shillington et al., 1992] thus making it an important element to consider alongside coastal upwelling and upper ocean dynamics in understanding the biological activity of a system [Thomas and Strub, 1989; Brink and Cowles, 1991]. [Sobarzo and Figueroa, 2001] however warn that filaments do not necessarily always contribute to the biological productivity of a system with the same intensity or geographic dimensions. Additionally, filaments, from the California system in particular, tend to have a distinctive core (or double core) containing fresher and cooler water, with different water masses present on either side [Flament et al., 1985; Huyer et al., 1991]. The exact distribution of water masses in and around a filament will greatly depend on the strength of upwelling related to the feature and thus the depth from which water has been pumped [Sobarzo and Figueroa, 2001]. In addition, they found that intrusions of water masses with different properties may result in the filament splitting. [Davis, 1985] also describes strong offshore jets, reaching depths of about 100 m, relative to cold filament cores. The equatorward front of a thermal filament also tends to be sharp while the poleward front tends to be more gradual [Flament et al., 1985; Rienecker et al., 1985; Kosro and Huyer, 1986], although, sharp surface fronts at the northern side of filament structures in the California Current system have also been recorded [Kosro and Huyer, 1986]. Filament waters tend to lose their distinctive characteristics through mixing with the surrounding water masses, and the feature appears to sink as it moves offshore [Van Camp et al., 1991; Nelson et al., 1998]. Subduction in near-surface isopycnal layers has additionally been noted as a cause for the rapid warming taking place in surface layers as the filament moves offshore [Washburn et al., 1991; Brink et al., 1991]. [Brink et al., 1991] suggest that convergence and downwelling tend to occur at the equatorward boundary of a filament while [Swenson et al., 1992] found evidence of it occurring at the poleward boundary. Several studies also found that turbulence enhances mixing at the fronts while at the core mixing tends to be restricted to the upper layers [Barton et al., 2001; Dewey et al., 1987].

In the 1980s satellite SST data was first used to observe the spatial and temporal scales of upwelling filaments in the Benguela region [Van Foreest et al., 1984]. This was followed by in situ measurements of the mesoscale activity within these filaments in the early 1990s [Shillington et al., 1990; Duncombe Rae et al., 1992; Shillington et al., 1992; Nelson

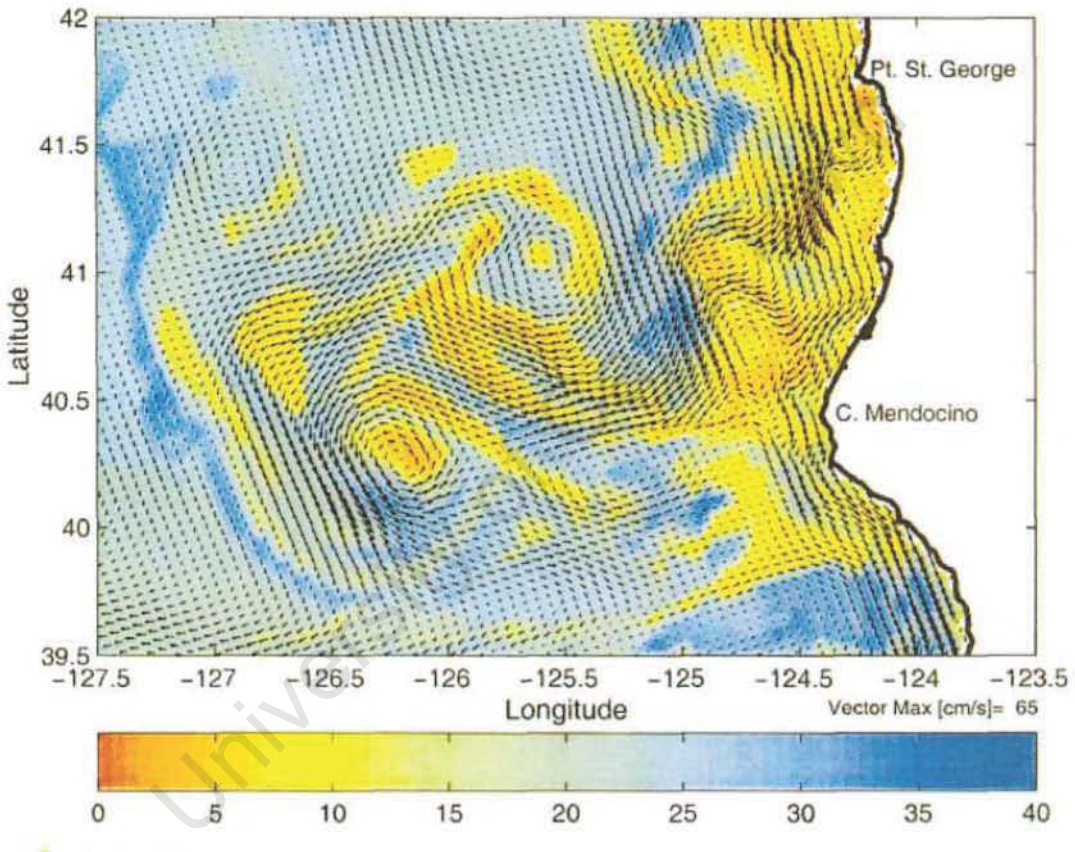

Fig. 1.11: SST and current vectors associated with an upwelling filament from [Marchesiello et al., 2003] showing dipole eddies surrounding the feature.

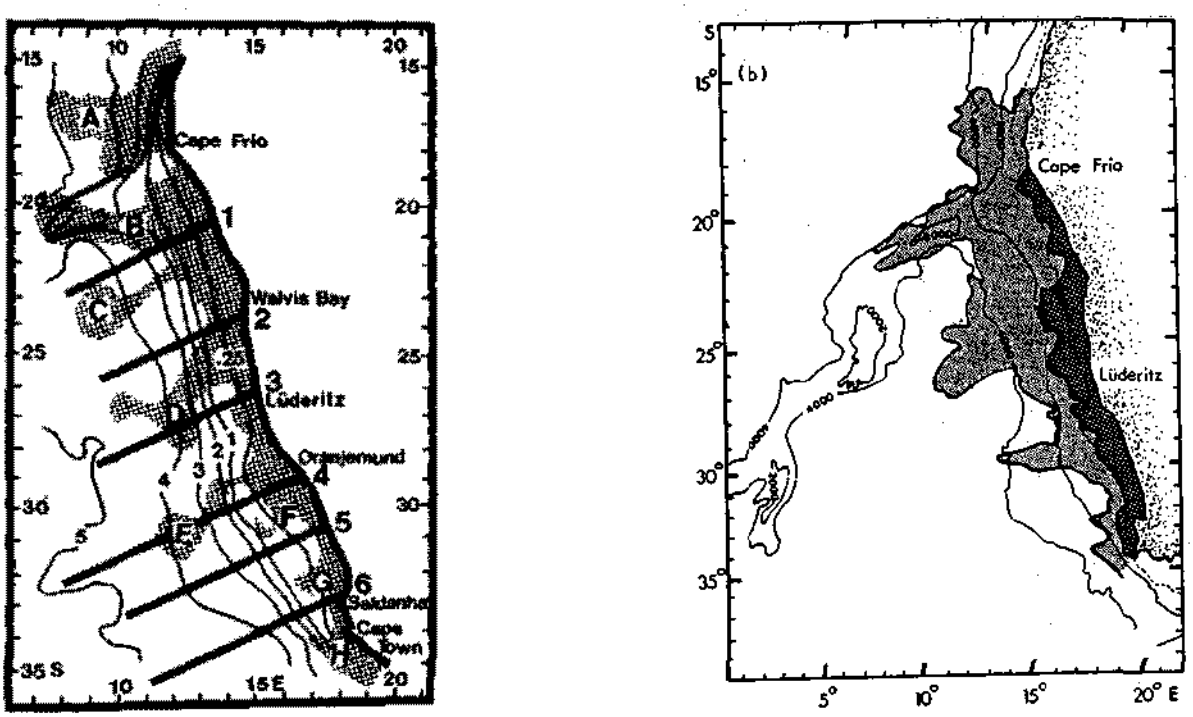

Fig. 1.12: Upwelling filaments across the Benguela. Left figure: Regions where high concentrations of upwelling filaments have been observed from numerous satellite studies can be seen in this figure from [Van Foreest et al., 1984] as the shaded features labelled A-E. Bathymetry contours presented in 1000 m intervals. Right figure: The main contiguous upwelling area (dark shading) and the full extent of upwelling filaments (lighter shading) from thermal infra-red METEOSAT imagery from August 1984 as per [Lutjeharms and Stockton, 1987].

et al., 1998]. None of these latter investigations however stretched much further north than Lüderitz, and the interaction of the filaments with warm cored Agulhas rings was often a primary point of interest [Lutjeharms et al., 1991; Duncombe Rae et al., 1992; Shillington et al., 1992]. [Van Foreest et al., 1984] did however observe a distinct difference in surface appearance of the features between the northern and southern Benguela from satellite data. They suggested that the filaments found north of 30°S have a greater offshore extent (up to 500 km) and that their longshore spacing is the same order of magnitude as their offshore extent, while those to the south of 30°S have a smaller offshore extent and tend to resemble frontal eddies. This means that northern Benguela filaments extend from the continental shelf, over the continental slope, to the abyssal plane, while southern Benguela filaments tend to be centered over the shelf break [Van Foreest et al., 1984]. [Nelson et al., 1998] therefore suggested that filament length in the Benguela corresponds roughly to shelf width. Based on extensive satellite observations it has further been suggested that Benguela filaments tend to propagate offshore approximately perpendicular to the upwelling front [Kostianoy and Zatsepin, 1996]. Early studies have also indicated that upwelling filaments correspond strongly with the major upwelling cells off the west coast of Namibia with regular filaments observed offshore from Oranjemund (∼29°S), Lüderitz (∼26°S), Walvis Bay (∼23°S), Rocky point (∼20°S) and Cape Frio (∼17°S) [Van Foreest et al., 1984; Lutjeharms and Stockton, 1987]. In a latter study, [Kostianoy and Zatsepin, 1996] listed high concentrations of filaments in three specific regions: 18-19°S, 22-23°30'S,26-27°30'S. Figure 1.12 shows two examples of regions where filaments are continuously observed across the Benguela.

There has however, been a lack of information on the subsurface structure and dynamics of northern Benguela upwelling filaments. Specifically, the contribution of these filaments to offshore transport within the region has not been sufficiently quantified. In this study both satellite SST and in situ measurements of hydrography, current velocity and turbulent processes which were made across two north-south transects through an upwelling filament located between 17.5 and 19.5°S. The aim was not only to provide insight into the mesoscale dynamics of a northern Benguela filament, but also on its role in the exchange of matter between the shelf and the open ocean in the region. These results are presented in chapter 5.

1.2 Summary and research motivation

This review of past research provides a platform from which to identify gaps and formulate new research objectives which could contribute to our understanding of the structure and dynamics of the northern Benguela in particular. There continues to be a need for a greater understanding of shelf edge exchange processes, specifically in eastern boundary current systems. In particular, the contribution of the shelf edge exchange and longshore processes

to ecosystem dynamics in the northern Benguela upwelling system has not been sufficiently investigated and quantified. This project aims to contribute not only to general knowledge about shelf edge exchange processes, but focus specifically on quantifying the contribution of processes within the northern Benguela upwelling (eco)system. As the literature summary thus far has shown, a great concordance exists regarding the large scale circulation dynamics of the northern Benguela, including the dominance of the poleward undercurrent and the LOW it transports, the contribution of the equatorward coastal jet to the oxygen structure on the shelf, the influence and influx of very distinct water masses from both the north and the south. In particular this research follows on from the recent work of [Veitch, 2009]. Veitch's research highlighted the strong link between wind-stress curl via the sverdrup relation and the poleward flow in the northern Benguela. It further showed that the deepening of the PUC is also related to the nature of the wind stress curl. In addition her research showed that there are regions in the central Benguela where local instabilities are generated and large filaments result. However, quantifying transport across the shelf edge has not yet been attempted for the system as a whole, and neither has it been attempted to quantify the contribution of upwelling filaments to cross-shore transport within the northern Benguela.

This project thus attempts to quantify where, how much and by what mechanisms water (as well as dissolved oxygen and nutrients) leaves or comes on to the Namibian shelf. This will largely be done by making use of the results from a regional ecosystem model which has been developed for more than a decade by the Theoretical Oceanography and Numeric Modelling working group at the Institute of Baltic Sea Research in Warnemünde under the guidance of Dr. Martin Schmidt. Due to the lack of literature dealing with the validation of this model, a section of this thesis is also dedicated to comparing model results with measured data across the northern Benguela. A further aim of the project is to gain a better understanding of the physical dynamics of upwelling filaments within the Benguela system and to try and quantify the contribution of upwelling filaments to the exchange across the shelf edge. This is done by making use of both data from a regional ecosystem model as well as cruise data and other direct measurements.

Therefore, section 2 will describe the model simulation and its configuration used for the analysis in this project. Additionally, in this section the satellite and in situ data sources will be outlined. In section 3 measured data from various sources will be compared with the model output in order to establish the validity of using this output for the analysis in this project. This will be followed by section 4, where model results will be used to analyze and quantify the variability in transport fluxes along the shelf in the northern Benguela. Then, in section 5, the results from a case study on an upwelling filament in the northern Benguela during October 2010 are presented and with the help of model output its contribution to cross-shore transport is examined. Finally, section 6 provides an overall summary of the limitations, recommendations and conclusions of this study.

Chapter 2

Research design and methodology

In this section a condensed description of the MOM-4 ecosystem model used for analysis in this project is presented. In addition, the procedures of data collection and analysis are described.

2.1 Introduction to the coupled ecosystem model adjusted for the Benguela region

The model description presented here is a condensed presentation of the technical report compiled by [Schmidt and Eggert, 2012]. The MOM-4 circulation model has been configure to include both the equatorial currents as well as their poleward extension along the coast of Africa. The model area extends to 10°W and thus considers the eastern part of the sub-tropical gyre [Fennel et al., 2012a].

2.1.1 Description of the model setup

Model grid and topography

Fig 2.1 shows the rectangular model grid in geophysical coordinates. Minimum grid cell size (both meridional and zonal) is about 8 km in the Namibian coastal region, whereas the grid is stretched towards the model boundaries (18 km). This resolution means that the Baroclinic Rossby radius is still resolved [Emery et al., 1984], except in shallow waters and near the shelf where the Rossby radius is much smaller. Vertical grid resolution is 3 m for

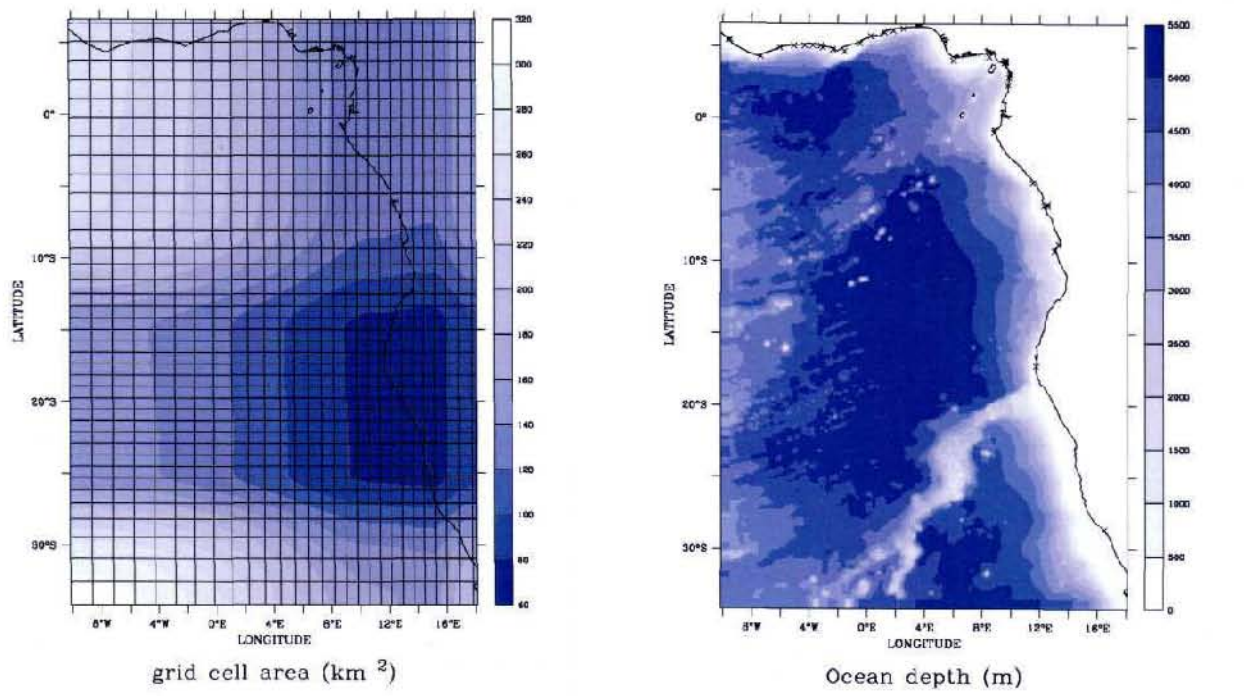

Fig. 2.1: Left: The rectangular model grid in geophysical coordinates. Right: ETOPO-5 topography data used in the coupled model. From [Schmidt and Eggert, 2012].

the top 200 m, after which the grid spacing increases like a cosine shape and at 5000 m depth a cell thickness of 500 m is found. The model grid has been generated with the off-line tools of MOM-4 [Pacanowski and Griffies, 2000] and contains 273 x 382 x 89 grid point overall [Fennel et al., 2012a].

ETOPO-5 (earth Topography 5-minute resolution) data, seen in figure 2.1, is used for model topography [NOAA, 1988]. Rivers known to have a significant influence on the surface water properties have been included in the model. The Congo river for example has an estimated outflow of more than 50 000 $m^3 \cdot s^{-1}$ and mass transports and river positions were obtained from aquarius1.gsfc.nasa.gov, referenced to Goddard Space Flight Center, and presented as a monthly climatology. The model is a level model and have so-called z*-coordinates which are derived from fixed z-levels. These coordinates allow a high vertical resolution along the shelf and was used instead of sigma coordinates which has been known to result in numerical errors in proximity of steep topography.

Boundary data and atmospheric forcing

The model grid is ARAKAWA B-grid (see Figure 2.2) and data from the MIT general circulation model from the ECCO consortium (Estimating the Circulation and Climate of the Ocean) is used to provide boundary values for sea-level and tracer concentration. Atmosphere

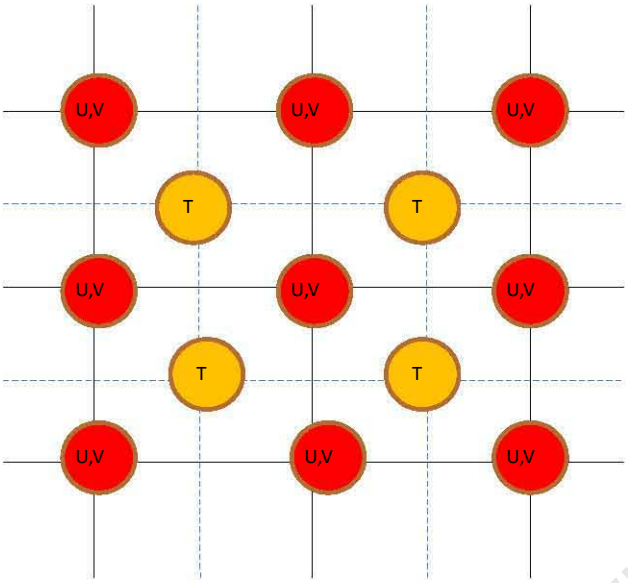

Fig. 2.2: Arakawa B-grid layout in model. Arakawa B-grid is a staggered grid arrangement which seperates the evolution of two sets of quantities, in this case velocities at the grid corners and a tracer at the grid center.

b) u,v components

data from NCEP reanalysis and scatterometer data (QuikScat) from NOAA are used to derive ocean-atmosphere fluxes used to force the model. The model needs the following fluxes: zonal and meridional wind stress, insolation, latent and sensible heat flux, thermal radiation budget and the fresh water flux. These fluxes are derived from the atmospheric variables: zonal and meridional wind at 10 m height, air pressure at sea level, air temperature at 2 m height, specific humidity at 2 m height, cloud coverage and precipitation. Thus, no atmosphere model is used, but the derived data are considered as realistic. The NCEP data have a spatial resolution of 1.875° and are available for every 6 hours, whereas QuikScat data have a spatial resolution of 0.25° and are provided daily as a composite made from a three day period. A combined data set from both NCEP and Quickscat data is therefore used where the QuickScat wind speed data are modulated with the diurnal cycle extracted from the NCEP data.

Ocean-atmosphere coupling

The ocean and atmosphere are coupled by a boundary layer model and the fluxes from ocean and atmosphere state variables are derived using bulk formulas. The fluxes are calculated explicitly. The atmospheric model is actually replaced by reading atmospheric data from files. Due to the feedback of the ocean to the atmosphere being neglected, NCEP and QuikScat data are considered a "realistic" representation of nature. This one-way coupling will keep the sea surface ocean variables near reality unless the ocean model drifts into a completely unrealistic state. The atmsophere-ocean boundary fluxes are calculated from

REMO based simulations which uses ERA-40 as the boundary values in conjunction with an ocean climatology. The coupling is done using the MOM-4 code and momentum and heat fluxes are calculated for a time segment in advance, using the atmosphere and ocean surface state variables. The model is coupled at two open boundaries, at 10°W and 35°S [Fennel et al., 2012a]. Time interpolated values of the atmospheric variables are used and the calculated fluxes are kept constant over the next time segment and used to drive the ocean model [Schmidt and Eggert, 2012].

Model initialization

Sea level, currents, temperature and salinity were initialized using a snapshot from ECCO group MIT general circulation model. Nutrients and oxygen were initialized using World Ocean Atlas 2001 [Conkright et al., 2002], while phytoplankton variables, zooplankton and detritus were initialized purely by a minimum value and its development is left to the model. Since the model is initialized using the ECCO output, which has a long spin-up time and because our model is small enough to adjust within a shorter time period, the model is assumed to be in statistical equilibrium. The model was run over 12 model years, with the first year being excluded from the statistics. In this analysis only data from the period 2000-2008 were used since Quickscat was replaced by Ascat in 2009 and it was thought that this may introduce inconsistencies.

2.1.2 The physical circulation model component

The MOM-4 circulation model is used for the calculations of currents and the advection and diffusion of tracers, with detailed documentation of this circulation model found in the manual by [Griffies, 2004]. The MOM-4 code solves the so-called primitive equations in Boussinesque approximation. Advection-diffusion equations for salinity and temperature supplement the momentum equations and density is calculated from temperature, salinity and pressure according to the revised seawater equation [Jackett et al., 2006]. Vertical velocity (w) is diagnosed from the divergence of the horizontal velocity field. Turbulence, though not represented explicitly, is incorporated into the equations as Reynolds stress, i.e. vertical and horizontal turbulent viscosity and mixing.

Turbulent closure

A nonlocal K-profile mode is invoked for turbulent vertical processes [Large et al., 1994] and provides not only vertical mixing and viscosity coefficients but also boundary layer depth (h). Below the surface boundary layer, shear induced turbulence and breaking of internal waves cause mixing and viscosity. Because the model implementation is "eddy resolving",

the turbulent terms are important not so much for parameterization of unresolved transport processes but for numerical stability of the advection scheme.

2.1.3 The 3D biogeochemical ecosystem model

A so-called Nutrient-Phytoplankton-Zooplankton-Detritus (NPZD) ecosystem model has been configured and embedded into the MOM-4 circulation model. The food chain levels include nutrients, three trophic levels of phytoplankton and zooplankton as well as dead particulate organic matter. After the zooplankton trophic level the food chain is truncated and higher trophic levels like fish is only implicitly presented as a mortality rate. Variables explicitly represented in the model are: nutrients like nitrate, ammonium, phosphate but also dinitrogen, elements of the sulfer cycle and oxygen. In contrast prokaryotes are not an explicit model variable but are assumed to be omnipresent, meaning the relevant metabolic processes mediated by them are implemented.

Chemical and biological variables are treated as Eulerian variables and as possible tracers within the circulation model. By passive tracers we mean they undergo the same physical advection and mixing as temperature and salinity. However, within the ecosystem model each of these chemical and biological variables contain dynamic equations describing all ecological activities and metabolic reactions. The model follows the cycling of nitrogen through the ecosystem and the conceptual diagram (Fig 2.3) from [Schmidt and Eggert, 2012] summarizes this.

2.2 Calculating volume transport fluxes

In chapter 4 an attempt will be made to quantify the contributions from the main driving forces to the transport fluxes along the Namibian shelf. This is important in order to gain a deeper understanding into the role that these processes and possible changes to them may have for oxygen and nutrient availability on the shelf. Here the Namibian shelf was defined as the region up to 300 m depth. This definition for the 300 m deep shelf was used in order to allow a unique view into the prosesses driving the dynamics close to the Namibian shore. Additionally, consideration was given to the findings of [Andrews and Hutchings, 1980] and [Shannon and Nelson, 1996] that the upwelling water reaching the surface over the shelf is primarily drawn from the central water masses (<180-200 m). Basic flux equations were used to compute flux profiles from the horizontal current velocity grid of the ecosystem model.

The general expression for the transport or flux (F) of a property equals the integral of the property (P) times velocity (v) over the area (dA). The area is a cross section, i.e. the

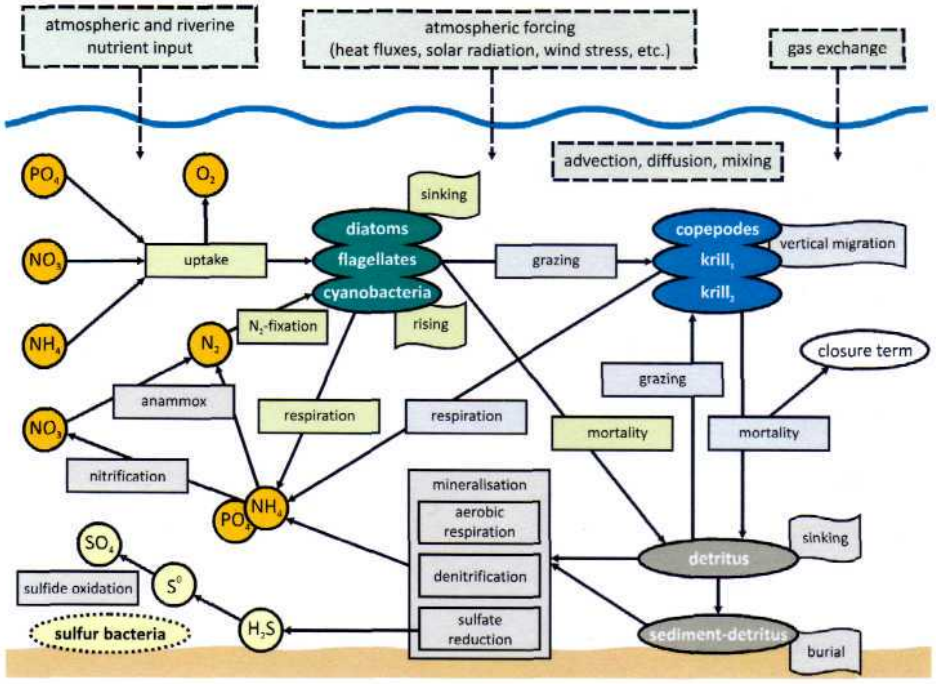

Fig. 2.3: The conceptual cycling of nitrogen through the ecosystem. From [Schmidt and Eggert, 2012].

width of the current times its depth.

$$F = \int P \cdot v \, \mathrm{d}A \tag{2.1}$$

Procedure

In the calculation of transport flux budgets a vertical plane is drawn across a current or region with x(y) and z being the zonal (meridional) and vertical dimensions respectively. Current velocity was computed from model data for the different sections of the plain and integrated for total transport through the cross-section. For this study the Benguela shelf between 16-28°S was divided into 4 regions of equal latitudinal dimensions. In Fig. 2.5 the four regions can be seen: A) 16°-19°, referred to in the text as the Cape Frio region, B) 19°-22°, C) 22°-25°, occasionally referred to as the region off Walvis Bay and D) 25°-28°S, referred to as the Lüderitz region. This selection of regions offer an opportunity to investigate the circulation dynamics surrounding the two major upwelling cells (Cape Frio and Lüderitz) and comparing these with the two central regions.

For each of the four regions a box was computed with three open planes and one closed plane, being the Namibian coast. The western plane of each box runs along the 300 m deep shelf edge. Calculations of the meridional volume transport fluxes for the budgets through

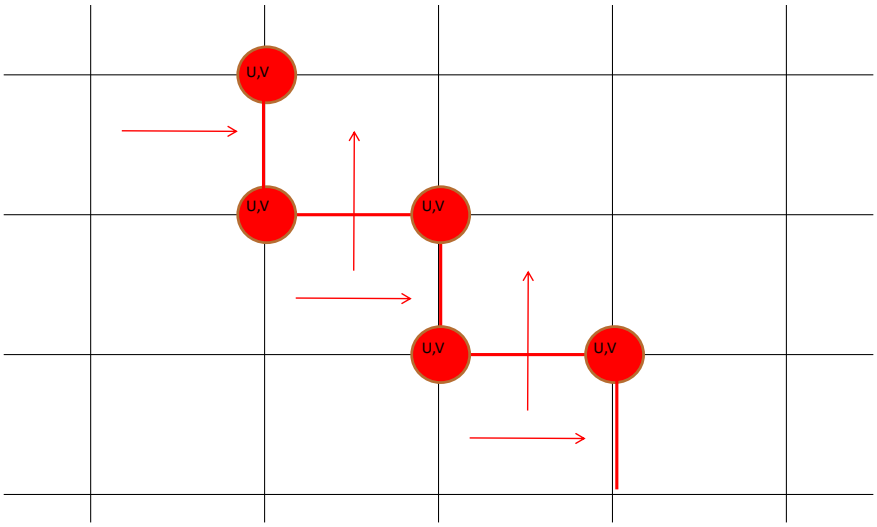

Fig. 2.4: The u,v components required for the cross-shore transport flux budgets. Due to grid alignment in the model the exchange "across" the inclined boundary includes both the zonal (u) and meridional (v) components.

the latitudinal cross-sections were standard (as described above). Due to the alignment of the model grids, the cross-shore fluxes along the 300 m shelf edge were more complicated. Figure 2.4 shows this graphically by indicating that both the zonal (u) and meridional (v) components have to be considered in order for the budget to balance.

2.3 Sampling an upwelling filament during October 2010

The methodology described here relates to the results of Chapter 5 and deals with the sampling of an upwelling filament in the northern Benguela during October 2010.

The filament survey was conducted aboard the R.R.S. Discovery from 1 to 5 October 2010 during leg 2 of the Geochemistry and Ecology of the Namibian Upwelling System (GENUS) cruise (10 Sept-10 Oct 2010) [Buchholz, 2010]. Figure 2.6 presents the SST image for the 2nd of October off the Namibian coast at Cape Frio. Visible is the surface signal of the upwelling filament as well as the two transects sampled across the feature. Due to extensive cloud cover during the sampling period no clear SST satellite images could be acquired. Optimum interpolated SST data from the Tropical Rainfall Measuring Mission Microwave

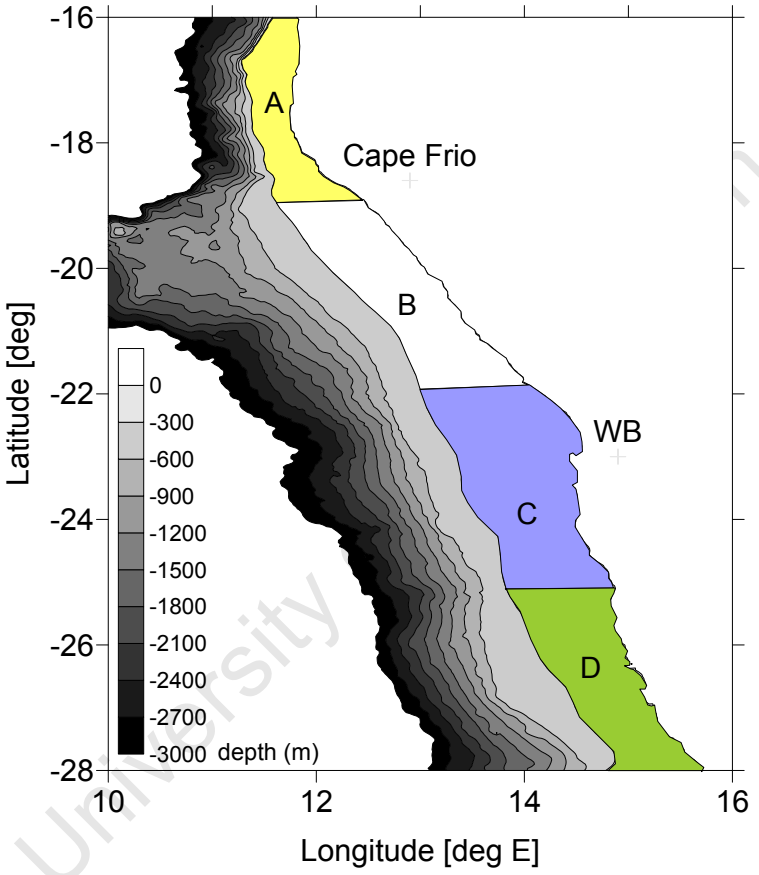

Fig. 2.5: Defining four geographic regions along the Namibian shelf: A) 16°-19°S, referred to in the text as the Cape Frio region, B) 19°-22°S, C) 22°-25°S, occasionally referred to as the region off Walvis Bay and D) 25°-28°S, referred to as the Lüderitz region. The western plane of each box runs along the 300 m deep shelf edge.

Imager (TMI) and Advanced Microwave Scanning Radiometer for Earth Observing System (AMSR-E), with a 0.25° longitude by 0.25° latitude grid resolution and an accuracy ranging between 0.2-1.0°C depending on the geographic region, were used instead to track the development of the filament. Two transects were chosen relative to the surface feature observed on the SST images with the aim being to sample one transect closer inshore and the other further offshore, closer to the western tip of the filament. The two cross-filament transects which were sampled can be recognized at approximately 11°E and 9.6°E. An AVHRR SST image (not shown) taken 10 days prior to sampling (21 September) showed the development of the filament (16°C surface temperature) at approximately 18.25°S, 11°E meandering westward to approximately 10.5°E. In the 7 day period following this (22-28 September) strong (9-17 $\mathrm{m{\cdot}s^{-1}}$) southerly winds dominated along the Namibian coast (Figure 2.7), as recorded in the onboard ships meteorological data. The favorable upwelling winds were a response to a high pressure cell centered at approximately 7°W, 30°S across the South Atlantic Ocean. In contrast, the hourly averaged surface winds during the sampling period were relatively weak, mostly lower than 7 $\mathrm{m{\cdot}s^{-1}}$ except for a few hours on the 4th of October. Wind direction during this period showed a distinctive diurnal pattern, oscillating between north-easterly and southerly winds. Weak north-westerly winds bridged the upwelling favorable period and the more diurnal quiet phase, in response to the weakening of the South Atlantic high pressure cell. Each transect was sampled twice. First a towed undulating CTD (ScanFish) was used to gain information on the general structure of the filament. This data set was limited to the top 100 meters and the resolution of the scanfish track through the water column can be seen in Figure 2.8. Each transect was subsequently sampled using a vertical CTD and a microstructure profiler (MSS). The eastern transect was sampled first with the ScanFish over a 14 hour period on the 1st of October (5h00 to 19h00 UTC). Five CTD and MSS stations were then sampled across the filament over a two day period (1-3 October 2010). Again, ScanFish measurements were taken across the western transect over an eight and a half hour period (8h50 to 18h20 UTC) on the 4th of October. This was similarly followed by a CTD and MSS transect of 5 stations over approximately 24 hours from 4 to 5 October.

The CTD measurements were made with a Seabird Electronic SBE 911Plus model with a sampling rate of 24Hz. In contrast, the ScanFish is a towed undulating vehicle, which collects profile data vertically through the water column over time. During the survey the ScanFish was also equipped with a SeaBird CTD SBE911+ probe. Additionally oxygen, fluorescence and backscattering sensors were mounted on the device. The SeaBird CTD SBE911+ has an accuracy of 0.001 K and 0.0003 $\mathrm{S{\cdot}m^{-1}}$ [SeaBird Electronics, 2013] and calibrations of our instruments following the RRS Discovery cruise showed that our residual errors after calibration was 0.002 K (temperature), 0.0061 $\mathrm{S{\cdot}m^{-1}}$ (conductivity) and -0.046 dBar (pressure).

The microstructure-turbulence profiler MSS 90-S, which is an instrument used for simultaneous microstructure and precision measurements of physical parameters in marine waters,

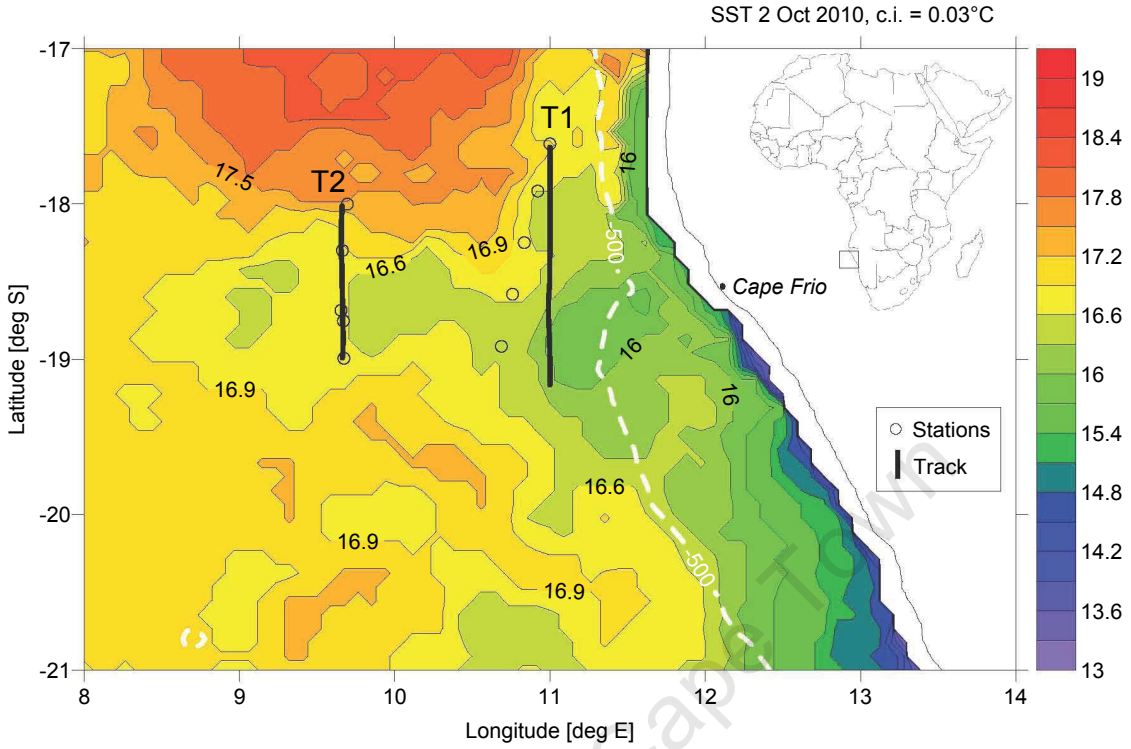

Fig. 2.6: Processed optimum interpolated Sea Surface Temperature (°C) image for 2 October 2010 from TMI and AMSR-E (NOAA) with a 0.25° longitude by 0.25° latitude grid resolution and an accuracy ranging between 0.2-1.0°C. The upwelling filament is evident between 18 and 19.5° South, extending from the coast of Namibia to 8.5° East. Transects (T1 and T2) surveyed with an undulating CTD (Scanfish) as well as the station locations across the filament are shown. The 500m depth contour is also indicated.

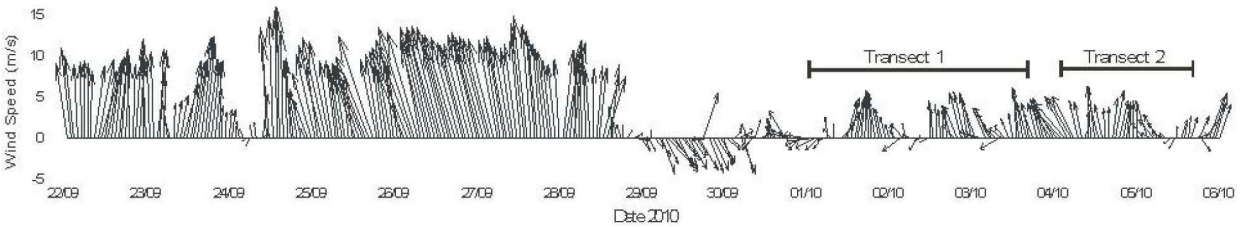

Fig. 2.7: Hourly averaged winds ($m \cdot s^{-1}$), taken aboard RRS Discovery, across the northern Benguela region between 22 September and 6 October 2010. Sampling intervals of transects 1 and 2 are marked.

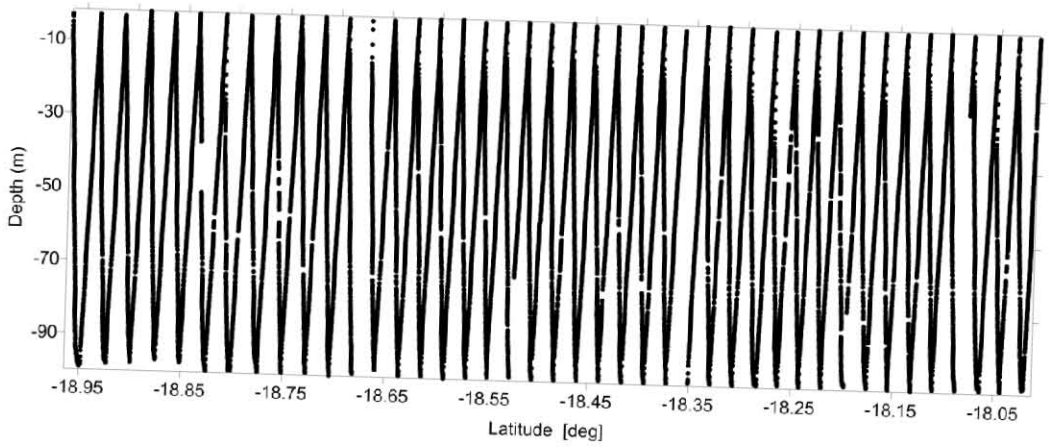

Fig. 2.8: Scanfish track through the top 100 m of the water column showing the undulation of the CTD instrument and the high resolution of measurements.

was equipped with two velocity microstructure shear sensors (for turbulence measurements), a microstructure temperature sensor, standard CTD sensors for precision measurements, an oxygen sensor, a turbidity sensor, and a vibration control sensor. The sampling rate for all sensors was 1024 samples per second. At each station a set of 4 subsequent profiles were gathered. The profiler was balanced with negative buoyancy, which gave it a sinking velocity of approximately 0.6 $m \cdot s^{-1}$. The dissipation rate of turbulent kinetic energy was calculated by fitting the shear spectrum to the theoretical Nasmyth spectrum in a variable wave number range from 2 to maximum 30 cycles per meter (cpm). The low wave number cut off at 2 cpm is to eliminate contributions from low frequent tumbling motions of the profiler.

Two VMADCPs (75 kHz and 150 kHz) from RDInstruments were mounted on the ships hull facing downwards. The output data from the ADCP was merged online with corresponding navigation data from the GPS output and additional heading information was provided by a gyro-compass. Post-processing of the VMADCP data was carried out using the Matlab® ADCP toolbox of IOW (Mohrholz, unpublished). The final profiles are 300 s averages of the single ping profiles.

As a supplement to station CTD data a few expendable bathythermographs (XBTs) were used to gather temperature data along transect 1. XBTs measure temperature using a thermistor contained within an expendable weighted casing. The depth is determined by the estimated rate with which a casing sinks and the time lapsed between the recorded values.

Calculating Ekman Transport

Ekman transport (Q) can be calculated in terms of wind speed at the 10 m level and the associated windstress (τ) using the following equations:

$$\tau = \rho\, C_D\, {U_{10}}^2 \tag{2.2}$$

and

$$Q = \frac{\tau}{f} \tag{2.3}$$

and

$$f = 2\Omega \sin(\theta) \tag{2.4}$$

Thus, mass transport = air density * drag coeff * |U| u in x direction or air density *drag coeff * |U| v in y direction where U_{10} is the wind speed at 10 metres above the ocean surface. Air density (ρ) with a value of 1.3 kg·m^{-3}, C_D is a dimensionless drag coefficient with value $1.25{\cdot}10^{-3}$, calculated from the wind speed at 10 m height after [Large and Pond, 1981]. f is the Coriolis parameter at latitude Ω. Q is thus the wind-generated mass transport per unit width integrated over the depth of the Ekman layer, with dimensions m^3·s^{-1}m^{-1}. ASCAT wind data was therefore used to calculate the Ekman transport across the region 5 to 15°E and 17 to 23°S.

2.4 Data description

2.4.1 SST satellite data

SST satellite NOAA-OI-SST-V2 data (0.25° resolution) provided by the NOAA/OAR/ESRL PSD, Boulder, Colorado, USA, from their Web site at http://www.esrl.noaa.gov/psd/ is used for model validation. The Sea Surface Temperature data is a blended analysis of daily SSTs, from a number of satellite platforms as well as in situ data from buoys and ships. The data are composites of monthly, seasonal, daily or hourly gridded variables. For more details on the analyses see [Reynolds et al., 2007].

2.4.2 World Ocean Atlas 2009 (WOA09)

Objectively analysed temperature and salinity from WOA09 [Conkright et al., 2002] are used to compare thermohaline properties both along the surface as well as vertical sections. Despite the low resolution (1° spatial resolution) of the WOA09 data, it provides a useful

tool for model validation due to its consistent global thermohaline climatologies. WOA data are typically interpolated into 33 standardised vertical intervals from 0-5500 m depth and in terms of spatial resolution it offers annual, seasonal and monthly time-scales.

2.4.3 CTD cruise data from BENEFIT programme

Hydrographic cruise data collected as part of the BENEFIT (Benguela Fisheries and Environmental Instructions and Training) programme [Boyd et al., 2006] has been used in this study.

2.4.4 Software tools

Primarily three software tools were used for the analysis and presentation of the results in this project:

Ferret. Seattle, USA. NOAA Pacific Marine Environmental Laboratory.

Surfer version 7. Golden, Colorado: Golden Software, Inc., 2012

MATLAB version 7.11.0. Natick, Massachusetts: The MathWorks Inc., 2010

Chapter 3

Validation of ecosystem model adjusted for the Benguela: observing regional features

In this section measured data from various sources, including remote sensing, field, and WOA (World Ocean Atlas) data will be compared with the output from the MOM-4 ecosystem model described in chapter 2 in order to establish the validity of using the output for the analysis in this project.

3.1 Surface patterns: Temperature and salinity

Readily available Sea Surface Temperature (SST) remote sensing data allows a regional comparison with model output. Figure 3.1(b) shows the 9 km resolution annual mean (mean for years 2000-2008 in order to compare with model output which spans this period) optimally interpolated (OI) SSTs, while Figure 3.1(a) shows the annual mean SST output from the model simulation and Figure 3.1(c) shows the difference between the two (i.e. model-satellite SST). For comparison purposes, the higher resolution satellite data were degraded slightly to approximate the model output.

At a first glance, the model is sufficiently able to simulate the cool coastal region as well as the warmer offshore region (Figure 3.1(a) and (b)). Additionally, the front separating these two zones is also clearly depicted in the model results (Figure 3.1(a)). Isotherm orientation between the two data sets was however slightly different. The strong Lüderitz upwelling cell (26°S) is evident in both satellite and model representations, with a slightly stronger (negative) annual signal from the model output. Similarly, the Angola-Benguela Frontal Zone (ABFZ) is accurately resolved in the model, but again it seems to overestimate the annual

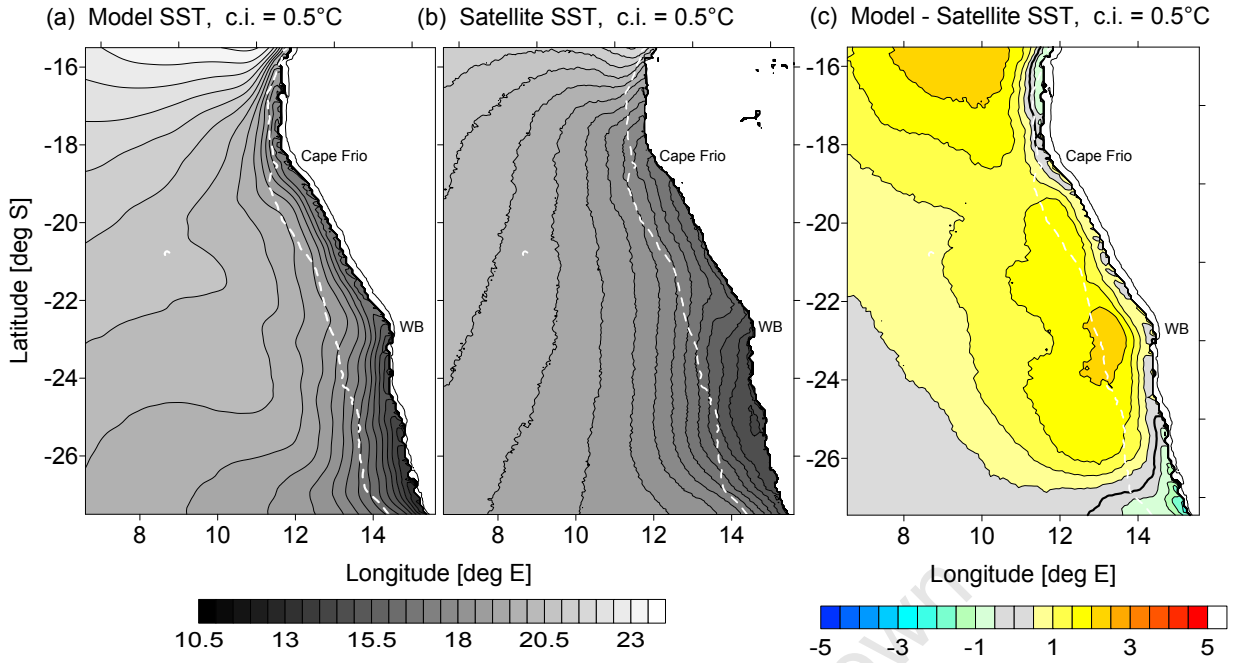

Fig. 3.1: Annual mean SSTs from model (a) and satellite (b) in the northern Benguela. The difference between the model and satellite SSTs is shown in (c). The broken white line indicates the 500 m isobath. Positive (negative) values indicate an over-estimation (under-estimation) of SSTs by the model.

mean temperature. Thus, despite the relatively good representation of the regional SST pattern by the model, a strong positive SST bias exists throughout the northern Benguela region as can be seen in Figure 3.1(c).

In Figure 3.2 the annual mean SST bias is compared for a region close to the coast (50 km coastal strip) and a region further offshore (250-350 km). The coastal region showed a weak positive bias between 18-25°S, and negative biases at the northern and southern borders. In particular the model seems to underestimate upwelling at the Lüderitz cell by as much as 2°C. In the region 250-350 km offshore the model tends to overestimate SSTs by up to 2°C throughout the region north of 27°S.

The SST model bias was subsequently computed for the summer (DJF) and winter (JJA) seasons respectively. This revealed that while in summer (DJF) the model slightly overestimates SSTs in the coastal region, particularly around Walvis Bay (20-26°S), this bias covers a much smaller region than what is observed for winter (JJA). During winter the model seems to substantially overestimate SSTs in the ABFZ (>3°C), while it also overestimates SSTs across the entire region except near the Lüderitz upwelling cell, where it underestimates SSTs slightly. A stronger SST bias is thus observed during winter. Due to the difficulties models face in simulating conditions at the surface boundary layer SST comparisons may not be the most stringent test of model performance, instead sub-surface conditions will subsequently be compared.

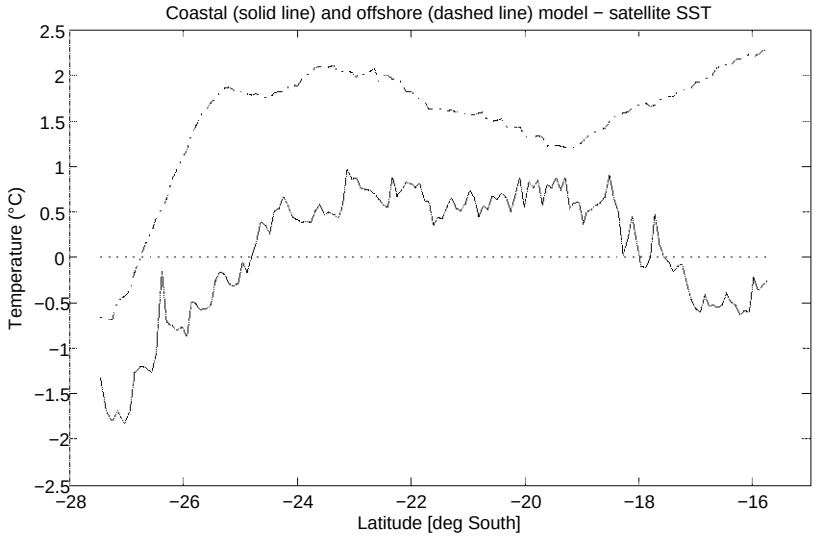

Fig. 3.2: Annual mean SST model bias (i.e. model - satellite) averaged in a 50 km coastal strip (solid line) and offshore, between 250-350 km (dashed line) in the northern Benguela. Positive (negative) values indicate an over-estimation (under-estimation) of SSTs by the model.

Despite a much lower resolution (1° spatial resolution), the annual mean Sea Surface Salinities (SSSs) from the objectively analyzed climatological fields of the World Ocean Atlas (WOA) allows a comparison with model-derived SSSs (see Figure 3.4). The large-scale regional patterns between the respective data sets are fairly similar. Similarly to the SSTs, lower SSSs are observed in the coastal regions, and in particular the southern coastal regions between Walvis Bay (23°S) and 28°S. Again the ABFZ is represented reasonably well in the model data, whereas the WOA struggles in this regard due to its low spatial resolution.

3.2 Vertical structures: temperature, salinity, oxygen and density

Narrow coastal longitudinal sections along 23°S, comparing the annual mean temperature and salinity profiles between the WOA climatological mean and model-derived data, can be seen in Figure 3.5. The highlighted 16°C isotherm has been taken to approximate the thermocline as it is centered within a region of tightly spaced isotherms in the model-derived profile (b). The model simulation fairly accurately represents the measured temperature data in terms of pattern, showing clearly the coastal upwelling as depicted by the upward sloping isotherms in the inshore region. At greater depths, there is evidence in both the temperature and salinity profiles from the model output for the presence of a poleward undercurrent, with downward sloping isotherms between 200 and 1000 m depths (see Figure 3.5 (b) and (d)). Due to the low coastal resolution of WOA data, this undercurrent signal is absent from these profiles (see Figure 3.5(a) and (c)). Despite the model overestimating the surface

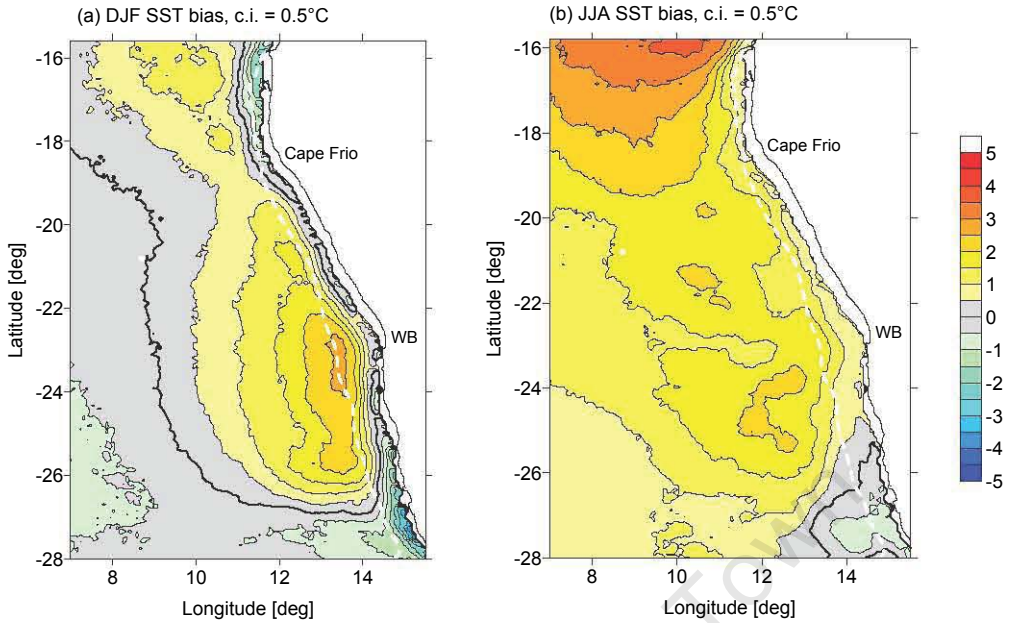

Fig. 3.3: Seasonal SST model bias (i.e. model - satellite) in the northern Benguela for (a) summer (DJF) and (b) winter (JJA). Positive (negative) values indicate an over-estimation (under-estimation) of SSTs by the model.The broken white line indicates the 500 m isobath.

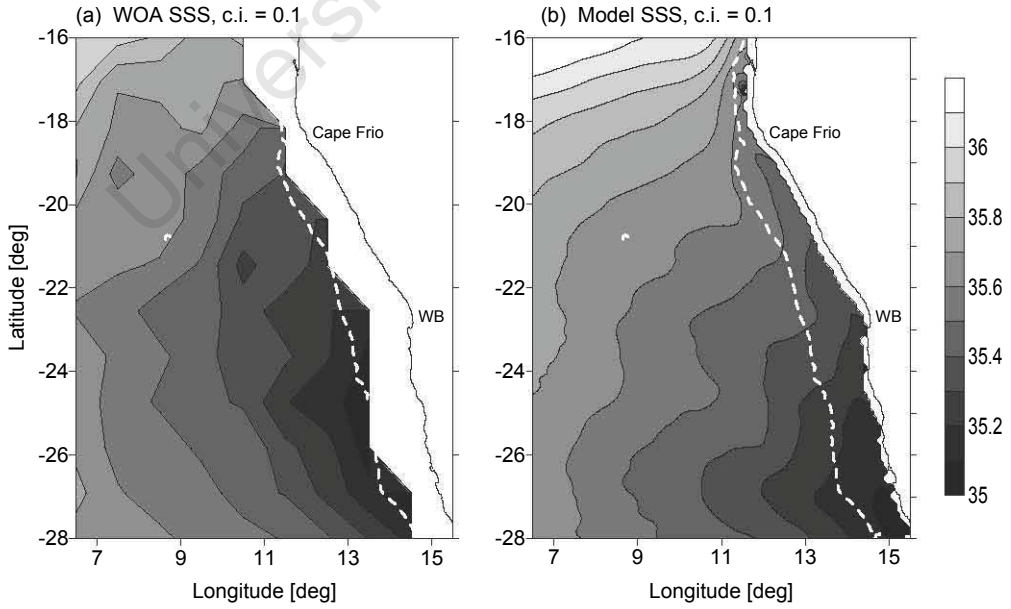

Fig. 3.4: Annual mean WOA (a) in situ and model (b) derived SSSs in the northern Benguela. The broken white line indicates the 500 m isobath.

temperatures by 1-2°C, below 300 m depth there is a better correspondence between the data sets.

In the salinity structure both the high salinity core at the shelf edge as well as a salinity minimum between 700 and 1000 m depth, which has previously been mentioned for the northern Benguela [Veitch, 2009], are present (see Figure 3.5 (c) and (d)). While the model accurately depicts the magnitude of this salinity minimum (34.55 psu), it underestimates its vertical extent if compared with what is observed in the WOA data.

The model also does a reasonable job in simulating the annual mean dissolved oxygen profile along the 23°S longitudinal section seen in Figure 3.6, with a steady decrease in dissolved oxygen with depth and with distance from the coast. This rapid decrease in oxygen below the thermocline has been largely attributed to the aerobic mineralisation of sinking organic material, e.g. [Brüchert et al., 2003].

Differences in temperature, salinity and density between model-derived and WOA values can be seen in Figure 3.7. In order to allow a more objective comparison of the model biases, the data were normalized with respect to the corresponding range of temperature, salinity or density. It appears that regions where large positive temperature biases are observed coincide with regions of large positive salinity biases. Despite the temperature and salinity biases being fairly large (>10% and >15% of the ranges), the density bias is less than 5% of the range of densities. This results in the density being closer to the measured data (WOA data) than what was observed for either temperature or salinity. Figure 3.7 shows that both temperature and salinity are over-estimated by the model in the top 200m of the water column, shown by the large positive biases for both summer (DJF) and winter (JJA) periods. Below 200 m depth the model seems to under-estimate temperature and salinity, for DJF up to 1000 m depth and for JJA up to 700 m depth.

Due to the low coastal resolution from the WOA data set, more than 400 data points from in situ CTD data taken in 2004 as part of the BENEFIT [Boyd et al., 2006] project were compared with model results in order to quantify model accuracy and deviation. Figure 3.8 presents vertical depth profiles for temperature and salinity up to 1000m depth in the northern Benguela region. The expected variability exists in the upper 100 meters of both temperature and salinity profiles, and it is in this region, comprising the thermocline, where model and measured results seem to differ most. Below 200 m depth, the mean temperature profiles from the two sources overlap and variability is low. Contrastingly, even at greater depths the model consistently overestimates the salinity by about 0.2 psu, despite the fairly similar shape of the curves. When the relationship between the measured and model values is examined statistically, temperature, salinity and oxygen all showed that there is in fact a significant correlation ($p < 0.001$). These statistics are summarized in Figure 3.9 and Table 3.1. Temperature and salinity both showed a strong positive correlation between the two data sets (r being 0.98 and 0.97 respectively), while for oxygen the correlation was

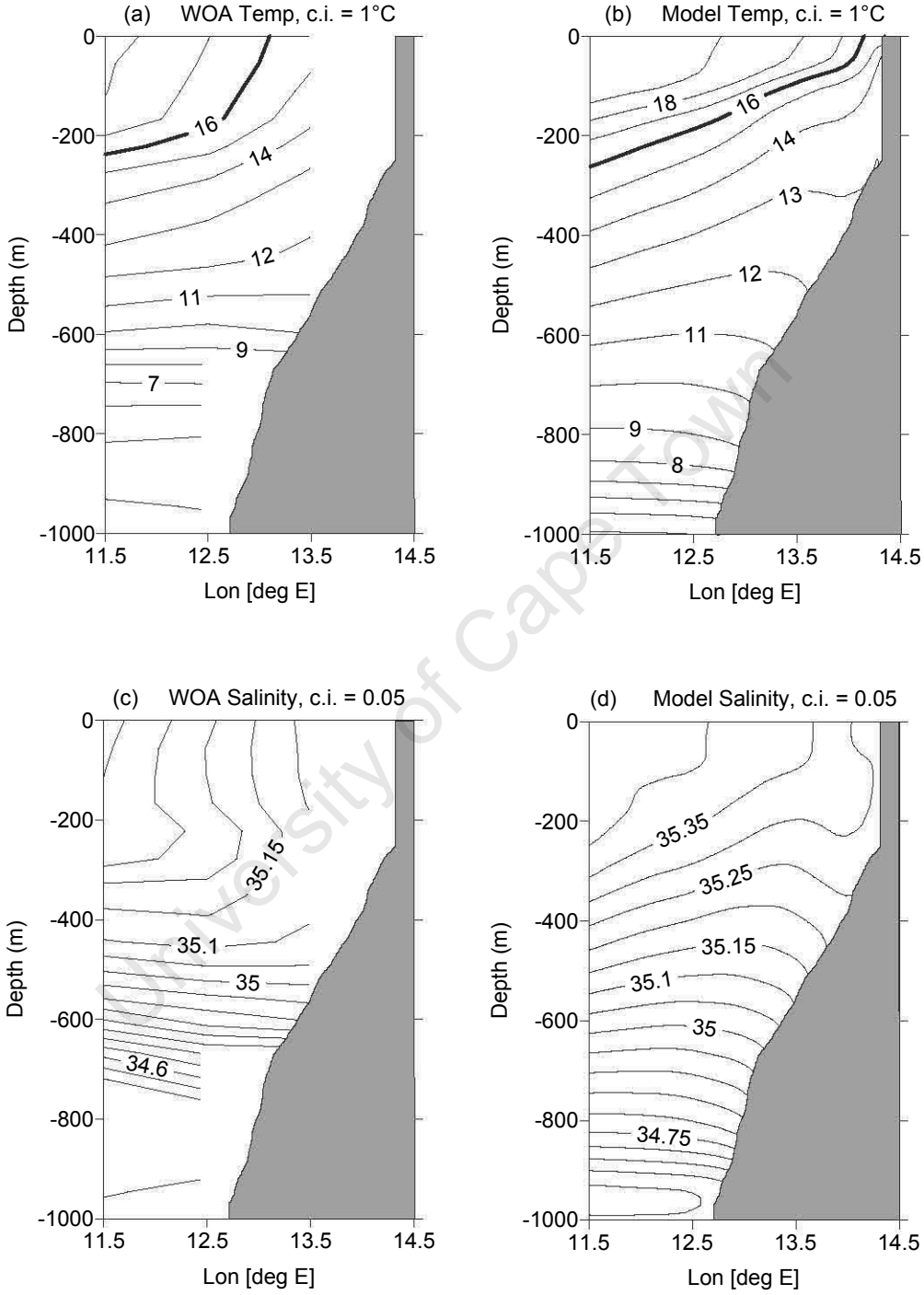

Fig. 3.5: Annual mean temperature (top) and salinity (bottom) comparison between WOA (left) and model-derived (right) data along 23°S.

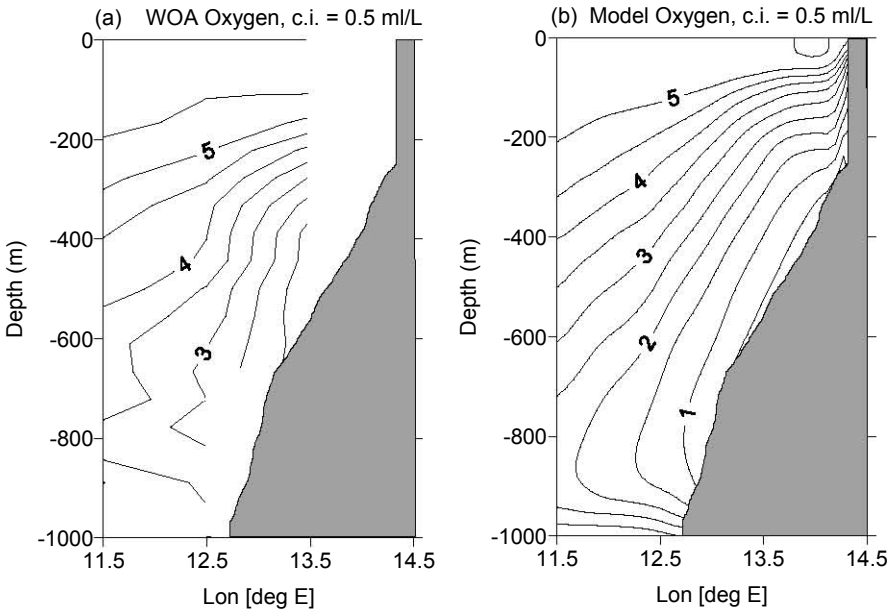

Fig. 3.6: Annual mean oxygen comparison between WOA (a) and model-derived (b) data along 23°S .

slightly weaker (r = 0.86). The level of accuracy for measurements should however also be considered in relation to the correlation statistics, as the error in oxygen measurements is normally considerably higher than for temperature and salinity. The root mean square error for each relationship was also calculated and is presented in Table 3.1. The typical error for temperature and salinity would thus be 0.8°C and 0.1 psu respectively. The root mean square error for oxygen was found to be relatively higher at 1.21 ml/l.

Tab. 3.1: Correlation statistics for model vs measured data

Variable	R	R^2	p-value	RMSE
temperature	0.9763	0.9532	<0.001	0.8281
salinity	0.9686	0.9382	<0.001	0.1140
oxygen	0.8627	0.7443	<0.001	1.2164

3.3 General regional features

Oxygen profiles (Figure 3.10) through the mixed layer and below suggest that the model is able to accurately represent the oxygen gradient expected, with inshore areas being oxygen poor and then an increase of oxygen is observed towards the shelf edge [Brüchert et al., 2006]. There is also a meridional oxygen gradient, which has previously been linked to a southward weakening of the PUC [Mohrholz et al., 2008]. Additionally, the decrease in oxygen through

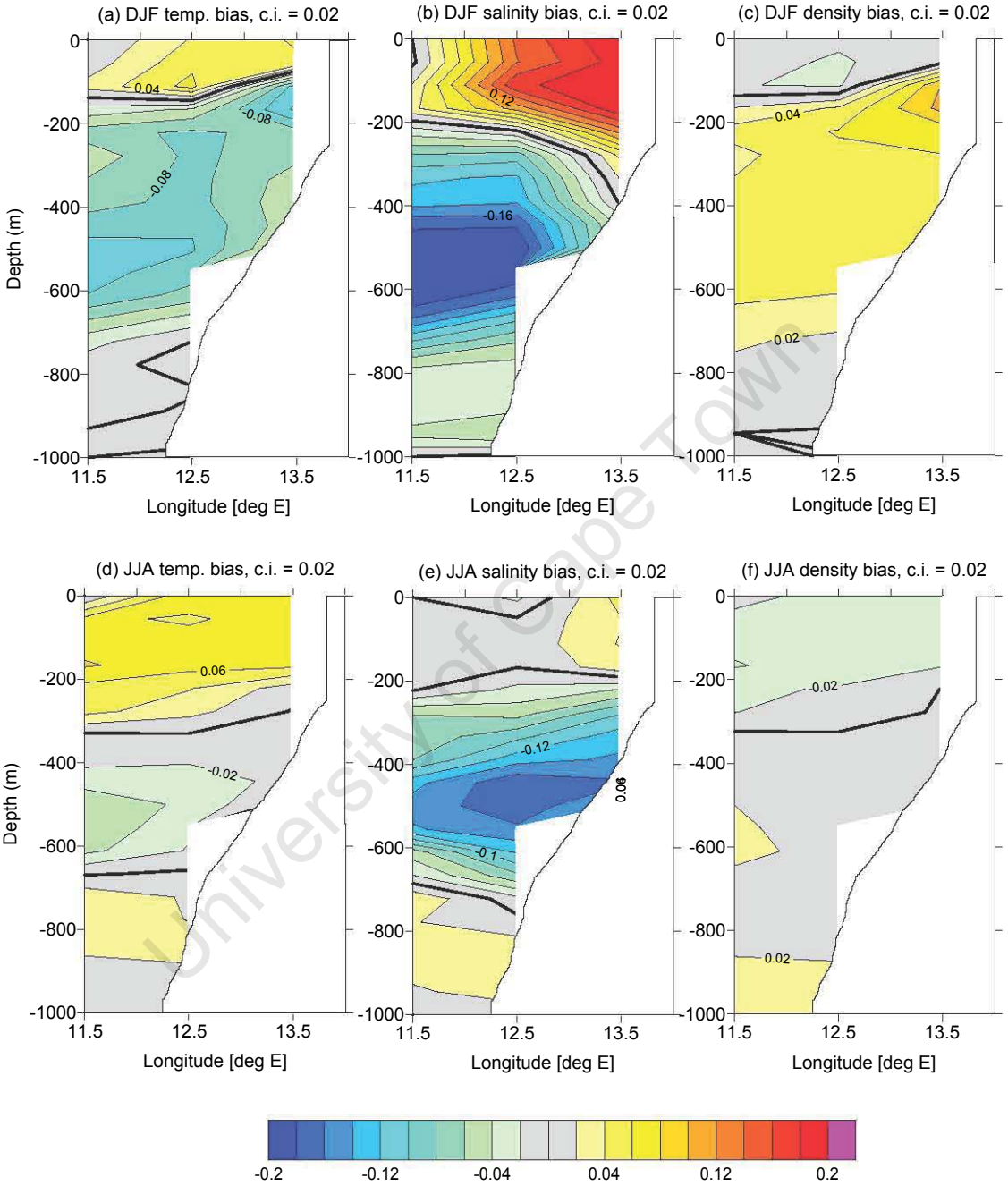

Fig. 3.7: Normalized temperature, salinity and density bias for summer (DJF) (above) and winter (JJA) (below) along 23°S. Positive (negative) values correspond to regions where the model overestimates (underestimates) WOA data.

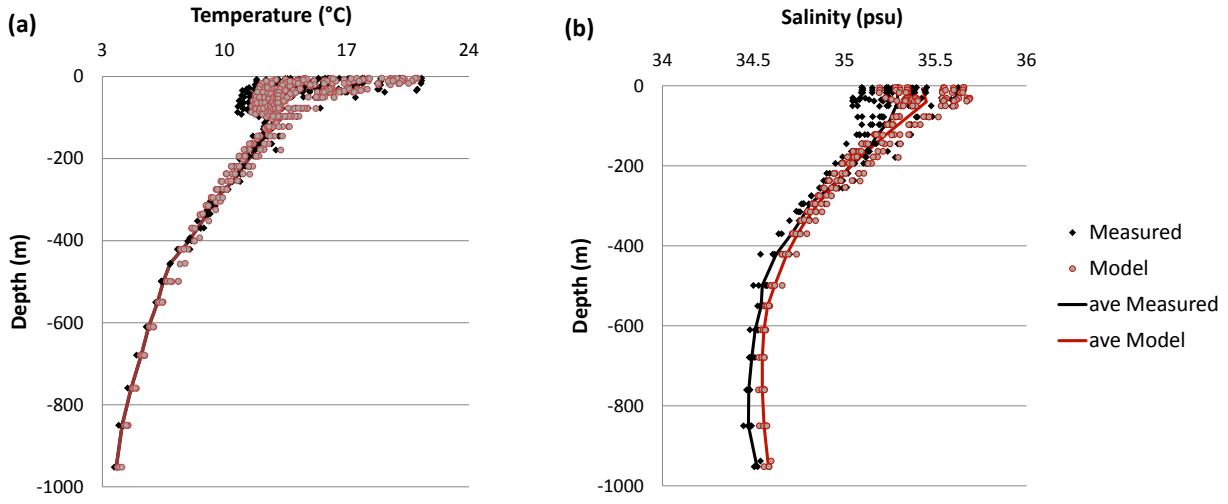

Fig. 3.8: Vertical depth profiles comparing temperature (a) and salinity (b) from in-situ CTD measurements (red) with model-derived (black) values through the water column.

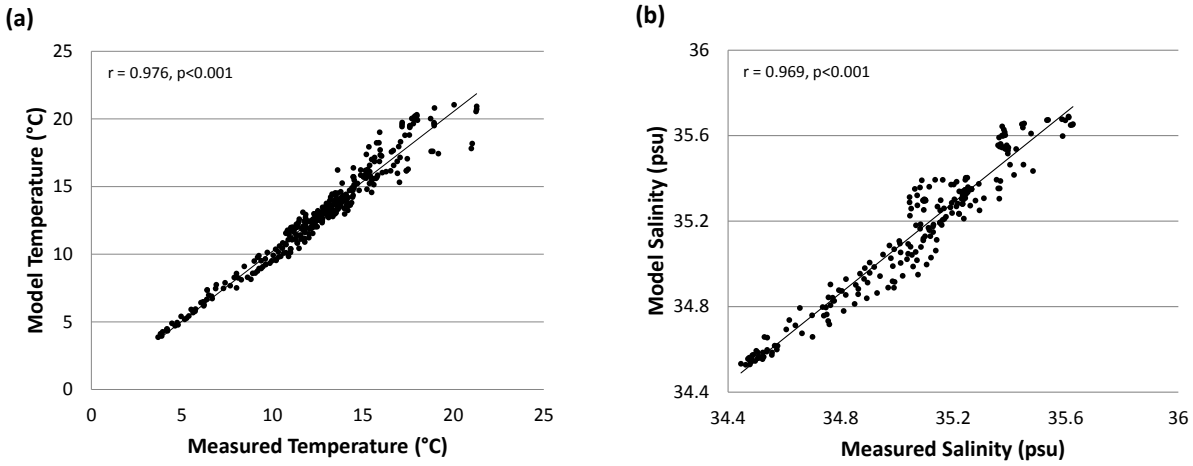

Fig. 3.9: Analyzing the relationship between in situ CTD measurements along the coast in the northern Benguela and the corresponding model-derived temperature (a) and salinity (b) values.

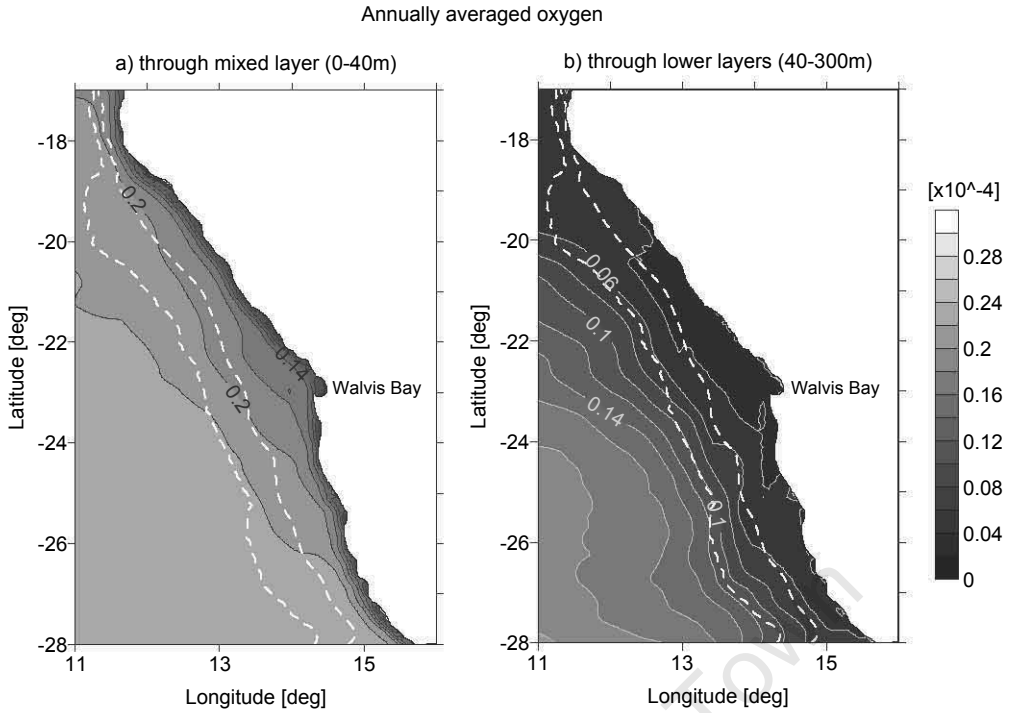

Fig. 3.10: Annual oxygen (mol·kg^{-1}) distribution across the shelf off Namibia as presented by the model: a) averaged through the mixed layer (0-40 m) and b) averaged through 40-300 m. Values represent 8 year (2000-2008) climatology. The broken white lines indicate the 300 m and 500 m isobaths respectively.

the water column is evident. Higher oxygen values were observed for winter (not shown), most likely signaling higher oxygen uptake during this period from the atmosphere for the surface layers, while in the deeper layers the expected ventilation of the shelf by oxygen rich ESACW could explain the higher oxygen content [Monteiro and van der Plas, 2006; Mohrholz et al., 2008].

Validation for current data between the model and measured data (Figure 3.11) proved difficult due to the differences in spatial and temporal resolution of the data sets. For a qualitative comparison model data is compiled and compared with published data from [Mohrholz et al., 2008]. Initial observations suggest a possible overestimation of northward flow across the time series by the model, and an underestimation of the poleward transport. The model is able to appropriately represent the seasonal variation across this time series. Observing an average (over 8 model years) annual representation of meridional flow shows that the model (Figure 3.12), depicts two key features, the coastal jet as well as the countercurrent [Fennel, 1988; Fennel et al., 2012b] or poleward current laying further west along the shelf edge. Similarly the zonal currents showed the expected annually averaged onshore compensatory flow one would expect in a wind driven upwelling system such as the Benguela. Further transport validation and more detailed results are presented in section 4.

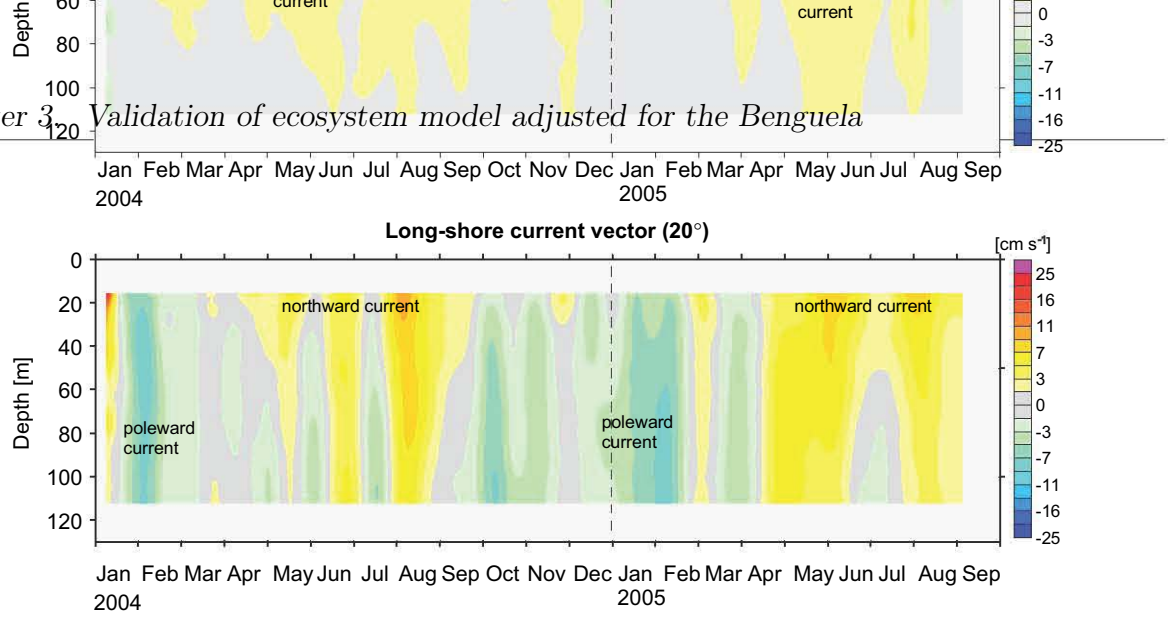

10. Time series of current components at the shelf off Walvis Bay. The velocities are projected to the cross-shelf (upper panel) and alongshore (lower el) directions. Low pass filter cut-off frequency: 30 d^{-1}.

ected at a period of 4–9 days and 14–17 days. These dings conform to the results of Lass and Mohrholz 05).

The data were low pass filtered with a Butterworth filter 30 d^{-1} cut-off frequency to remove the short-term cesses from the current time series. Additionally, the rent vectors were projected to its cross-shelf (110°) and gshore (20°) components. The time series showed a clear sonal signal in both the cross-shelf and longshore mponents (Fig. 10). The cross-shelf circulation is racterised by the wind driven Ekman regime. The shore transport in the upper 20–30 m surface layer was mpensated for by a subsurface onshore directed flow. hough the upper 16 m of the Ekman surface layer were sufficiently covered, the current measurements indi- ed the presence of a year round Ekman offshore nsport in the surface layer that peaked between April August with a mean offshore flow of 3 cm s^{-1} at 16 m th. In the longshore direction a poleward current is st pronounced from mid-January to mid-March and ers nearly the entire water column below the surface ked layer with a mean southward current speed of about cm s^{-1}. A second period with a moderate poleward flow s observed in October/November 2004. From April to tember the longshore current is mostly northwards or sists of an alternating regime of weak poleward and atorward flow.

The time series was divided into three half-year periods order to elucidate the seasonal characteristics of the rent field: winter 2004 (April–September), summer ctober 2004–March 2005) and winter 2005 (April–Sep- ber). Mean current profiles were calculated for each of these periods and projected to the cross-shelf and long- shore direction of 110° and 20°, respectively (Fig. 11). The depth of the wind-driven Ekman layer was 30–35 m in winter and only 20 m in summer. The enhanced Ekman offshore transport during winter is closely linked with the stronger trade winds at this time of the year. Most of the variability observed in the cross-shelf component was associated with the depth of the onshore compensation flow. In winter, it covered the entire water column below the surface mixed layer—the maximum onshore flow (1–1.5 cm s^{-1}) was found between 50 and 70 m. Bottom velocities were approximately 0.5 cm s^{-1}. In summer, the maximum onshore flow was shallower at 30–35 m and also weaker (1 cm s^{-1}). Below 80–90 m depth it vanished completely.

The mean longshore current component was different in all three seasons. During the 2004 winter period the surface flow was northwards with maximum velocities of around 3.5 cm s^{-1}, which decreased to 0.0 cm s^{-1} at 90 m depth. The situation during the 2005 winter was similar but with a northward offset of 2 cm s^{-1} throughout the water column. In summer, the mean longshore flow was generally poleward. It increased from 1.5 cm s^{-1} at 20 m depth to 3 cm s^{-1} at 50 m depth and remained at this level down to 10 m above the bottom. The maximum poleward flow occurred at 100 m (3.5 cm s^{-1}).

Progressive vector diagrams of the current time series provide the meridional and zonal displacements (Fig. 12). The displacement in the surface layer (16 m depth) was mainly meridional and amounted to ~100 km poleward in summer and ~600 km equatorward in winter, with a total northward displacement (2000–2008) of ~500 km per annum. Ekman

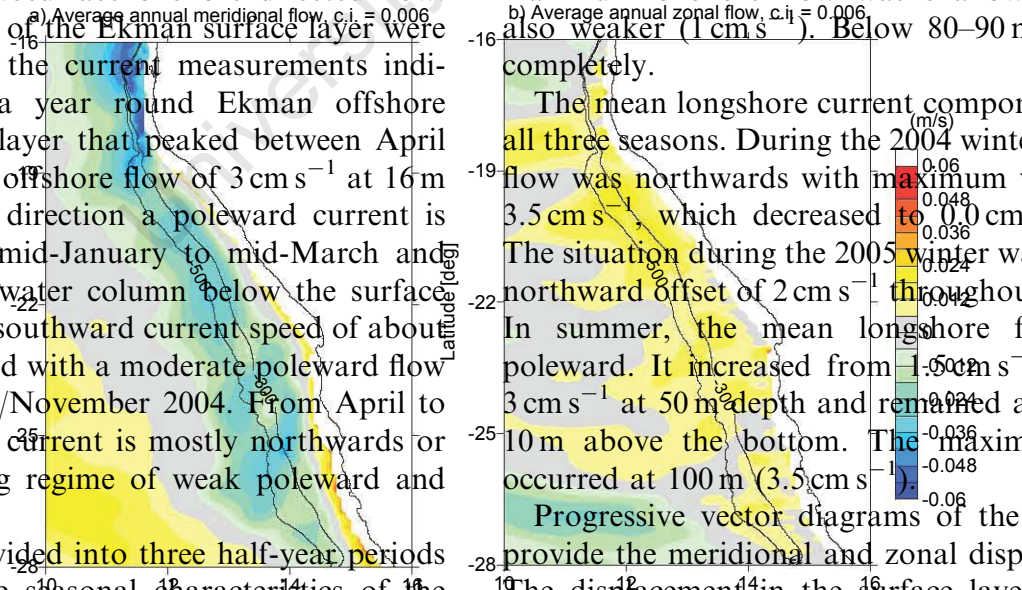

Fig. 3.12. Annual meridional and zonal flow off Namibia averaged through the top 300 m of the water column as presented by the model. Values represent 8 year (2000–2008) climatology. The 300 m and 500 m isobaths are presented.

3.4 Section summary

Overall the MOM-4 adjusted ecosystem model is able to simulate regional patterns and features across the northern Benguela region sufficiently well, and therefore provides a unique tool for evaluating both large scale circulation as well as coastal processes. This is invaluable in the context of the critical role the regional circulation plays in the modification of both the shelf conditions as well as water mass properties. The ecological dynamics of the Benguela are in fact known to be largely influenced by the water mass fluxes entering the system through its borders. An accurate simulation of the main processes driving these fluxes is therefore crucial. The MOM-4 model is able to simulate both the poleward flow of the PUC [Nelson, 1989; Shannon, 1995; Monteiro and van der Plas, 2006; Mohrholz et al., 2008; Monteiro et al., 2008], as well as the equatorward transport of the Benguela coastal current [Shannon and Nelson, 1996; Moroshkin et al., 1970; Wedepohl et al., 2000]. Additionally, the seasonal variation associated with these is also resolved. Furthermore, the main upwelling cells of the northern Benguela, i.e. Lüderitz, Walvis Bay, Namibia, and Cape Frio, [Bakun and Nelson, 1991; Shannon and Nelson, 1996; Hardman-Mountford et al., 2003] are also resolved.

Despite the present chapter having been dedicated to validation of the MOM-4 model, it was merely done within the context of the rest of this document and the feasibility of making use of this data set for the analysis of transport fluxes across the northern Benguela. There is thus not a focus here on improving model performance within the time constraints of the present study. Rather the discrepancies observed here should be adressed by the Theoretical Oceanography and Numeric Modelling working group at the Institute of Baltic Sea Research in Warnemünde. Another note of caution is that our analysis has focused primarily on comparing annual and seasonal means and work therefore remains to be done on the evaluation of model performance with reference to dynamical behavior.

However, possible reasons for the overestimation of the temperature by the MOM-4 model are presented based on the analysis done: 1) One consideration was that it could likely be related to so called ocean biology-induced heating. In short this concerns the fact that total phytoplankton biomass and its vertical distribution can influence the way in which incident solar radiation is absorbed in the mixed layer [Zhang and Busalacchi, 2009]. For example with stronger biological activity, the penetration of the incoming solar irradiance (ISI) is reduced and more heat is trapped in the mixed layer. Alternatively, as biological activity decreases ISI penetrates deeper, reducing mixed layer heating, and heating the subsurface layers [Chavez et al., 1998, 1999; Strutton and Chavez, 2004]. The differential heating in the vertical which results can lead to changes in the oceanic density field, stability, vertical mixing and even mixed layer depth [Zhang and Busalacchi, 2009]. Despite it being a less

likely cause of the warmer SST in our findings, without proper investigations this cannot be excluded as a cause. 2) Another possibility is that the nonlocal K-profile Parameterization (KPP) mixing scheme, used insufficiently represents the mixed layer and therefore the top layers of the water column are warmer in the model. The KPP scheme unifies treating a variety of unresolved processes involved in the vertical mixing [Large et al., 1994]. It has been shown by [Large et al., 1997] that the KPP scheme is able to realistically represent mixed layers and boundary layers both temporally and spatially. An attempt to substantiate whether the KPP scheme is misrepresenting the mixed layer for the Benguela region was unsuccessful as data from both WOA as well as measured CTD data showed no clear discrepancy in the mixed layer depth presented in the model. The differences in both spatial and temporal scales between the data sets do however make it difficult to simply dismiss this as a possible cause of the overetimation of SST. Particularly, since it has previously been shown that this effect could be observed in relation to the KPP scheme employed in MOM models. For example, [Junker, 2011] compared observed vertical profiles of temperature and salinity from the Baltic Sea in the winter 2006/2007 with the results of a numerical model run (MOM3, kpp mixing scheme). In this study he found that the model underestimates the mixed layer depth in all of the analysed profiles by up to 30 m. 3) A third possible cause could be the low resolution (1.875° spatial and 6 hourly) of the NCEP (temperature) data used to force the model, particularly near the Namibian coast. Wrong heat fluxes computed from this lower resolution data would result in a deviation of the surface layer temperatures similar to what is observed here. Forcing the model with newly available higher resolution NCEP data from the CISLs Research Data Archive [Saha et al., 2010] is therefore recommended.

It is thus important that attention should be paid and more research be done on the above-mentioned suggestions for the future simulations of the MOM-4 ecosystem model adjusted for the Benguela. In the current study, the model deviations will be accepted as reasonable, as is the model performance in accurately similating the regional features and their seasonal variability, for the purposes of the presented analyses.

Chapter 4

Longshore and cross-shore advection associated with the northern Benguela shelf

The main focus of this section is to analyze and quantify regional transport fluxes along the 300 m deep shelf in the northern Benguela. The working hypothesis is that the ventilation of the Namibian shelf is driven primarily by the longshore advection, and only modified by the cross-shore advection. This hypothesis will be tested by making use of data from the regional MOM-4 ecosystem model described in chapter 2.1. An important note to aid interpretation and understanding of the results in this chapter is that due to the alignment of the coast, there is a rotation of 30° from north to south and therefore what is depicted here as zonal flow do not necessarily reflect the on/off-shore flow properly. These terms will however be used interchangeably with u- and v- components.

4.1 Seasonal and geographic variability in longshore and cross-shore current flow in the northern Benguela

4.1.1 Regional transport

For a regional perspective on transport across the Benguela upwelling system, through both the mixed layer (defined here as approximately the upper 40 m of the water column) as well as the deeper compensatory layers (defined here as 40-300 m) across the shelf, monthly ocean climatology (2000-2008) flow vectors were compiled for four seasons DJF, MAM, JJA, and

SON. The investigated area was limited to 16-28°S, 10.5-15.5°E. Through the mixed layer (0-40 m) a number of interesting features can be observed (see Figure 4.1). Firstly, at the Lüderitz upwelling cell (∼27°S) a strong, persistent offshore flow dominates throughout all four seasons. Persistent offshore flow is also observed elsewhere in the region, but is not of the same magnitude as the flow west of Lüderitz. In addition, a strong southward flow is observed in the northern part of the system year round. However, the southward extent of this flow and the latitude where it turns westward and offshore varies seasonally. During winter (JJA) the flow bends offshore north of 18°S, while in spring and early summer (SON) it does so further south at 20°S. Furthermore, during both JJA and SON a strong equatorward jet can be observed close to the coast of Namibia. This coastal jet weakens during summer (DJF) and autumn (MAM).

When the flow is averaged over the deeper compensatory layers (40-300 m), as seen in Figure 4.2, a broad region of south-eastward transport is observed along the coast during spring (SON) and summer (DJF). In contrast, during winter (JJA) this southward signal vanishes and in close proximity to the coast a thin but relatively strong equatorward jet is observed. The eastward flow related to the Lüderitz upwelling cell can be observed during summer (DJF) even through the deeper layers (40-300 m). This is consistent with the past results which showed a spring/summer maximum in upwelling favourable winds between 25-30°S [Boyd, 1987].

4.1.2 Meridional and zonal current flow through the mixed layer and below

For a clearer perspective on the spatial and temporal variability in the longshore and cross-shore flow through the region, the meridional and zonal flows were separated for the same 4 seasonal periods and plotted relative to the 300 m depth contour line. Figure 4.4 shows the meridional flow below the mixed layer (40-300 m). The broad southward flowing undercurrent is the dominant feature in the region, supporting [Shannon and Nelson, 1996]'s suggestion that the net flow through the water column tends to be poleward. The undercurrent is much stronger ($>0.1\,\mathrm{m{\cdot}sec^{-1}}$) during spring (SON) and summer (DJF). Additionally, during summer it is located closer inshore and its core is observed primarily along the shelf. During spring (SON) the undercurrent is at its strongest but shifted slightly to the west, with its core now located directly along the 300 m depth shelf-break. During winter (JJA) the much weaker undercurrent migrates even further offshore, with the core lying completely off the shelf. Additionally, during winter a relatively strong ($0.06\,\mathrm{m{\cdot}sec^{-1}}$) equatorward flow

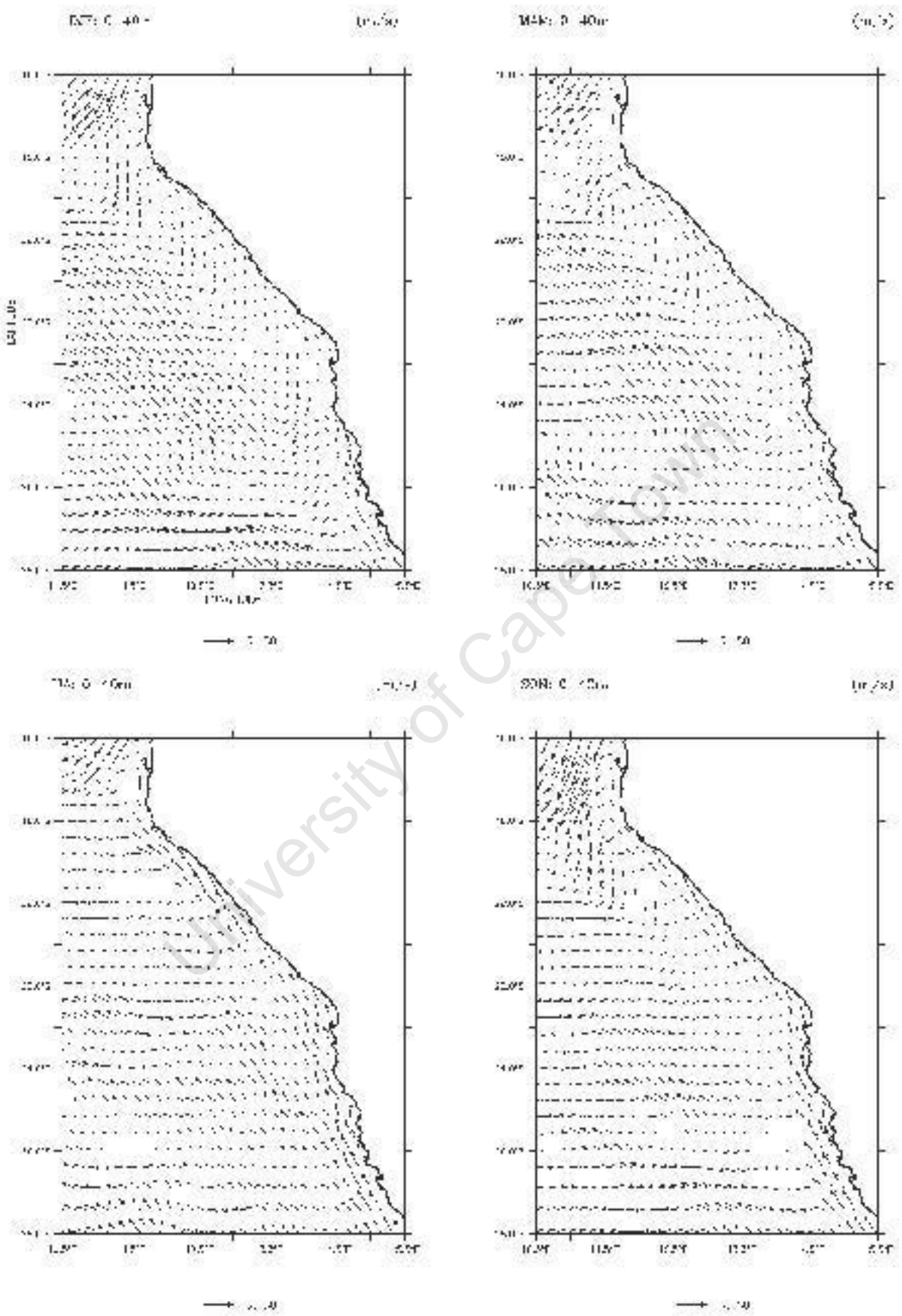

Fig. 4.1: Current vectors (m·sec^{-1}) (2000-2008 climatology) averaged through the mixed layer (0-40 m) in the northern Benguela for four seasons: a) summer (DJF), b) autumn (MAM), c) winter (JJA) and d) spring (SON), showing the seasonal and spatial variability in regional circulation.

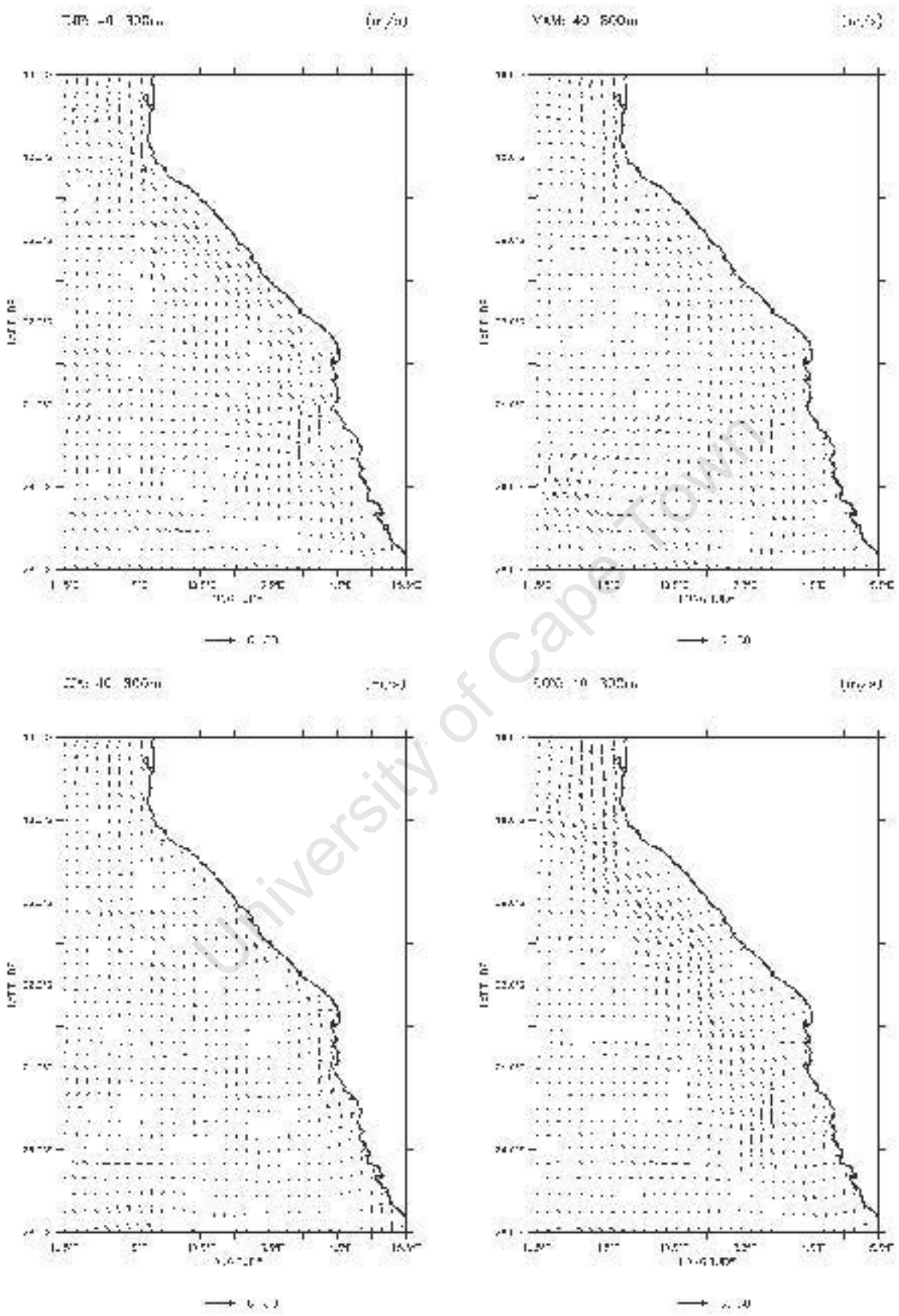

Fig. 4.2: Current vectors ($m \cdot sec^{-1}$) (2000-2008 climatology) averaged through 40-300 m depths in the northern Benguela for four seasons: a) summer (DJF), b) autumn (MAM), c) winter (JJA) and d) spring (SON), showing the seasonal and spatial variability in regional circulation.

is observed subsurface next to the coast of Namibia. A similar northward coastal flow is also observed through the mixed layer (0-40 m) year round (see Figure 4.3). During winter (JJA) this coastal jet reaches its maximum strength and width, while the southward undercurrent weakens substantially and is only observed north of 18°S. In contrast, the northward coastal jet decreases in width during spring (SON), summer (DJF), and autumn (MAM), while the poleward undercurrent increases in strength as it moves on to the shelf, both through the mixed layer as well as the deeper layers.

The cross-shore flow variation is less distinct as can be seen in Figures 4.6 and 4.5. A steady offshore flow is observed through the mixed layer and throughout the region, with very strong ($>0.14\,\mathrm{m{\cdot}sec^{-1}}$) offshore flow off Lüderitz (27°S) and off Cape Frio (∼17°S), and to a lesser extend off Rocky Point (∼19°S) and Walvis Bay (23°S). This cross-shore transport is particularly strong during winter (JJA) and extends from the coast far offshore. These four zones of offshore flow correspond to the major upwelling cells off the west coast of Namibia, where upwelling filaments are also regularly observed [Van Foreest et al., 1984; Lutjeharms and Stockton, 1987; Kostianoy and Zatsepin, 1996]. At the prominent cells, like Lüderitz and Cape Frio, there is strong evidence for year round circulation across the shelf edge. Below the mixed layer (Figure 4.5) strong onshore flow across the shelf edge is observed during spring (SON), summer (DJF) and autumn (MAM). Both spatial and temporal variability is observed in this onshore transport, with the most persistent feature between 19-21°S and more seasonal features of onshore flow across the shelf edge during summer and spring. These patches of subsurface onshore flow are observed just south and north of Walvis Bay and also north of the Lüderitz upwelling cell. During winter (JJA) there is evidence for only sparse subsurface onshore flow across the shelf edge, particularly outside of the 19-22°S region.

Figure 4.7 presents the density integrated vertical velocity averaged through the water column from the surface to 300 m depth and shows the expected strong positive vertical motion close to the Namibian coast. Strong year round vertical motion is observed off Cape Frio (∼17°S) and Lüderitz (∼27°S). Whereas in winter (JJA) large regions along the shelf showed strong positive vertical motion, i.e. upwelling, during summer (DJF) upwelling is weaker and confined to the known upwelling cells, specifically the zone 26-28°S, which has been defined as a region where upwelling persists nearly year round [Hagen et al., 2001].The winter season (July-September) has previously also been identified as the main season of cold water coming to the surface through upwelling [Hagen et al., 2001].

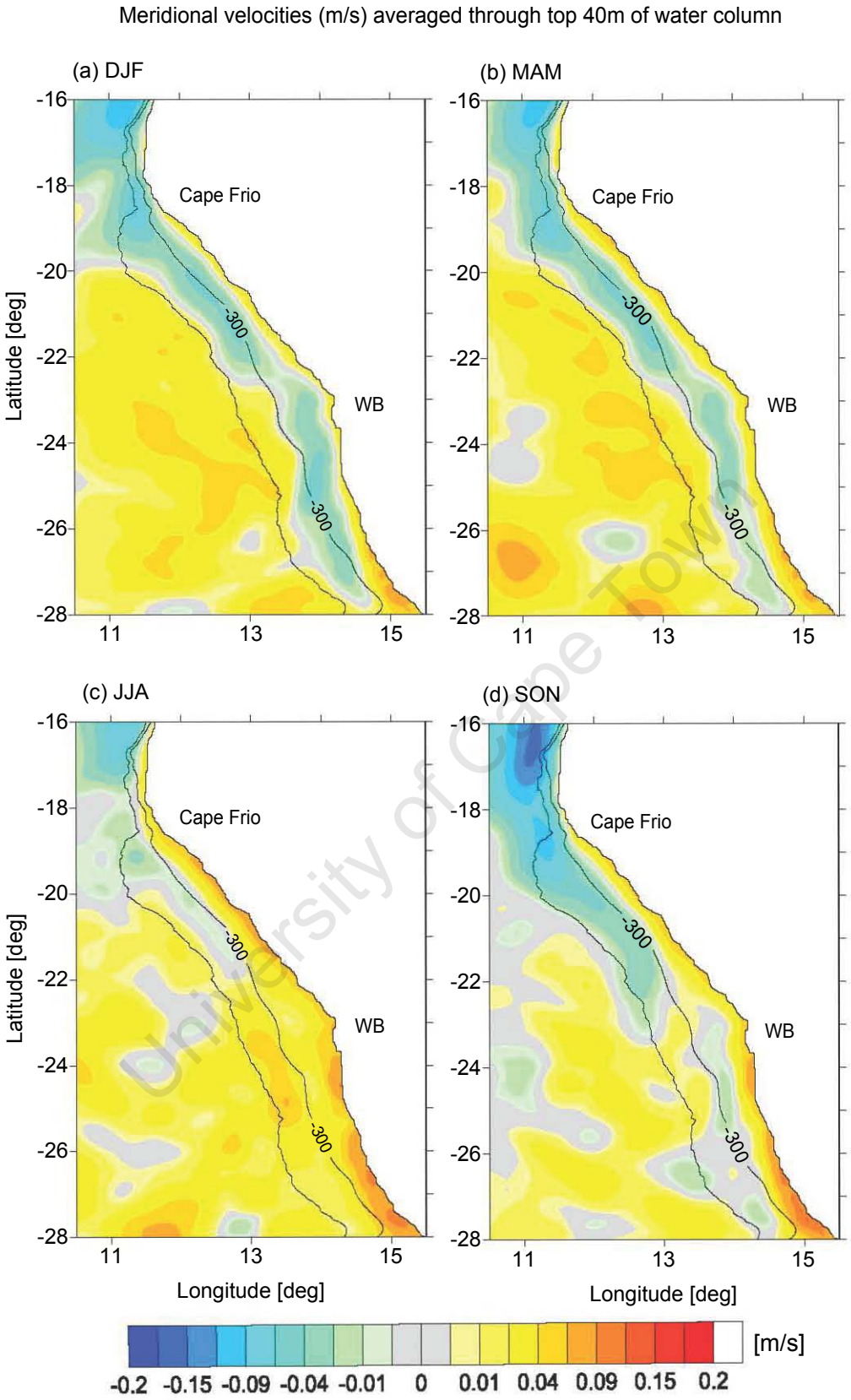

Fig. 4.3: Meridional current (m·sec^{-1}) (2000-2008 climatology) averaged through the mixed layer (0-40 m) for four seasons: a) summer (DJF), b) autumn (MAM), c) winter (JJA) and d) spring (SON). Positive (negative) is northwards (southwards). Strong poleward undercurrent (PUC) dominates along the 300 m shelf edge during spring (d), summer (a) and spring (b), whereas during winter (c) the PUC disappears and strong northward flow is observed across the shelf. The 300 and 1000 m isobaths are indicated.

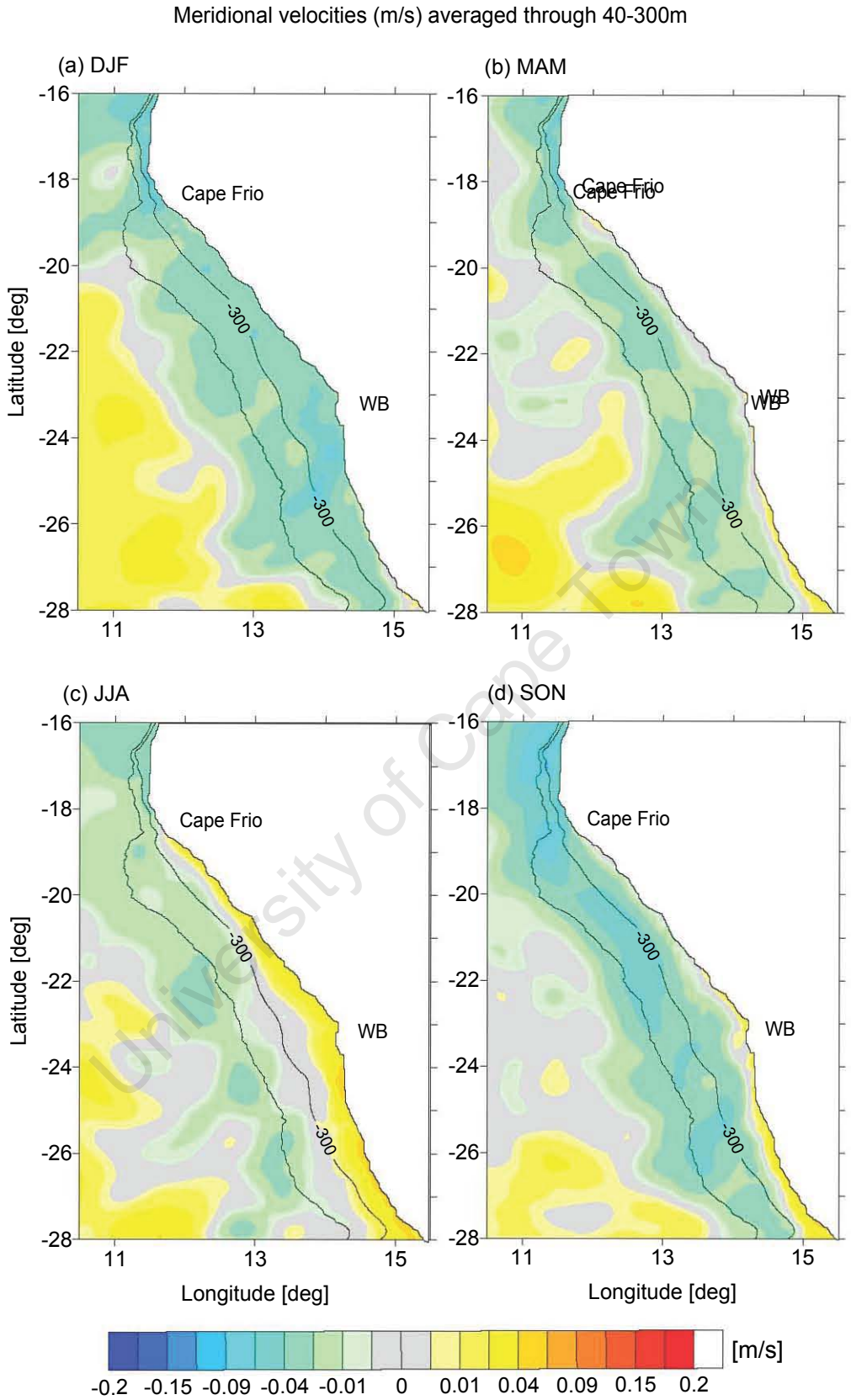

Fig. 4.4: Meridional current (m·sec^{-1}) (2000-2008 climatology) averaged through 40-300 m depth for four seasons: a) summer (DJF), b) autumn (MAM), c) winter (JJA) and d) spring (SON). Positive (negative) is northwards (southwards). The strong southward PUC is observed across the shelf during spring (d), summer (a) and autumn (b), whereas it weakens during winter (c) and a strong northward transport is observed along the coast of Namibia. The 300 and 1000 m isobaths are indicated.

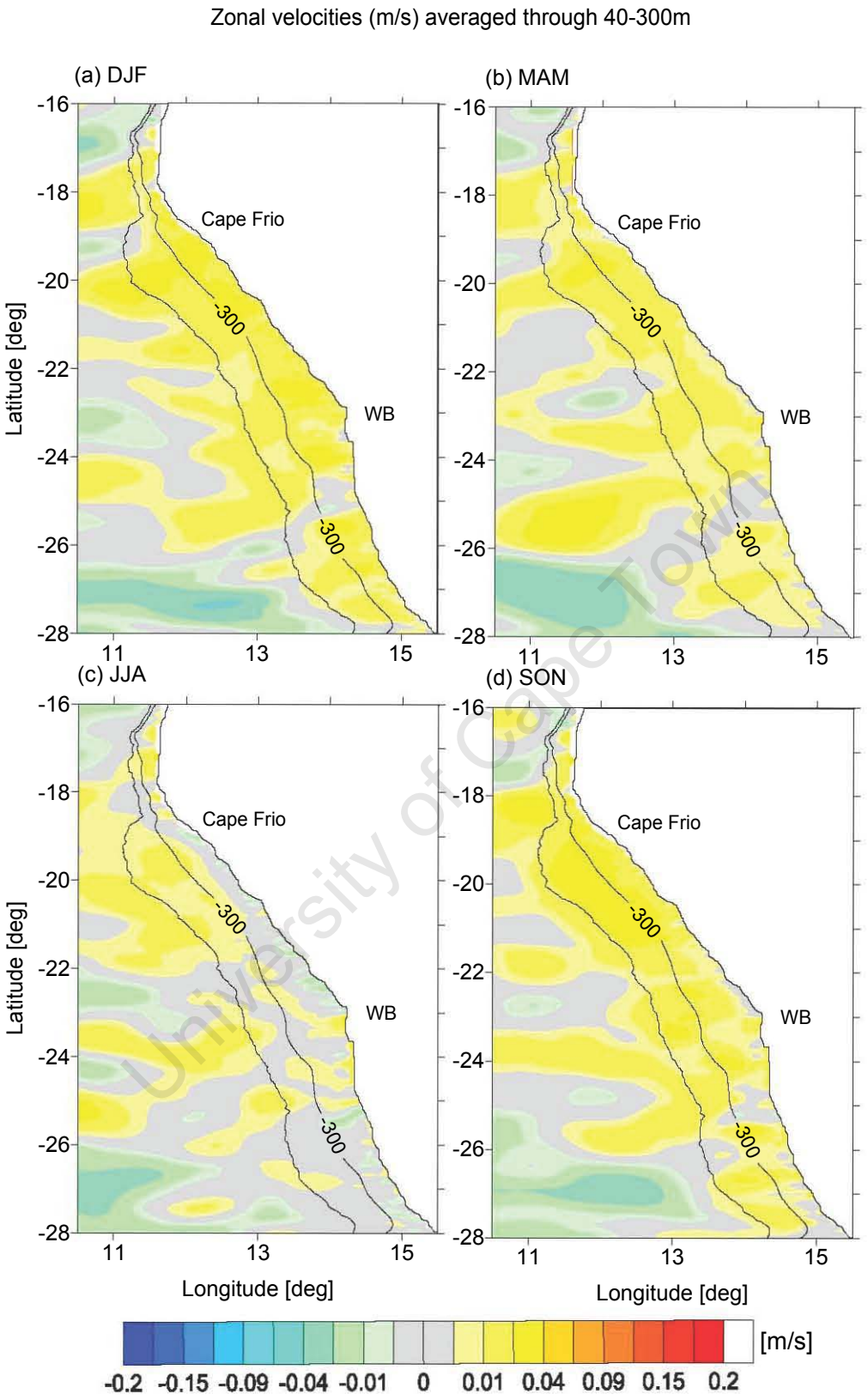

Fig. 4.5: Zonal current (m·sec^{-1}) (2000-2008 climatology) averaged through 40-300 m depth for four seasons: a) summer (DJF), b) autumn (MAM), c) winter (JJA) and d) spring (SON). Positive (negative) is eastward (westward). Onshore compensatory flow is observed onto and across the shelf, being particulary strong in spring (d), summer (a) and autumn (b). The 300 and 1000 m isobaths are indicated.

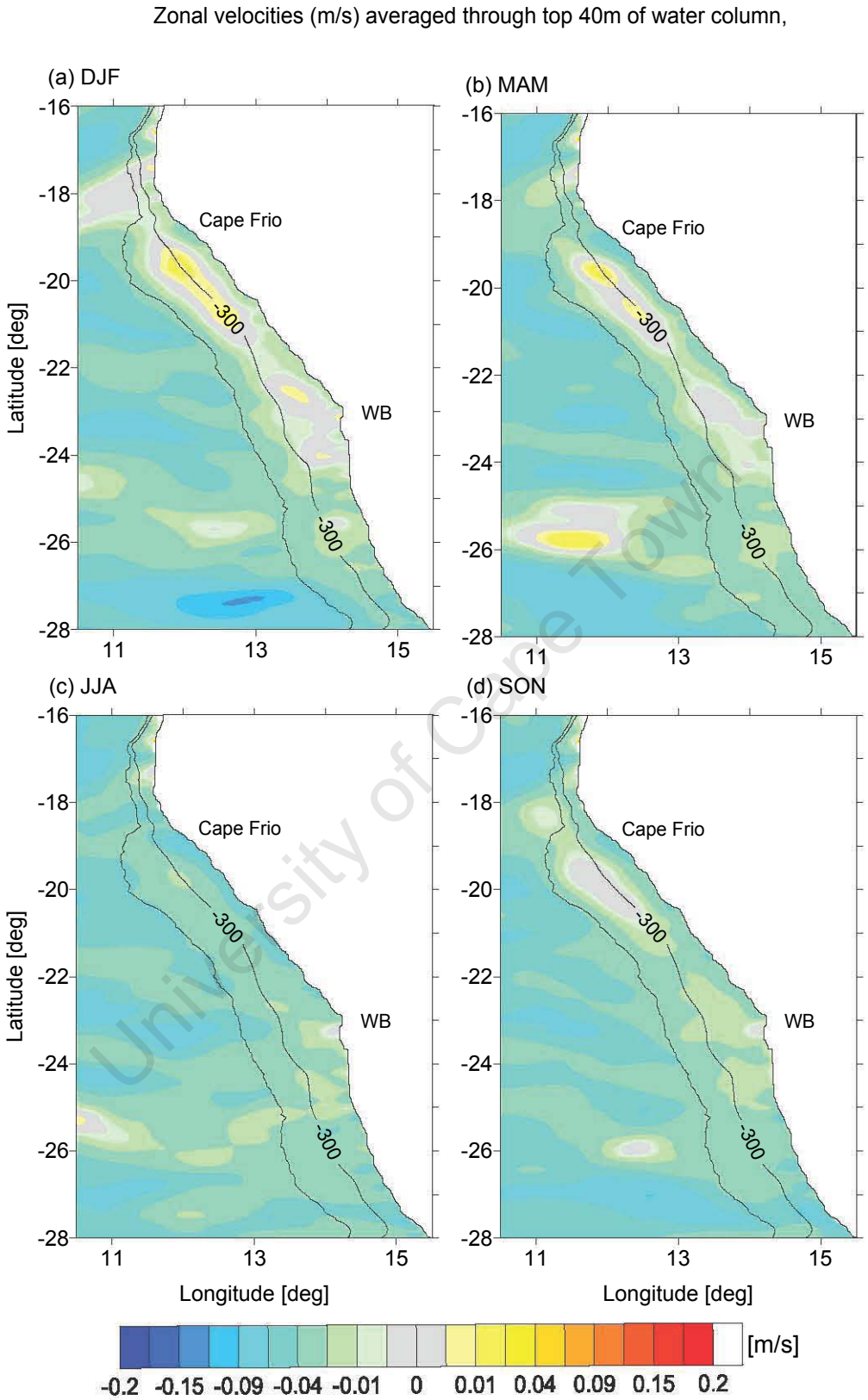

Fig. 4.6: Zonal current ($m \cdot sec^{-1}$) (2000-2008 climatology) averaged through the mixed layer (0-40 m) for four seasons: a) summer (DJF), b) autumn (MAM), c) winter (JJA) and d) spring (SON). Positive (negative) is eastward (westward). Strong offshore Ekman flow is observed across the region year round. The 300 and 1000 m isobaths are indicated.

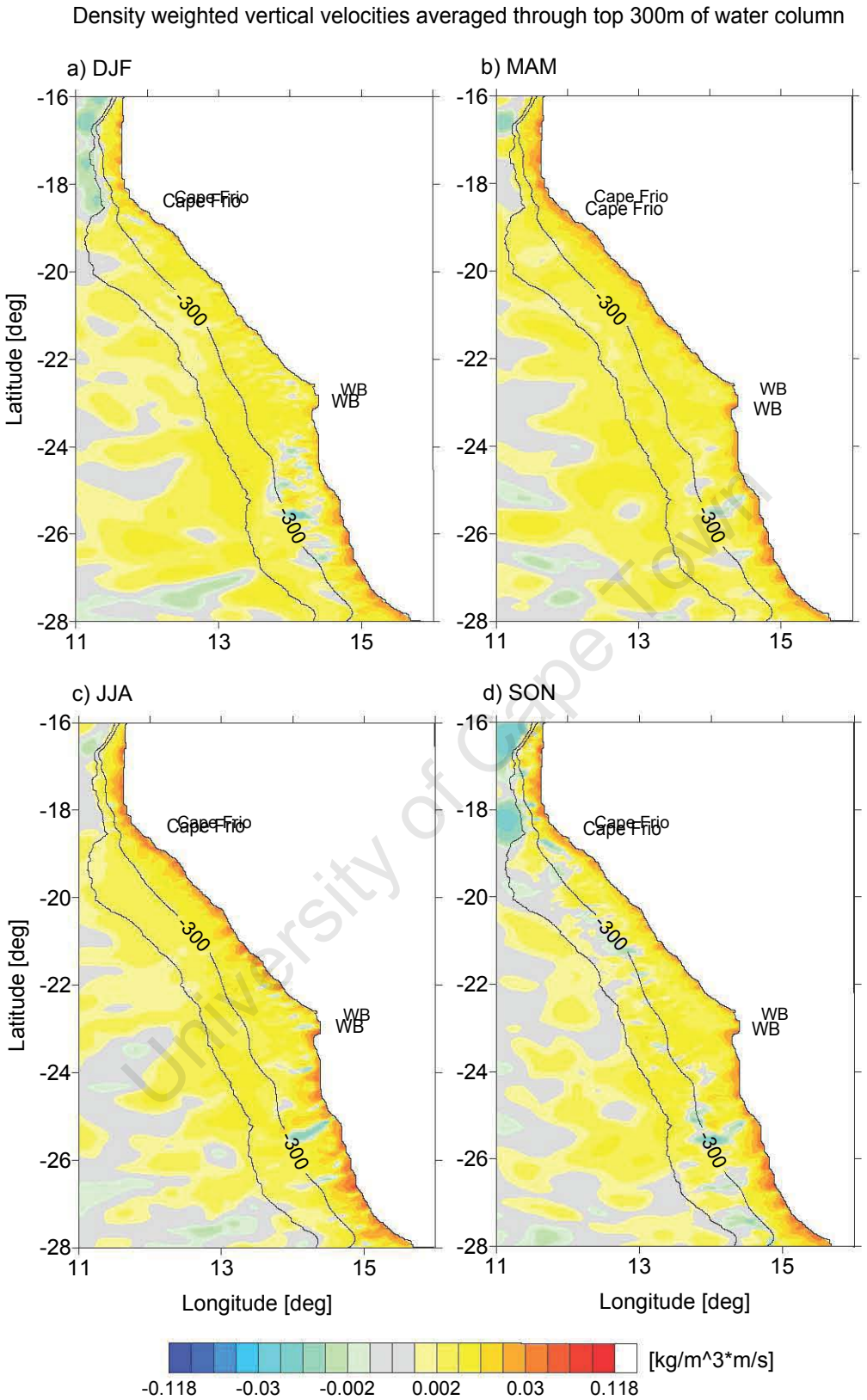

Fig. 4.7: Density integrated vertical velocity ($kg{\cdot}m^{-3}{\cdot}m{\cdot}sec^{-1}$) averaged through 0-300 m for four seasons: a) summer (DJF), b) autumn (MAM), c) winter (JJA) and d) spring (SON). Positive (negative) shows upwelling (downwelling). Strong upwelling is observed across the region during winter (c), whereas upwelling is confined to major upwelling cells during summer (a). The 300 and 1000 m isobaths are indicated.

4.1.3 Seasonal and geographic variation in circulation through the water column

For the rest of this section our main focus will be to examine the seasonal differences in current flow between summer (DJF) and winter (JJA), although spring and autumn will not be completely ignored during the discussion. The reasoning behind this decision is that upon evaluation of the initial results the winter season (JJA) was most distinguishable from the other three seasons and in order to investigate this in more depth the focus was narrowed to include predominantly results from summer and winter.

Variation of flow with depth along the shelf as well as off shelf at five latitudinal cross-sections (16°S, 19°S, 22°S, 25°S and 28°S) for summer (DJF) and winter (JJA) respectively are presented in Figures 4.8 and 4.9. With a narrow shelf at 16°S, the PUC persists at the shelf edge, but is stronger and wider in summer (DJF) as can be seen in Figure 4.8 (a). At the southernmost cross-section (28°S) the PUC is only observed deeper than 100 m in summer (DJF) and is only weakly present in winter (JJA). Here strong northward flow is observed along the coast in the upper 100 to 200 meters. At the central latitudes (19°S,22°S and 25°S) the PUC is weaker than at 16°S during DJF, yet still has a fairly wide span and is also still relatively strong. There is thus clearly a deepening of the PUC with latitude from north to south. In addition, this southward flow is located on the shelf and along the shelf edge, with shallow northward surface flow along the coast and west of the PUC. During winter the deepening of the PUC can be observed with increasing latitude as can the strengthening and increase in vertical dimensions of the equatorward coastal flow. During winter it is also evident that the PUC migrates to almost entirely off the shelf at the higher latitudes. Another interesting feature during winter is that at 25°S the PUC seems to have two core maxima, despite its offshore migration.

Observing zonal flow along the same five latitudinal cross-section (Figures 4.8 (b) and 4.9 (b)) a relatively thin (<50 m) Ekman offshore flow is observed in all cross-sections during summer (DJF), whereas at 19°S,22°S and 25°S a subsurface (50-300 m) onshore flow across the shelf is observed. During winter (JJA) the Ekman layer nearly doubles in vertical dimension and much weaker onshore flow is observed at all latitudes but 19°S (Fig 4.8 (b)). During both JJA and DJF very strong offshore flow is observed through the water column at both 16°S and 28°S, with limited subsurface onshore flow.

Figures 4.8 (c) and 4.9 (c) show the density intergrated vertical flows along the same five cross-sections. There is evidence for upwelling along all the latitudinal sections during both seasons. Due to the fact that only summer and winter are considered, it was difficult to formulate conclusions regarding the observed changes in upwelling strength with latitude as well as the seasonal variations. For example, confirming results from the upwelling indexes

like that from [Weeks et al., 2006] which showed peak upwelling season for the northern Benguela to be autumn, was not possible.

Based on the assumption of the conservation of potential vorticity in a region where the Rossby number is generally low, and the subsequent negligence of the relative vorticity term, [Veitch et al., 2010] was able to calculate the depth of the base of the poleward flow in the Benguela system. The results from the five cross-sections presented above are similar to what [Veitch et al., 2010] found. For example, they observed an annual mean depth of approximately 300 m for the PUC at 16°S, and then calculated a subsequent southward deepening to 373m at 20°S, 427 m at 23°S and 512m at 28°S. In these results there is a similar increase in the depth of the PUC, although the bottom depth is not indicated in the graphs of the higher latitudes. Additionally, [Veitch et al., 2010] also observed a secondary maximum of the PUC starting at 20°S and being pronounced at 23°S. Despite the plot not being showed, due to 23°S not being a main cross-section of interest in this study, the double cored PUC was also particularly pronounced at 23°S in the MOM-4 data set. Additionally there is evidence of the double core at 25°S during winter in Figure 4.9 (b). [Veitch et al., 2010] attributed the inshore and offshore maximums to the meridional flows on the shelf driven by the upwelling as well as the South Equatorial undercurrent respectively. Again, the Benguela is not the only system where this double maximum poleward flow is observed, as [Penven et al., 2005] found a similar feature in the Peru Coastal Current (PCC).

Another cross-section was taken along the 300 m depth contour between 16°S and 28°S and zonal flow was computed for a comparison of the cross-shore exchange between the summer (DJF) and winter (JJA) seasons (see Figure 4.10 (a) and (b)). A dominant feature is the difference in depth of the mixed layer between the two seasons. During winter (JJA), the layer of strong offshore Ekman related flow is at maximum depth (40-50 m), while in summer (DJF) it is only half as deep. In addition, during JJA the compensatory onshore flow is almost entirely absent through most of the region (Figure 4.10 (b)). In contrast, during summer (DJF) (Figure 4.10 (a)) there is strong onshore flow below the mixed layer, specifically in the region between 18-22°S. Strong zones of increased offshore flow along the surface and across the shelf edge can be observed at Lüderitz (27-28°S) and Cape Frio (16-18°S) during both seasons and again in winter these offshore pulses are also observed at 23°S and 19°S, zones identified as the major upwelling cells [Lutjeharms and Stockton, 1987; Kostianoy and Zatsepin, 1996]. Again the pattern of cross-shore flow was found to be very similar to that of [Veitch et al., 2010] although they considered the annual mean as well as assumed the shelf-edge to be at 500 m depth. Their results however similarly showed offshore Ekman flow confined to the upper 40 meters while zones of onshore pulses exist at greater depths. The meridional current for summer (DJF) presented in Figure 4.10 (c) similarly portrays the distinct shelf-edge poleward flow which [Veitch et al., 2010] observed in the annual mean

velocities for the northern Benguela. The deepening of the PUC southward is also clearly visible. Contrastingly, in winter (JJA) the PUC mostly disappears across the shelf-edge south of 20°S and there is a strengthening of the northward flow along the surface (Figure 4.10 (d)). With regards to density weighted vertical velocities shown in Figure 4.11, there is evidence for upwelling during both seasons and particularly in zones offshore of the major upwelling cells: Cape Frio (16-18°S), 22-25°S and a thin band off Lüderitz (27-28°S).

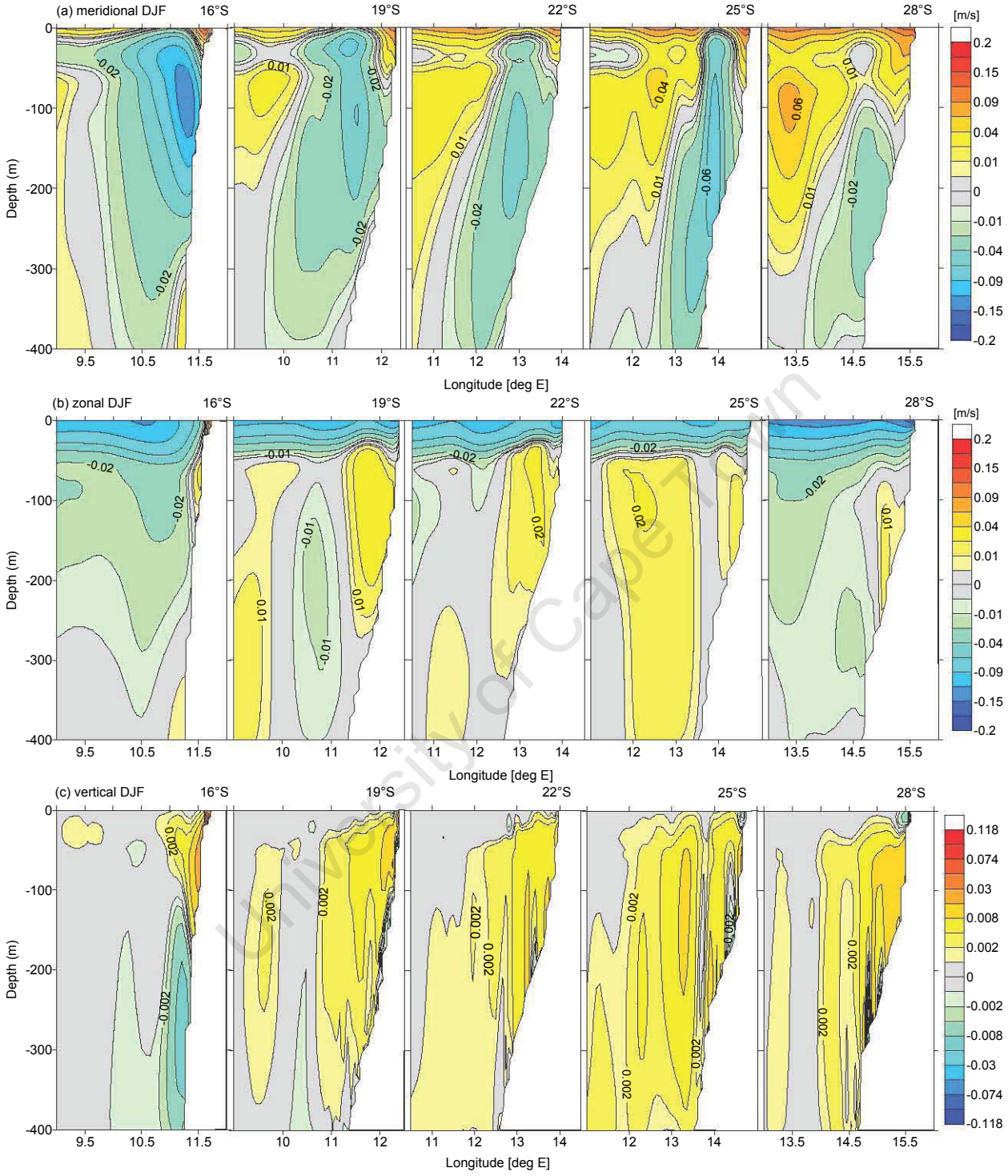

Fig. 4.8: (a) Meridional current, (b) zonal current and (c) density weighted vertical current ($kg{\cdot}m^{-3}{\cdot}m{\cdot}sec^{-1}$) during summer (DJF) along the cross sections at 16°S, 19°S, 22°S, 25°S and 28°S respectively. Calculated from the 2000-2008 climatologies. In (a) positive (negative) is northward (southward), (b) positive (negative) is east/onshore (west/offshore) and (c) positive (negative) is upwelling (downwelling).

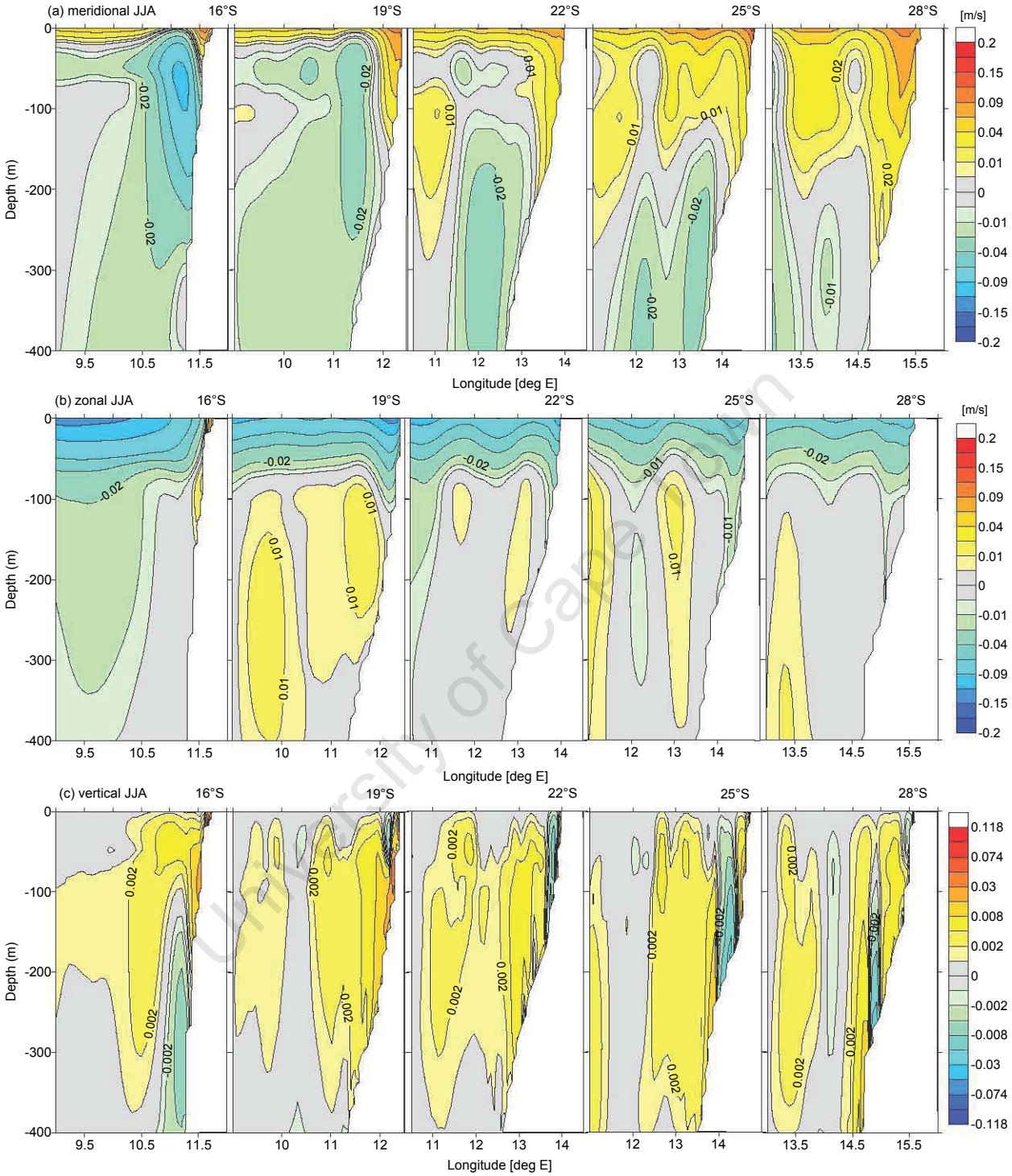

Fig. 4.9: (a) Meridional current, (b) zonal current and (c) density weighted vertical current ($kg{\cdot}m^{-3}{\cdot}m{\cdot}sec^{-1}$) during winter (JJA) along cross sections at 16°S, 19°S, 22°S, 25°S and 28°S respectively. Calculated from the 2000-2008 climatologies. In (a) positive (negative) is northward (southward), (b) positive (negative) is east/onshore (west/offshore) and (c) positive (negative) is upwelling (downwelling).

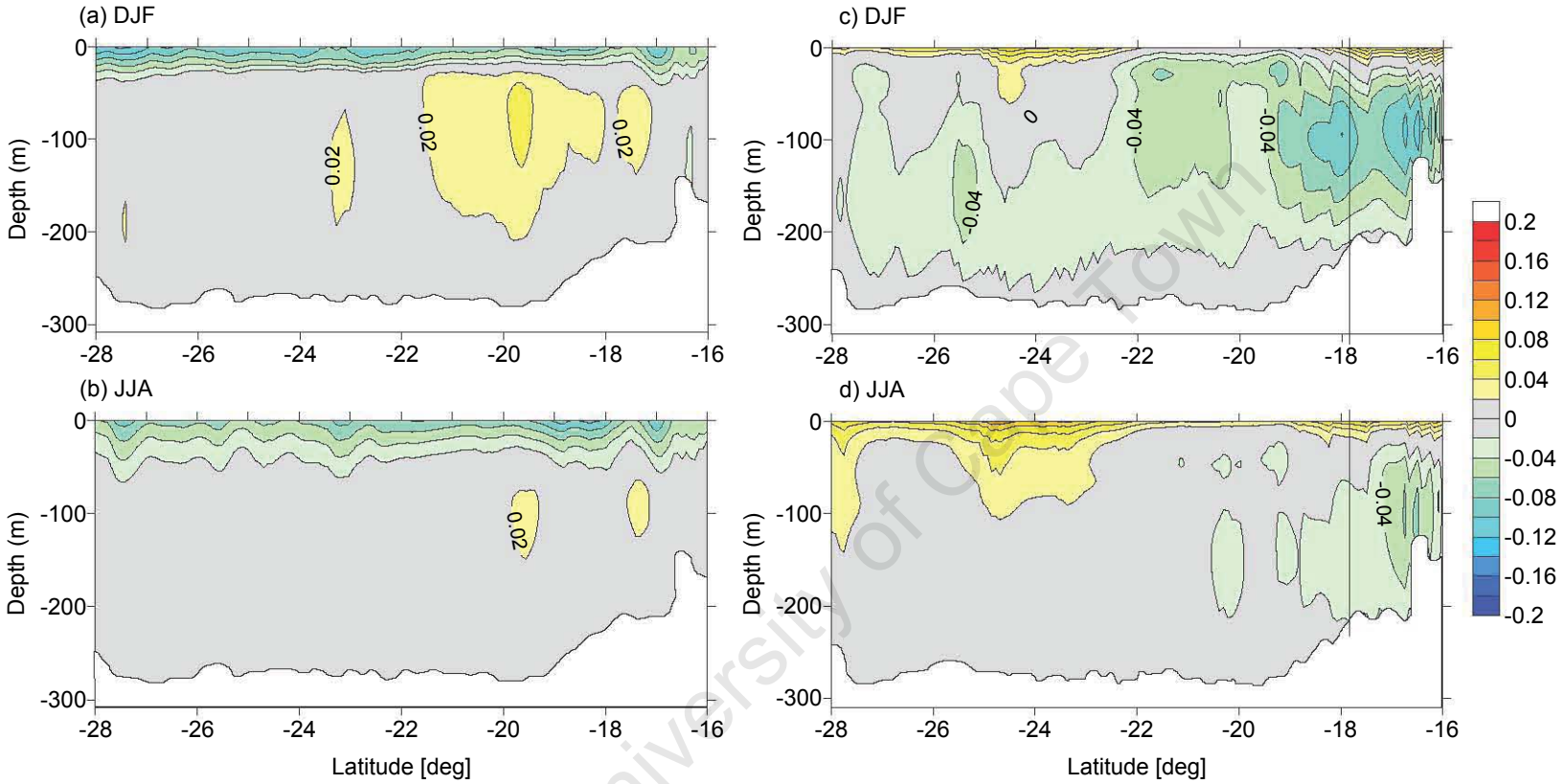

Fig. 4.10: Zonal and meridional current (m·sec^{-1}) through a transect along the 300 m depth shelf-break for summer and winter. In (a) and (b) positive (negative) is eastward (westward), and in (c) and (d) positive (negative) is northward (southward). In (a) and (b) surface Ekman flow as well as the compensatory subsurface onshore flow is observed. Additionally, in summer (c) the PUC is observed along the shelf edge throughout the region, whereas during winter (d) the PUC weakens and equatorward flow in the surface 100 m dominates the southern part of the region.

Hovmöller diagrams of the depth integrated transport allow a final qualitative examination of the seasonal and geographic variation in transport across the northern Benguela region, before a quantitative analysis in the next section. Four latitudinal sections, scaled to shelf width, can be seen in Figure 4.12 and the longitudinal section in Figure 4.13.

Figure 4.12 shows that at 16°S the PUC dominates transport along the very thin shelf, with particularly strong southward (15-20 $m^2 \cdot sec^{-1}$) transport during autumn (SON) and summer (DJF). The narrow shelf however means only a moderate influence of transport through the cross-section at this latitude. Further south at 19°S the shelf is wider and despite a similar PUC signal along the western edge of the shelf, a medium strong (5 $m^2 \cdot sec^{-1}$) northward transport is observed along the coast. The width of northward transport stretches west during winter and also increases in strength. South of Walvis Bay (25°S) the pattern changes slightly. Here, the PUC signal strengthens, especially during early and late summer, and also migrates to being more centered on the shelf. In contrast to the two northern transects, essentially no southward transport is observed at 25°S during winter. Again, this is a direct effect of the offshore migration of the PUC during this time, also supported by Figures 4.3 to 4.5. The strong northward transport during winter (JJA) is also observed south of Lüderitz (∼28°S), when the PUC influence again shifts west to the edge of the shelf. Here the PUC is weaker than what was observed at the northern transects. In contrast to the other transects stronger northward transport can be observed close inshore even during the summer months. The northward transport in winter is also stronger and more persistent. There thus appears to be a bimodal pattern for the transects 19°S, 25°S and 28°S.

Figure 4.13 provides a perspective on transport across the shelf-edge. As expected from past research [Stander, 1964; Parrish et al., 1983; Lutjeharms and Meeuwis, 1987] offshore transport is observed just north of the Lüderitz upwelling cell nearly year round, with strongest values during the winter months. A similar pattern is observed for the region between 16°S and 17°S where two strong offshore bands persist. This pattern is similar to results from [Parrish et al., 1983], who showed maximum Ekman drift off both Lüderitz and Cunene. The region between 22°S and 25°S shows a relatively clear seasonal variability with weak offshore transport during winter, while during summer a medium strong onshore transport (4 $m^2 \cdot sec^{-1}$) is observed. Finally, in contrast to the surrounding regions the area between 19°S and 22°S shows predominantly strong (7 $m^2 \cdot sec^{-1}$) onshore transport almost year round, with a strengthening during SON and DJF and slight weakening during JJA.

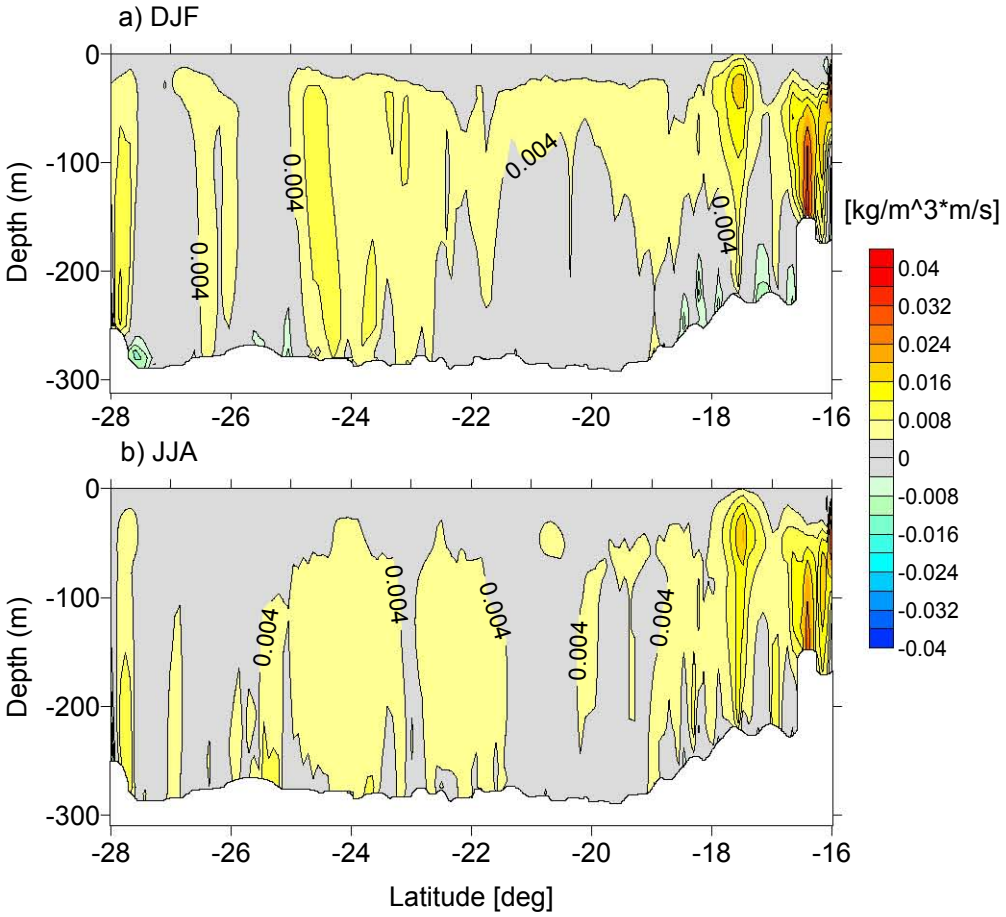

Fig. 4.11: Density weighted vertical current ($kg{\cdot}m^{-3}{\cdot}m{\cdot}sec^{-1}$) through a transect along the 300 m depth shelf break for summer (DJF) and winter (JJA). Positive (negative) is upwelling (downwelling).

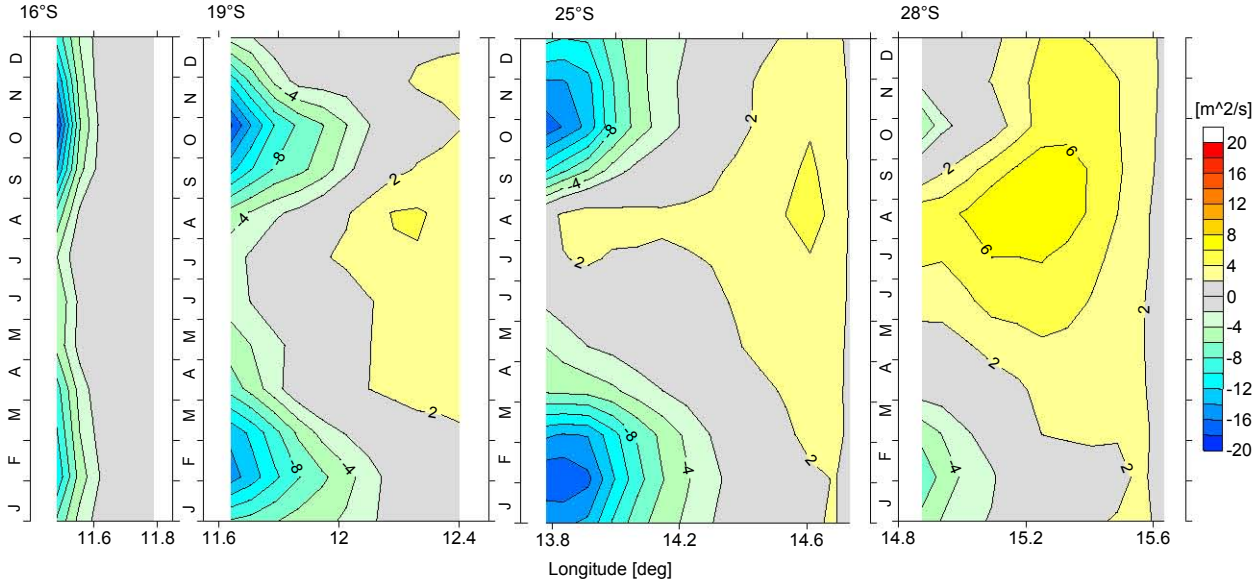

Fig. 4.12: Hovmöller diagrams of integrated transport ($m^2{\cdot}sec^{-1}$) through transects at 16°S, 19°S, 25°S and 28°S. Transects have been scaled according to longitudinal width. Positive (negative) is northwards (southwards).

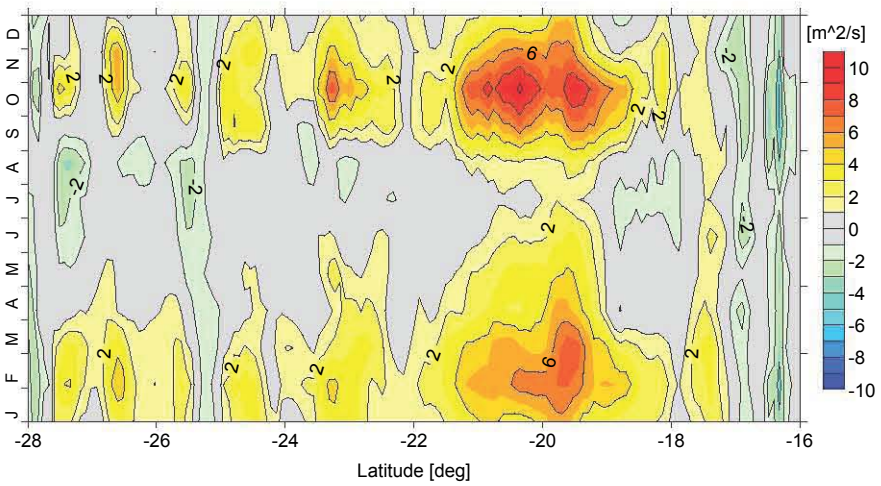

Fig. 4.13: Hovmöller diagram of integrated zonal transport ($m^2 \cdot sec^{-1}$) through a transect along the 300 m deep shelf break, showing bands of year round offshore transport at 16-17°S, 25°S and 28°S, as well as a zone of strong onshore transport almost year round between 19-22°S. Positive (negative) is east/onshore (west/offshore).

4.2 Quantifying transport flux budgets for the northern Benguela shelf

4.2.1 Annual budgets

For a first quantitative impression of the contributions of major features across the northern Benguela, the mean annual transport fluxes, based on the 8 year climatologies (2000-2008), were calculated for 4 geographic sections of equal latitudinal proportions: 16-19°S, 19-22°S, 22-25°S and 25-28°S. See section 2.2 for the explanation of the rational behind region selections and method details. Fluxes were calculated through the northern and southern boundary of each section as well as along the 300 m depth contour along the western edge of the shelf. The eastern boundary was considered closed. The annual results are presented in Fig 4.14.

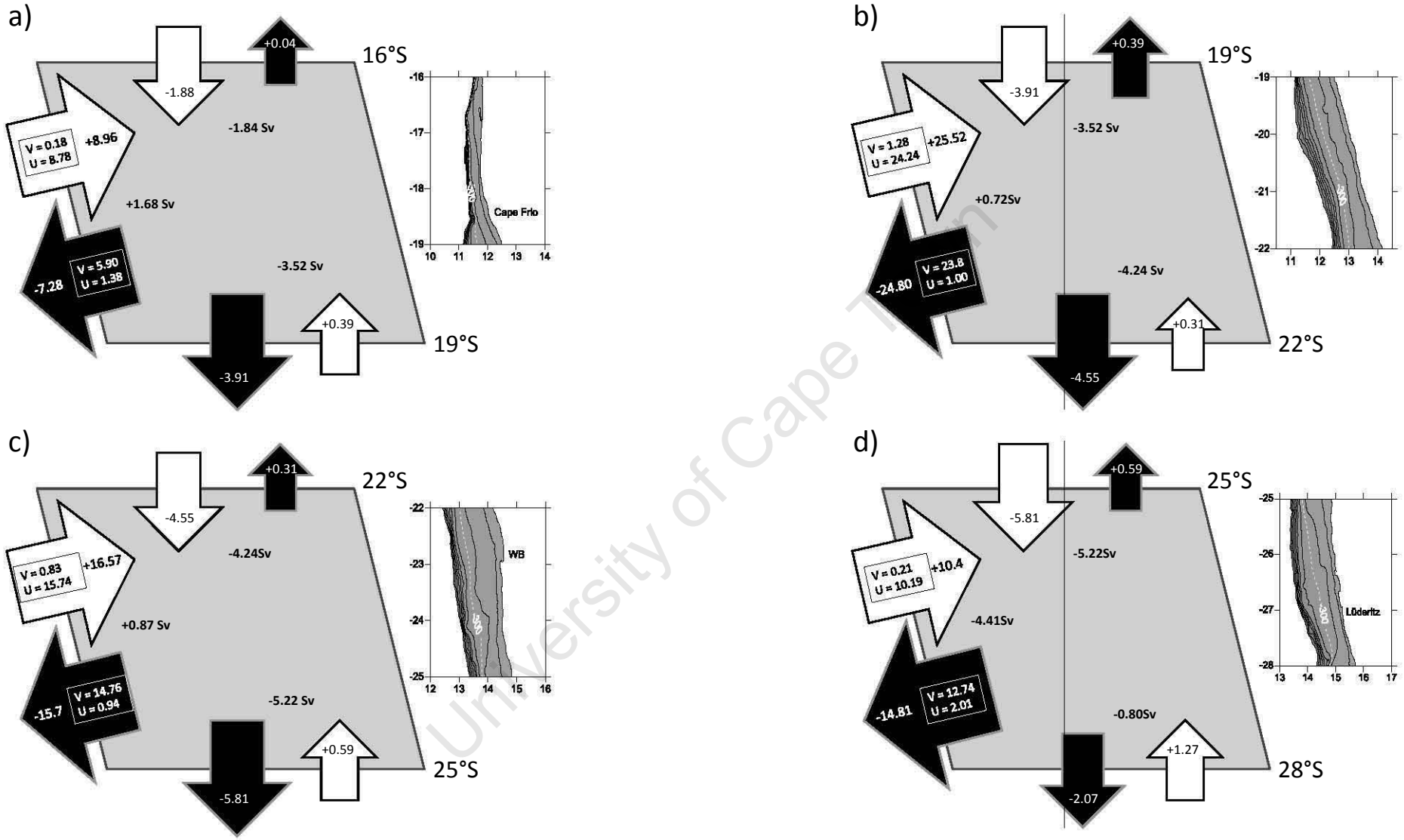

Fig. 4.14: Mean annual volume transport flux budgets (Sv) for four box regions along the northern Benguela shelf: a) 16-19°S, b) 19-22°S, c) 22-25°S and d) 25-28°S. The western border actually runs along the 300 m deep shelf edge. The inset maps show the actual shape of the western border, as well as the width of the southern and northern borders of each box.

A number of general observations on the annual volume transport fluxes:

Due to the widening of the shelf from equator to pole, the southward flux associated with the PUC increases from 16 to 25°S. From north to south the transports are: -1.88 Sv at 16°S; -3.91 Sv at 19°S; -4.55 Sv at 22°S and -5.81 Sv at 25°S. In contrast, the northward transport flux associated with the equatorward jet decreases from south to north and is thus strongest at 28°S. From south to north the transports are: +1.27 Sv at 28°S; +0.59 Sv at 25°S; +0.31 Sv at 22°S; +0.39 Sv at 19°S and +0.04 Sv at 16°S.

The contribution of the PUC to the offshelf transport is also substantial, see section 2.2 for details. Particularly the regions where the bathymetry changes most dramatically in longitude from north to south show a strong meridional component to the transport fluxes leaving the western edge of the box. For example the meridional component (v) accounts for approximately 95% of the offshelf transport flux between 19-22°S and 22-25°S. In contrast this reduces to less than 85% for the Cape Frio and Lüderitz regions, where the offshore Ekman flux makes a much larger contribution to the offshore exchange. In contrast to the offshore exchange, the onshore compensatory flux is dominated by the contribution of the zonal (u) component (>95% for all regions).

The cross-shore transport fluxes support the qualitative results in Figure 4.10 by showing the very strong onshore subsurface compensatory flux between 19-22°S. The zonal flux (24.24 Sv) is nearly double that found in any other other of the four regions. It seems that this strong onshore flux compensates for the equally strong PUC driven meridional transport flux, which "leaves" the shelf due to its inclination. The region 22-25°S shows a similar, yet weaker pattern with an annual onshore zonal flux of 15.74 Sv. The very narrow shelf of Cape Frio (16-19°S) makes it difficult to compare transport fluxes here with the three southern regions. The Lüderitz cell in contrast, is most distinct from the other regions in that this is the only region where offshore transport exceeds the onshore compensation on an annual basis. Additionally, at the 28°S border there is a relative balance between the northward and southward flux balance, with a pronounced weakened PUC and a stronger equatorward flux close to the coast. [Mohrholz et al., 2008] have suggested a maximum southward extent for the PUC at 27°S. The flux results here sugget that this may be a reasonable estimate.

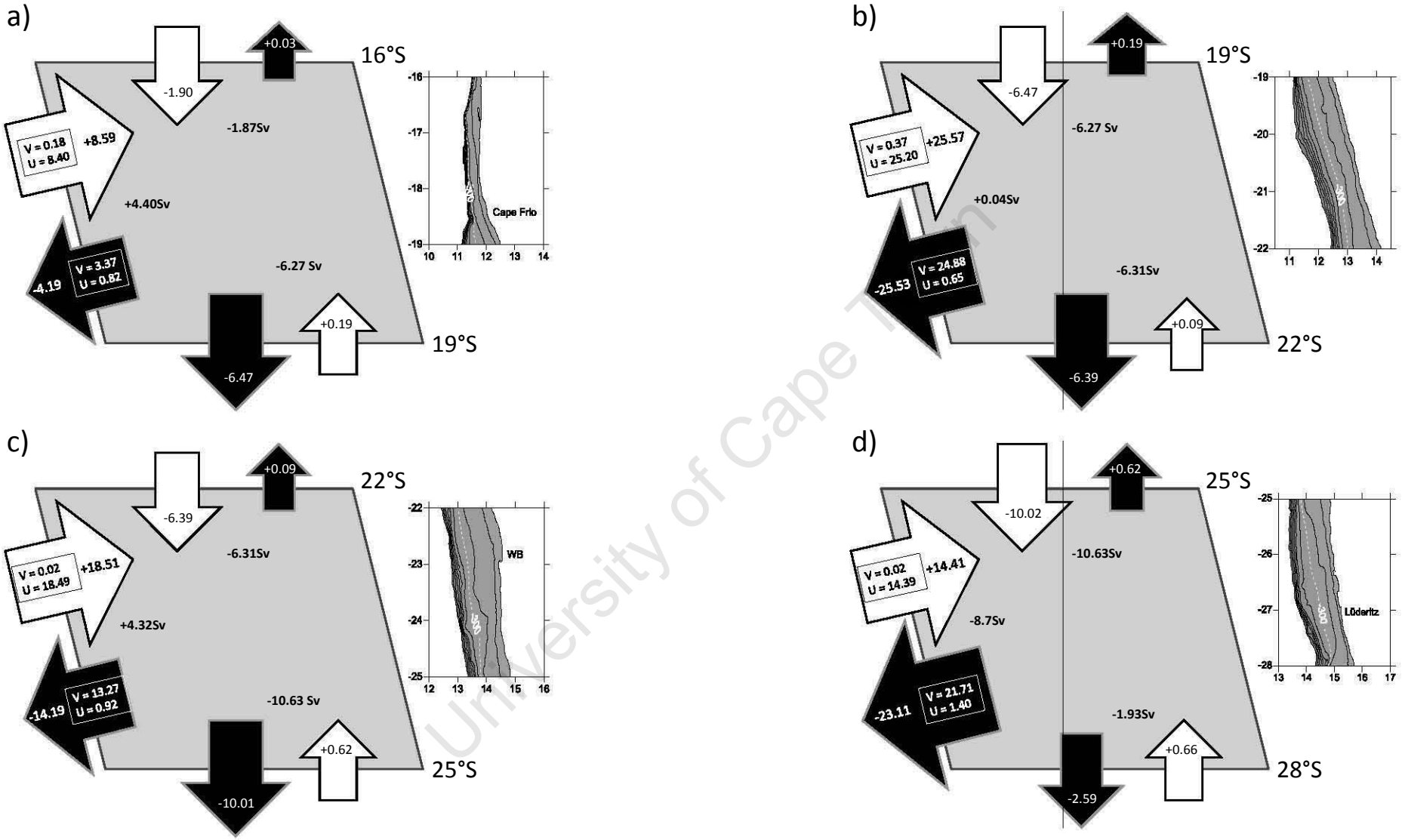

Fig. 4.15: Mean summer volume transport flux budgets (Sv) for four box regions along the northern Benguela shelf: a) 16-19°S, b) 19-22°S, c) 22-25°S and d) 25-28°S. The western border actually runs along the 300 m deep shelf edge. The inset maps show the actual shape of the western border, as well as the width of the southern and northern borders of each box.

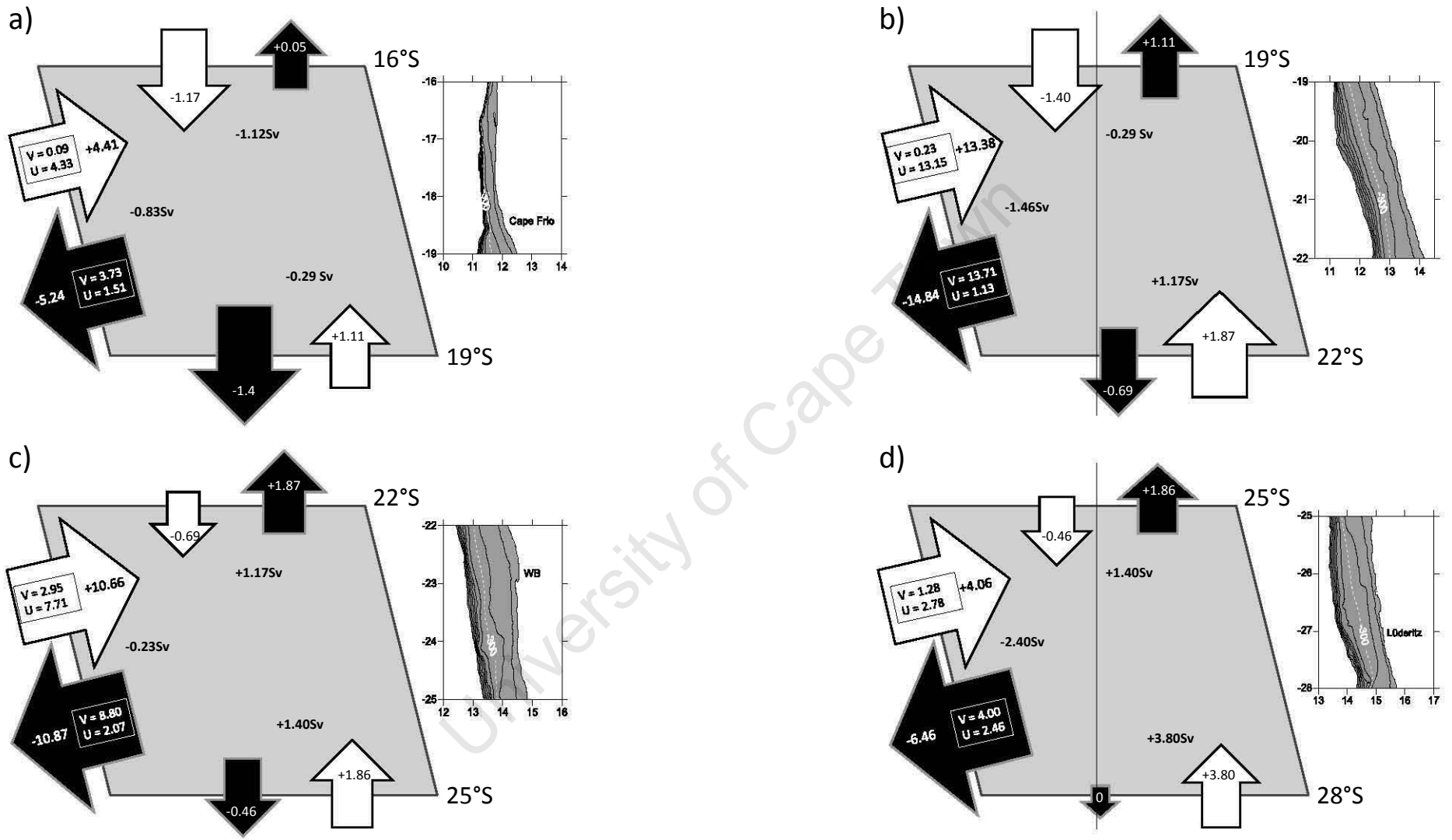

Fig. 4.16: Mean winter volume transport flux budgets (Sv) for four box regions along the northern Benguela shelf: a) 16-19°S, b) 19-22°S, c) 22-25°S and d) 25-28°S. The western border actually runs along the 300 m deep shelf edge. The inset maps show the actual shape of the western border, as well as the width of the southern and northern borders of each box.

4.2.2 Summer (DJF) and winter (JJA) budgets

The summer profiles (Figure 4.15) broadly resemble the annual volume transport fluxes (Figure 4.14) in so far as the PUC driven poleward flow dominates the longshore transport fluxes and the three northern sections (16-19°S, 19-22°S and 22-25°S) all show a mean onshore flux across the shelf edge, whereas at the Lüderitz box (25-28°S) an offshore flux is observed. However, the summer values were much larger than the annual values, with the poleward fluxes from north to south being: -1.90 Sv at 16°S, -6.47 Sv at 19°S, -6.39 Sv at 22°S and -10.01 Sv at 25°S. Even at 28°S the mean southward summer flux was higher than the annual flux. At the Lüderitz cell (25-28°S) the offshore summer flux (-8.7 Sv) is nearly double the annual flux, whereas the onshore fluxes at Cape Frio (16-19°S) and between 22°S and 25°S is four times as large (+4.40 Sv and +4.32 Sv respectively).

In contrast to both the annual and summer flux budgets, the winter profiles show that instead of the PUC driven poleward transport, the coastal jet (northward coastal branch of the Benguela current) forces the transport fluxes during this season. This is clear from the decreasing southward fluxes from north to south: -1.17 Sv at 16°S, -1.4 Sv at 19°S, -0.69 Sv at 22°S, -0.46 at 25°S and 0 at 28°S. In contrast, the equatorward driven fluxes increases from north to south during winter: +0.05 Sv at 16°S, +1.11 Sv at 19°S, +1.87 Sv at 22°S, +1.86 Sv at 25°S and +3.80 Sv at 28°S. This switch co-exists with an offshore transport flux across all four regions, the northern three regions having shown onshore transport fluxes both for the annual and summer budgets. At Lüderitz the offshore flux is much weaker in winter (-2.4 Sv) than in summer (-8.7 Sv). With reference to both the cross-sections in Figure 4.10 as well as Figure 4.13 the observed difference in flux budgets between summer (DJF) and winter (JJA) is expected. Figure 4.13 in particular shows the switch in zonal transport between summer and winter and this is presented quantitatively here.

4.3 Section summary

Figure 4.17 summarizes the findings of this section quantitatively. It has previously been suggested by [Mohrholz et al., 2008] that a distinct seasonal cycle of both meridional and cross-shelf circulation exists in the northern Benguela region. Similar to their findings the results presented in this section showed the dominant role played by the strong PUC (poleward undercurrent) during summer (DJF) in the meridional volume transport fluxes. Additionally, in winter the equatorward coastal current drives the meridional fluxes. In Figure 4.17 (b) the PUC dominated summer showed negative (poleward) budgets through all five cross-

sections (16°S, 19°S, 22°S, 25°S and 28°S), this pattern being similar to the annual budgets (a) but much stronger. In contrast, the equatorward coastal current dominates in winter (Figure 4.17 (c)) resulting in a switch from weak negative or poleward fluxes at 16°S and 19°S to positive or equatorward fluxes increasing in strength from 22°S to 28°S.

These results, however, showed that [Mohrholz et al., 2008]'s and [Brüchert et al., 2003]'s simplified suggestion for the cross-shore transport is not entirely sufficient for the whole northern Benguela region. For example, the pattern of increasing poleward fluxes from 16°S to 25°S and a decrease at 28°S seem to add to the cross-shore fluxes observed during summer (Figure 4.17 (b)), meaning an increased negative or offshore flux off the Lüderitz upwelling cell (25-28°S) and an increased positive or onshore fluxes for the three northern regions (16-19°S, 19-22°S and 22-25°S). In contrast, during winter (Figure 4.17 (b)) the unique meridional pattern seems to add to an offshore flux along the shelf edge for all four sections. Results presented here thus suggest a much more complex exchange across the shelf edge than the suggested simplified view of upwelled water from intermediate depths balancing the wind driven offshore Ekman transport of surface water [Brüchert et al., 2003]. In addition, this cross-shore exchange seems to be greatly affected by the seasonal and spatial variability in the meridional currents.

Furthermore, there is evidence in our results that the four regions examined exhibit unique longshore and cross-shore dynamics: The Lüderitz cell (25-28°S) is unique with an offshore flux across the shelf edge year round. This result does not deviate from past results and in fact enhances the view of the Lüderitz zone being a barrier making it difficult for certain fish species to pass through [Agenbag and Shannon, 1988; Hutchings et al., 2009]. Additionally, this result may add support to [Monteiro, 1996]'s "gate hypothesis", which essentially suggest that wind controlled upwelling and changes in topography maintained the inhibition of the poleward flow. The budget results here show that the PUC influence diminishes rapidly in strength south of 25°S. However, it is seen that a stronger influx from north, associated with the PUC, adds to the offshore flux observed at the Lüderitz cell during summer (Figure 4.17 (b)). In contrast, during winter a strong flux from the south is seen to contribute strongly to the offshore flux (Figure 4.17 (c)). These influences however only form part of the number of forcings (including atmospheric forcings, open ocean circulation and turbulent interactions) shaping the upwelling dynamics associated with the Lüderitz upwelling cell. This result confirms again the unique interplay between the water mass being transported poleward by the PUC [Mohrholz et al., 2001] and that transported northward via the Benguela coastal current [Poole and Tomczak, 1999] in determining the shelf condition next to the coast of Namibia.

Circulation dynamics of the Cape Frio region (16-19°S) appears more complicated. [Monteiro

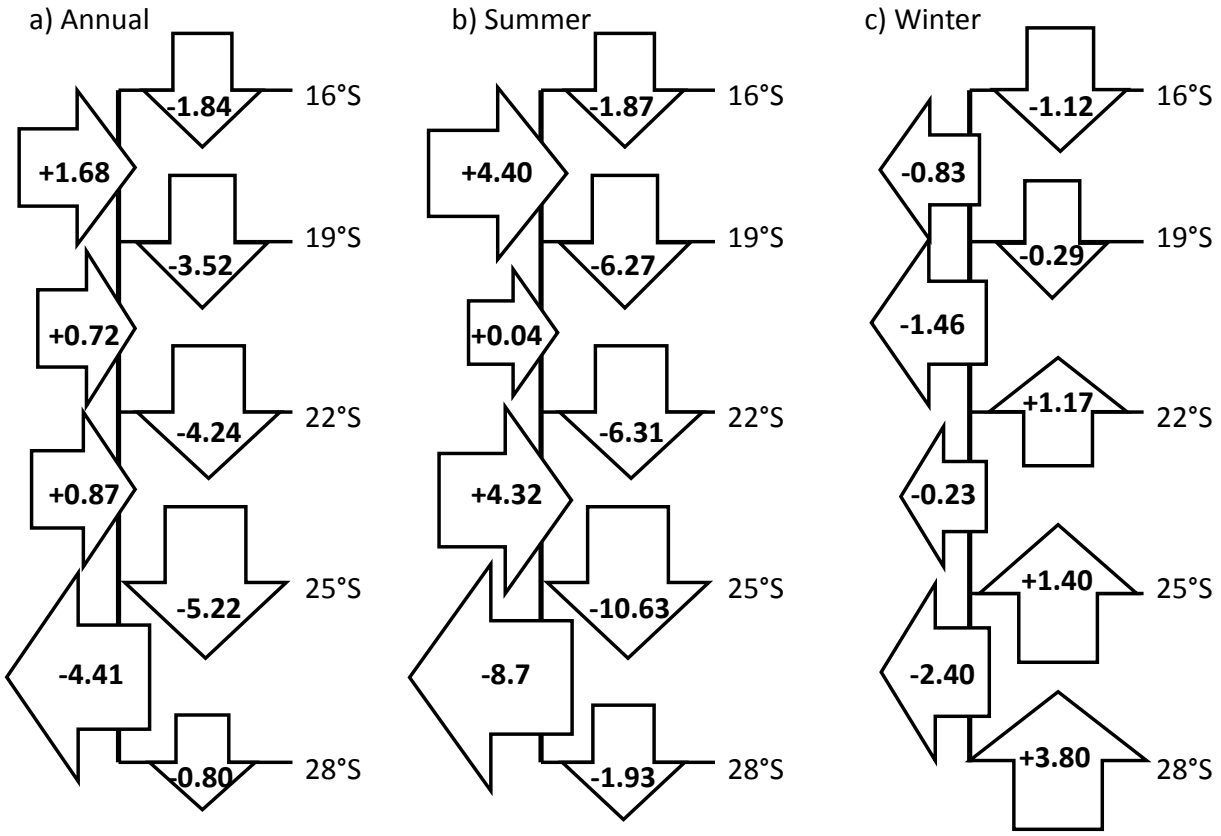

Fig. 4.17: (a) Annual, (b) summer (DJF) and (c) winter (JJA) volume transport flux budgets (Sv) across the northern Benguela shelf. For details see Figures 4.14, 4.15 and 4.16.

and van der Plas, 2006] suggested a strong uplift onto the shelf at Cape Frio in their work on LOW (low oxygen water) whereas it is also known that surface upwelling filaments persist off Cape Frio. This can be seen in Figure 4.13 where both the offshore channels associated with the Cape Frio upwelling cell (16-17°S) as well as the region south of this where year round onshore transport dominates (18-19°S) can be seen. The dynamics of this region are therefore averaged out somewhat in the budget calculations. The difference between the summer and winter budgets, however, shows something of the unique cross-shore dynamics present along the shelf edge in this region. Unlike the Lüderitz region, the Cape Frio region would not appear to be a persistent barrier, but rather a dynamic zone exhibiting high spatial and temporal variability.

The two central regions both show offshore fluxes during summer and onshore fluxes during winter. The summer fluxes indicate the extreme weakening of cross-shore ventilation in the bottom layers previously suggested by [Mohrholz et al., 2008] from data collected offshore of Walvis Bay. The offshore transport in these central regions, associated with surface Ekman transport, is also less than for the Cape Frio and Lüderitz regions.

The results presented here therefore support past work which suggest that SACW, that is oxygen poor and nutrient rich, would flush the shelf during summer whereas during winter ESACW, which is oxygen rich and has a lower nutrient concentration, would ventilate the shelf [Poole and Tomczak, 1999; Mohrholz et al., 2001; Brüchert et al., 2003; Monteiro and van der Plas, 2006]. What these results add is that the geographically variable cross-shore circulation of each sub-region has the capability to uniquely modify local oxygen conditions along the shelf. Figures 4.18 and 4.19 show this result graphically. Here oxygen transports are presented for the northern Benguela region both through the mixed layer (0-40 m) and below (40-300 m). It should however be cautioned that the oxygen transport values through the upper 40 meters does not take into consideration the oxygen uptake through the air-sea interface. The winter flushing of the shelf with oxygen rich water is clearly evident particularly along the surface (Figure 4.18 (b)) but also in the deeper layers. Figures 4.19 (c) and (d) also show the much weaker but none the less present transport of oxygen across the shelf in the deeper (40-300 m) layers.

These results therefore again highlight the great seasonal as well as spatial variability in both meridional and cross-shore exchanges which exist within the northern Benguela system. Furthermore, the results provide new evidence with regard to the ventilation of the Namibian shelf and the processes driving this, i.e. the unique interplay between the longshore currents greatly shaping the seasonal and geographic variability in transport across the shelf edge. These results, however, only provide a mean view of the system based on climatologies from 2000-2008, and thus does not portray the great interannual variability in the circulation of the northern Benguela shelf which has been recorded [Brüchert et al., 2003, 2006; Monteiro and van der Plas, 2006; Hutchings et al., 2009].

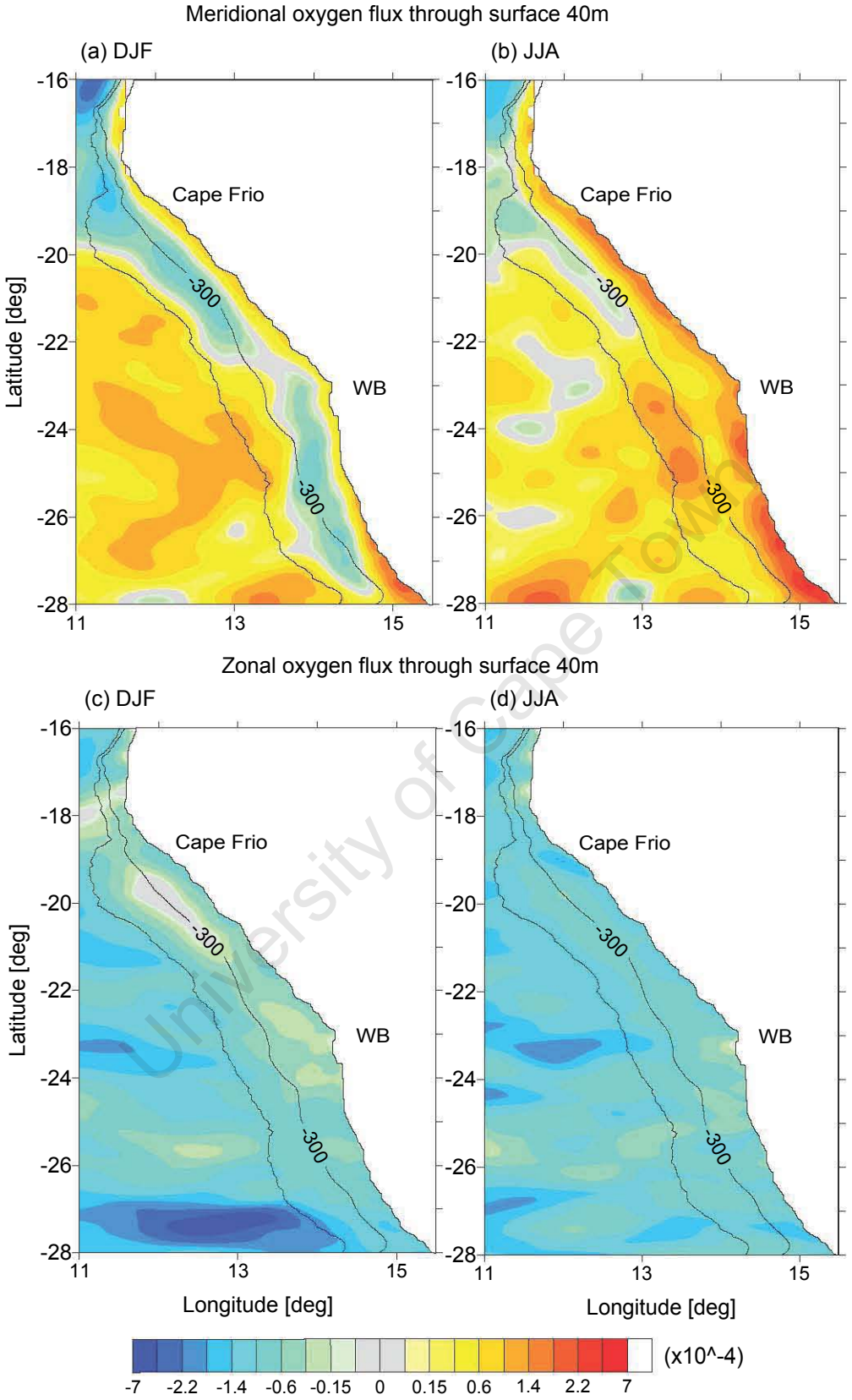

Fig. 4.18: Oxygen transport ($m \cdot mol \cdot s^{-1} \cdot kg^{-1}$) along and across the Namibian shelf through the mixed layer (0-40 m) for summer (left) and winter (right). Values represent 8 year (2000-2008) climatology. For meridional transport positive (negative) is northward (southward), for zonal transport positive (negative) is east (west). The 300 and 1000 m isobaths are indicated.

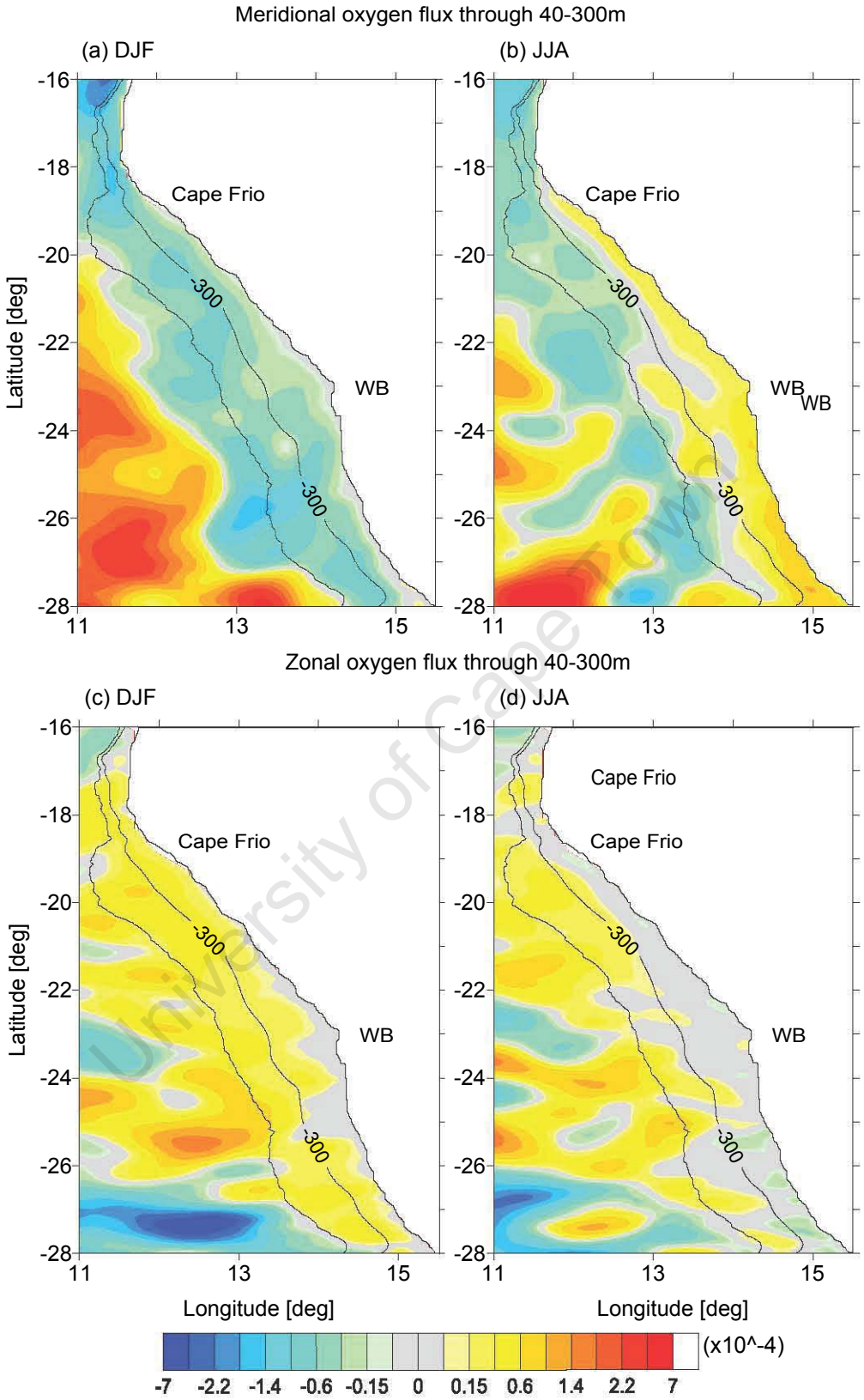

Fig. 4.19: Oxygen transport ($m \cdot mol \cdot s^{-1} \cdot kg^{-1}$) along and across the Namibian shelf through depth 40-300 m for summer (left) and winter (right). Values represent 8 year (2000-2008) climatology. For meridional transport positive (negative) is northward (southward), for zonal transport positive (negative) is east (west). The 300 and 1000 m isobaths are indicated.

Chapter 5

The circulation dynamics associated with a northern Benguela upwelling filament during October 2010

In this section the focus will be the examination of a particular upwelling filament sampled in a region off Cape Frio, where filaments are a common feature [Van Foreest et al., 1984; Lutjeharms and Stockton, 1987] in the northern Benguela, during October 2010. A unique high-resolution hydrographic dataset of the top 100 m of such a filament is presented in combination with remote sensing satellite data as well as results from a regional ecosystem model. The instruments and sampling design as well as the model description are presented in Chapter 2. In light of the transport regimes described in Chapter 4, the importance of understanding mesoscale features like upwelling filament and the contribution they may make to the cross-shore exchange within a marine system is highlighted in the current chapter.

5.1 Surface structure of the upwelling filament

The surface signal of upwelled water being transported offshore as well as the local westward protrusion of the upwelling front, which generally separates the cool freshly upwelled coastal waters and the warmer oceanic waters, could clearly be observed in the interpolated SST satellite data (Figure 5.1) of the 2nd of October 2010. This feature extended from the coast of Namibia offshore to approximately 18.5°E and was centered between 18 and 19°S, with an average width of 110 km. The present feature therefore conformed to the filament definition set by [Kostianoy and Zatsepin, 1996] with L/d $>$ 2 (L being length and d being width of the filament), and the feature protruding more than 50 km from the main thermal upwelling front. Strong temperature gradients clearly defined the filament width, with a particularly strong equatorward gradient and a more subtle one at the poleward boundary. Further

SST images obtained prior and subsequent to the survey period (Figure 5.2) indicated that filament development most likely commenced at the Cape Frio upwelling cell following initial coastal upwelling on the 24th of September. With strong southerly winds still dominating the period prior to the 28th of September some of the upwelled water seemed to have been pushed northward in a tongue-like feature, while a narrow truncated patch of similar temperature at 10°E suggested the filament was already extending offshore. Once the winds relaxed, the upwelled water spread southward and further offshore to reach its maximum westerly span (400 km offshore) by the 30th of September. Over the subsequent six day period the surface signal of the feature decayed rapidly. The periods observed here for filament growth and decay are similar to results from [Van Foreest et al., 1984] who suggested that filaments in the Benguela north of 30°S tend to form and decay over approximately seven day periods. In contrast to their results however, the satellite observations seem to suggest that the filament did not remain stationary and unchanged for an extended period (5-35 days), but that decay commenced only days after its maximum offshore extension was reached. In their study [Kostianoy and Zatsepin, 1996] however, also mentioned that cold filaments were only observed in the SW African upwelling region for 1-3 day periods based on about 100 IR images. Results discussed in section 5.5 from a MOM-4 model however revealed the subsurface presence of the filament for approximately 20 days, which is in line with [Van Foreest et al., 1984]'s findings and show potential discrepancies between what is visible at the surface and what is actually occurring subsurface.

5.2 Vertical structure of the upwelling filament

Thermosalinograph temperature measurements along transect 1 revealed that the minimum temperature value within the core at the surface was 1 °C colder than the surrounding waters, while the difference in salinity was only 0.2 (Figure 5.3). A sharp drop in specifically temperature was observed at the equatorward boundary of this transect. Current data presented below will reveal that these sharp boundaries are caused by the complex cross-shore circulation pattern in and around the upwelling filament. Both temperature and salinity profiles from transect 1 do however, suggest two possible cores, one centered at 18.85°S and another at 18.35°S. Along transect 2 the surface temperature and salinity profiles showed no clear evidence of the filament core (Figure 5.4). The only pronounced feature along this transect is a very dramatic increase in both temperature and salinity at the equatorward boundary (18.10°S).

Concurrently measurements were taken through the water column up to 100 m depth with an undulating CTD. Transect 1, sampled on the 1st of October and located closest to the Namibian coast, revealed a thin (<10 m) warmed surface layer across. However, below this depth (10-100 m), a colder, fresher cored feature was clearly visible (Figure 5.5 (a) and (c))

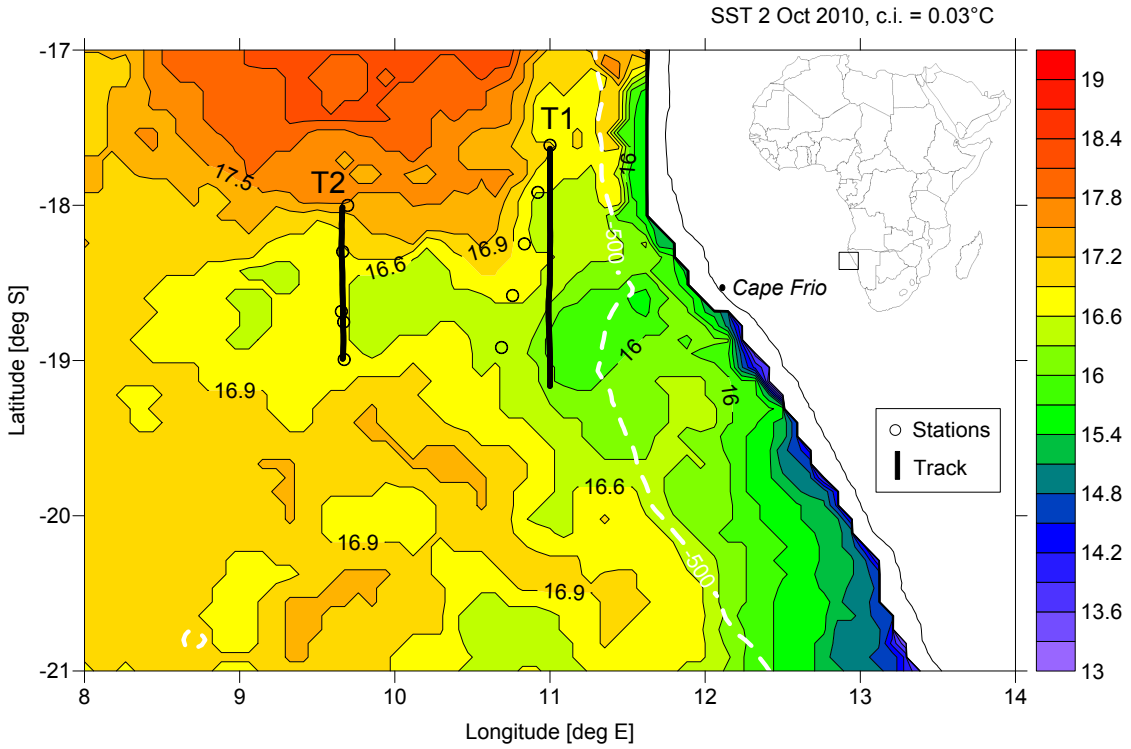

Fig. 5.1: Processed optimum interpolated Sea Surface Temperature (°C) image for 2 October 2010 from TMI and AMSR-E (NOAA) with a 0.25° longitude by 0.25° latitude grid resolution and an accuracy ranging between 0.2-1.0°C. The upwelling filament is evident between 18 and 19.5° South, extending from the coast of Namibia to 8.5° East. Transects (T1 and T2) surveyed with an undulating CTD (Scanfish) as well as the station locations across the filament are shown. The 500 m depth contour is also indicated.

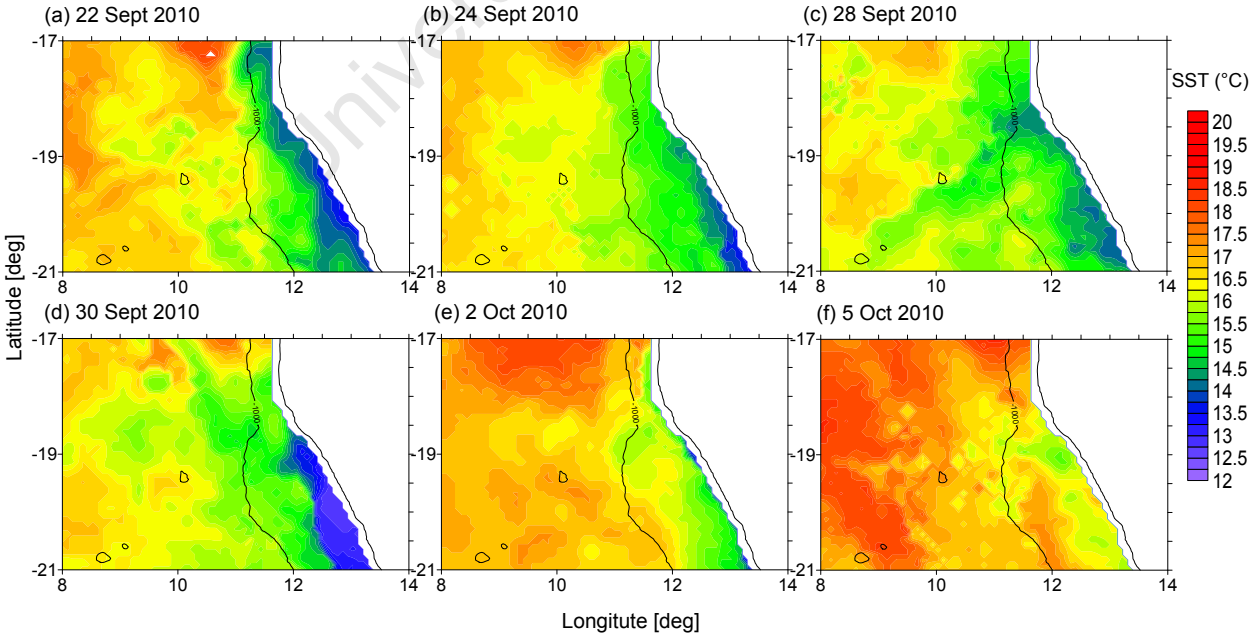

Fig. 5.2: Tracking the development and decay of the Oct 2010 upwelling filament from SST satellite images from 22 Sept to 5 Oct 2010. The 1000 m isobath is indicated.

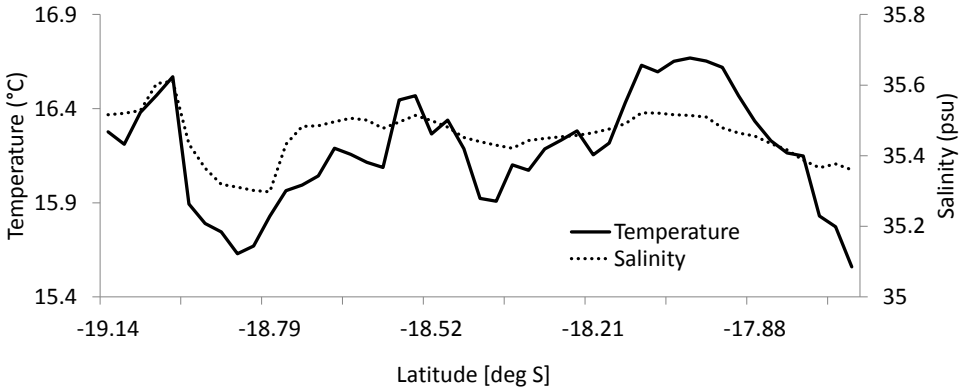

Fig. 5.3: Sea surface temperatures and salinities from the salinograph along transect 1 (11°E).

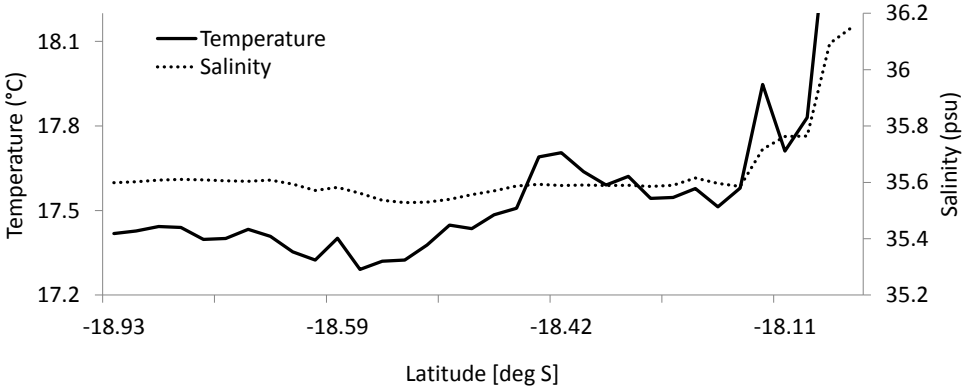

Fig. 5.4: Sea surface temperatures and salinities from the salinograph along transect 2 (9°E).

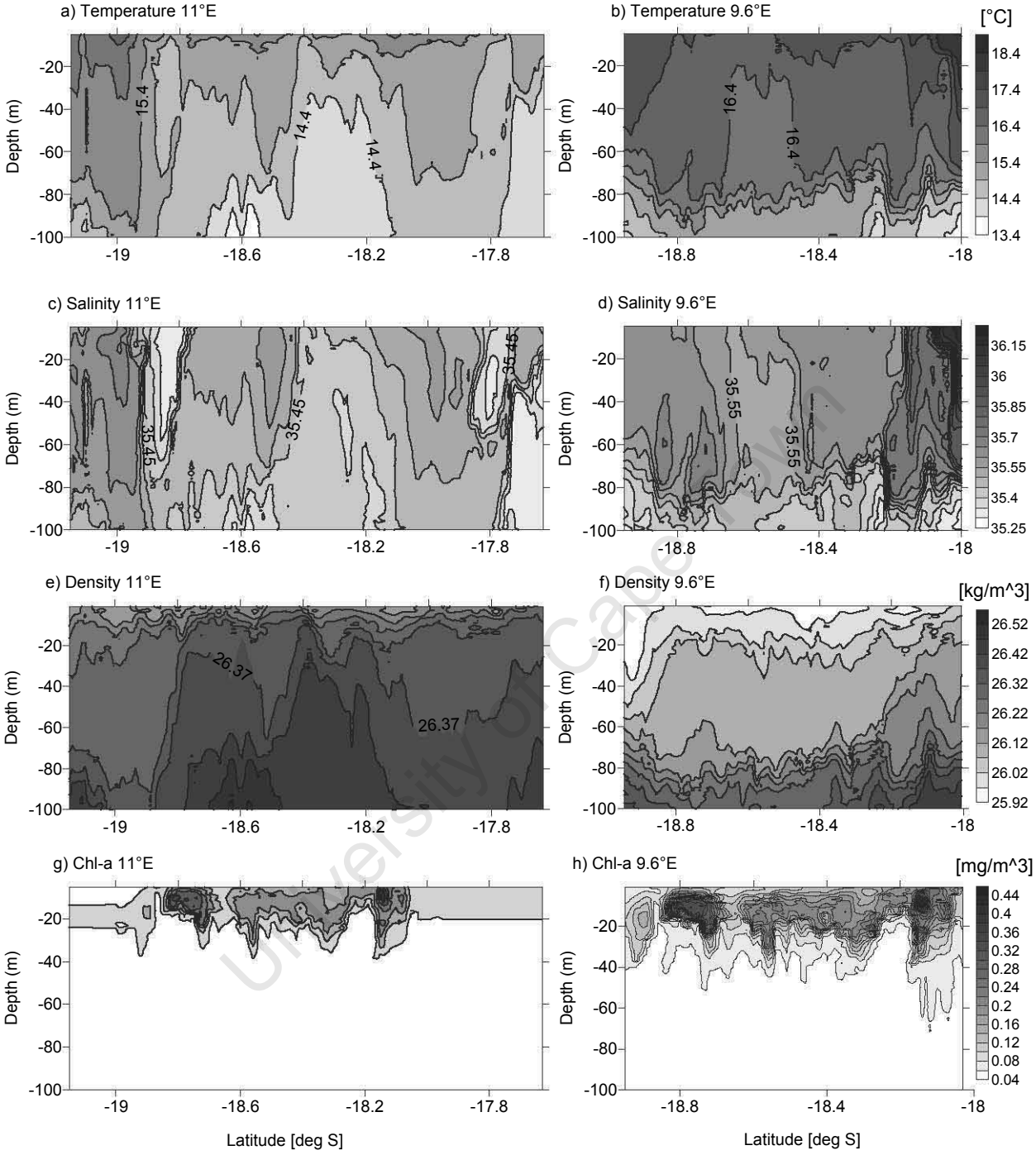

Fig. 5.5: Transects across the upwelling filament: (a) Vertical temperature (°C) profile through transect 1 (11°E), (b) Vertical temperature (°C) profile through transect 2 (9.6°E), (c) Vertical salinity profile through transect 1 (11°E), (d) Vertical salinity profile (°C) through transect 2 (9.6°E), (e) Vertical density (kg·m^{-3}) profile through transect 1 (11°E), (f) Vertical density (kg·m^{-3}) profile through transect 2 (9.6°E), (g) Vertical fluorescence chlorophyll (mg·m^{-3}) profile through transect 1 (11°E), (h) Vertical fluorescence chlorophyll (mg·m^{-3}) profile through transect 2 (9.6°E). Maximum depth of available data is 100 m.

centered at approximately 18.25°S and with a horizontal width of 38 km. On either side of the core the near-surface isotherms and isohalines sloped up very steeply from 70 m to about 10 m below the surface. Temperature within this central core was approximately 1.6 °C and salinity 0.26 lower than water at the same depth south of the filament (at 19°S). Directly south of the central core there appeared to be a weaker core, centered at 18.65°S, containing slightly warmer (0.4 °C warmer) and more saline (0.04) water than the main core but it was, nevertheless, still colder and fresher than the water mass to the south. Similarly, steep isotherms and isohalines marked the edges of this weaker core, which had a horizontal extend of 35 km.

Two very distinctive cold (14.9°C) and fresh (35.3) fronts at 18.85 and 17.80°S, extending from the surface to approximately 70 m, could also be observed in both the temperature and salinity profiles, while a warm (15.4°C) more saline (35.6) front was present at 18.5°S. Strong horizontal gradients were associated with the density profile of transect 1 (Figure 5.5 (e)), with the dense filament core or double core (26.4-26.5 $kg{\cdot}m^{-3}$) present in the centre of the transect (18.1-18.9°S) and an additional upward sloping of the isopycnals north of 17.9°S. Vessel-mounted ADCP data revealed the associated flow pattern (Figure 5.6 (a)) associated with the filament, by showing strong offshore velocities (0.10-0.25 $m{\cdot}sec^{-1}$) in the region 18.9-18.6°S as well as north of 18.1°S and the compensatory onshore velocities (0.14-0.32 $m{\cdot}sec^{-1}$) further north between 18.5-18.1°S as well as south of 18.9°S. Despite the surface currents being much stronger, the associated on and off-shore transport can be observed up to 400 or 500 m depths. Fluorescence chlorophyll measurements along this transect showed two zones where phytoplankton was present in high concentrations (>0.6) (Figure 5.5 (g)). These zones corresponded to the relatively warmer and more saline regions around the central core, where mixing between filament water and ambient oceanic water would occur. This observation is consistent with previous findings which suggest high productivity or high phytoplankton standing crop tends to have their local maxima at the border or just outside of upwelling fronts [Dengler, 1985; Simpson et al., 1979]. The chlorophyll maximum was confined to the top 10 m, with very little chlorophyll observed at deeper levels. Additionally, the filament cores contained water with a much lower dissolved oxygen (DO) content ($<$ $2\,ml{\cdot}L^{-1}$), with the water mass present at the less dense 18.65°S core being nearly depleted of dissolved oxygen (not shown), and regions of high DO corresponding to regions of high primary production.

In contrast, transect 2, located 140 km west of transect 1, showed that the top 30 meters of the water column had already been stratified (Figure 5.5(b) and (d)) by the 4th of October. This stratification can most likely be attributed to a combination of surface warming as well as either advection of warmer surrounding water into the filament or filament subduction beneath a surrounding water mass of lower density. The latter argument will be discussed in more detail in section 5.5. However, a single distinctive cold, less saline core could still

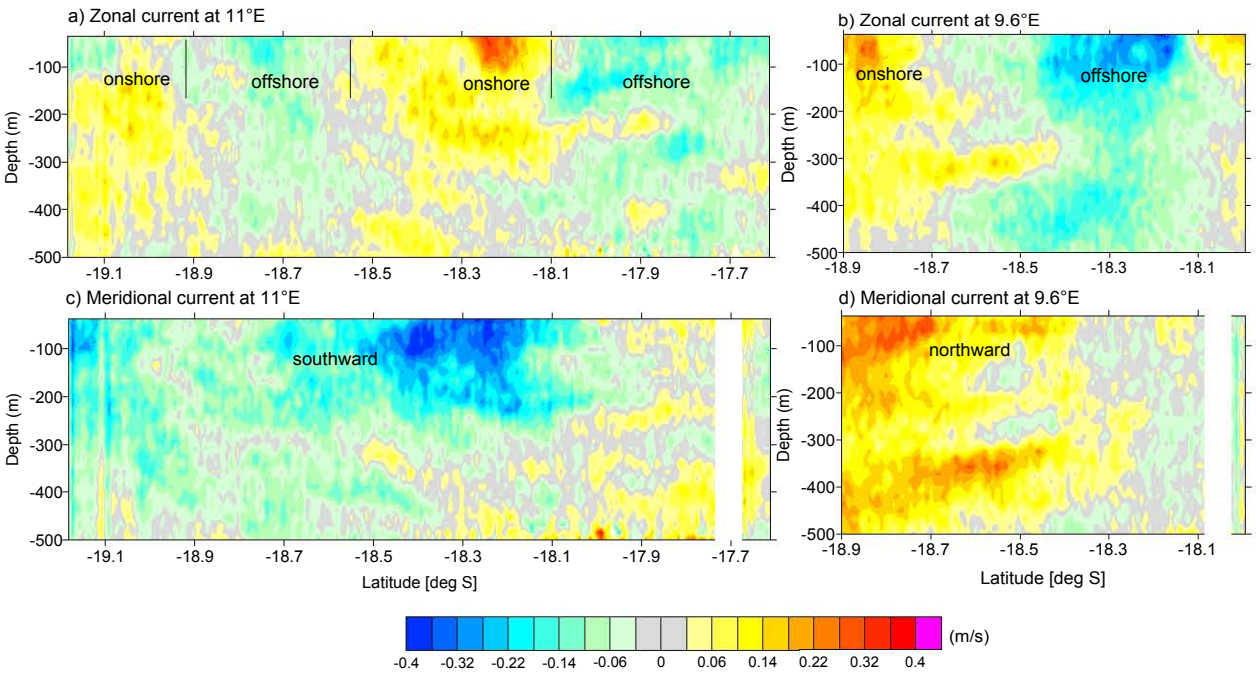

Fig. 5.6: Zonal current from ADCP (m·sec^{-1}) along (a) transect 1 and (b) transect 2 and meridional current (m·sec^{-1}) from ADCP along (c) transect 1 and (d) transect 2. Positive is northward (onshore), negative is southward (offshore). Note: maximum depth is 500 m.

be observed between 30 and 70 m depths, across the transect.

The isohalines sloped up very sharply from 70 m depth to the surface, while the isotherms only sloped up to 20 m below the surface. Even though the feature was much weaker than in transect 1, the core was still 0.8 °C colder and 0.12 fresher than the surrounding water masses. Below the filament feature the steady thermocline could be observed up to 100 m depth. An interesting feature observed in both the temperature and salinity profiles was however a very sharp equatorward front between 18°S and 18.1°S, where there was a nearly 2 °C and 0.24 change in temperature and salinity over a horizontal distance of less than 11 km. Despite being in a decaying state the filament core could still be observed as the zone, between 30-70 m depth, with weaker vertical density gradients along transect 2 (Figure 5.5 (f)). ADCP measurements (Figure 5.6(b)) along this transect showed that strong offshore transport (0.4 m·sec^{-1}) dominated the equatorward two thirds of the profile, whereas south of 18.7°S onshore transport was observed to depths of 500 m but with the strongest currents in the surface 100 meters.

Horizontal profiles of latitude versus temperature or salinity from three different depths along each transect allowed comparisons not only between the two transects at the same latitude but also latitudinal variation down the water column along each transect. The warmer water mass (16°C) to the south is clearly visible at all three depths across transect 1 (Figure 5.7). This is followed by a sharp temperature drop of approximately 1 °C throughout the water column. At 80 m depth the initial temperature drop (north of 19°S) steadily proceeds down

to the lowest levels (14.2°C) attained at this depth. In contrast, at 20 and 40 m depths there is the initial (1 °C) temperature drop and then a second drop (0.5 °C) north of 18.5°S. The 80 m profile suggest a wide cold core feature stretching from 18.8 to 18.2°S, while higher up in the water column further evidence for the two cores described above could be seen. The weaker southerly core can be seen at 18.6°S with minimum temperatures of just below 15 °C and the more pronounced central core at 18.3°S with 14.4 °C temperatures at 40 m depth. Equatorward of the northern core temperature rises again but only attains intermediate values (14.7-15.7 °C). North of 17.9°S temperatures at 40 and 80 m depths drop to values even lower than those observed at the central core, suggesting a possible third core or sharp front at the equatorward end of the data. The limitations of the present data set makes it difficult to substantiate the presence of the suggested second core. In contrast to transect 1, temperatures in transect 2 were at least 0.5 °C and up to 1.5 °C warmer. A similar pattern of temperature increase could however be observed at the poleward end, with the cold core (at depths 40 and 60 m) observed between 18.7 and 18.5°S. The rise in temperature at the equatorward end of transect 2 was thus sharper than at the poleward end. The filament core also showed a south-westerly displacement of about 33 km between the two transects. The horizontal salinity profiles for transect 1 are similar to the temperature profiles described above, the very sharp fronts, containing fresher water, at approximately 18.85 and 17.8°S being the exceptions (Figure 5.8). Most of transect 2 had a very similar structure to that of transect 1 in terms of temperature structure. Within the salinity structure there was a very pronounce increase at the northern border. Similar also to the temperature profiles, salinity values along transect 2 were higher at all depths than along transect 1. For large sections of the core, the salinity values were similar to the more mixed section of the core in transect 1.

The general hydrographic properties of the filament thus conformed well to what had previously been recorded in the Benguela and other eastern boundary upwelling systems and clearly at least two different water masses contributed to the dynamics of the feature. The high resolution data set also allow a fresh insight into the mesoscale structure within such a feature. In particular the fronts on either side of the core have up to present not been recorded in such detail. Of real interest was the cold, fresh water at the poleward fronts of what appears to be two cores along transect 1. The direct current measurements particularly along transect 1 additionally revealed a very complex circulation pattern associated with the filament where both on- and offshore exchange persist.

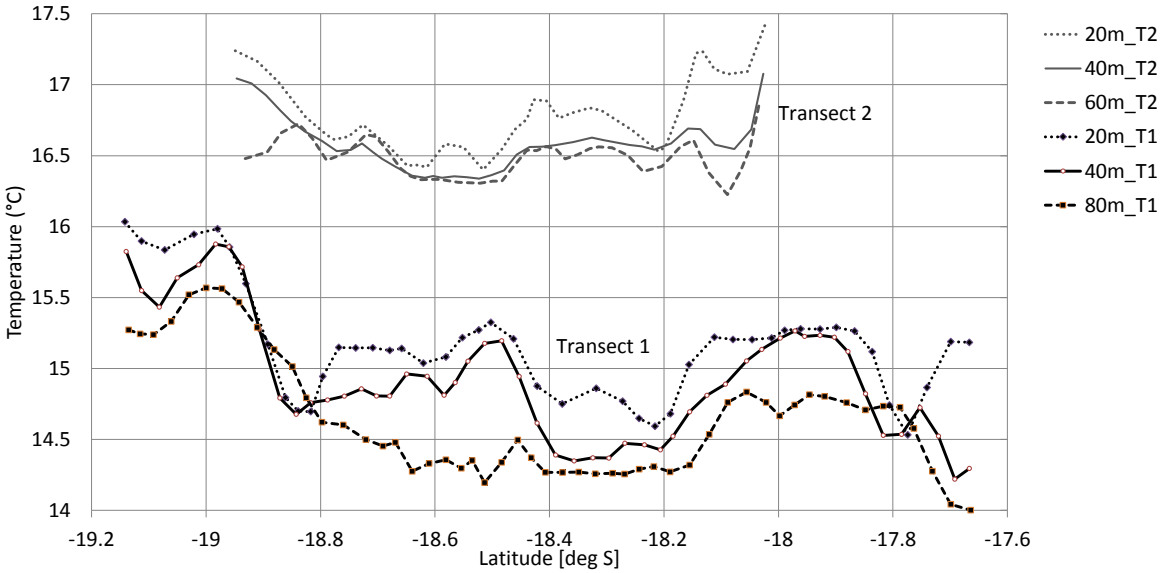

Fig. 5.7: Horizontal latitude vs temperature profiles extracted from three different depths (20,40 and 60/80 m) along each transect.

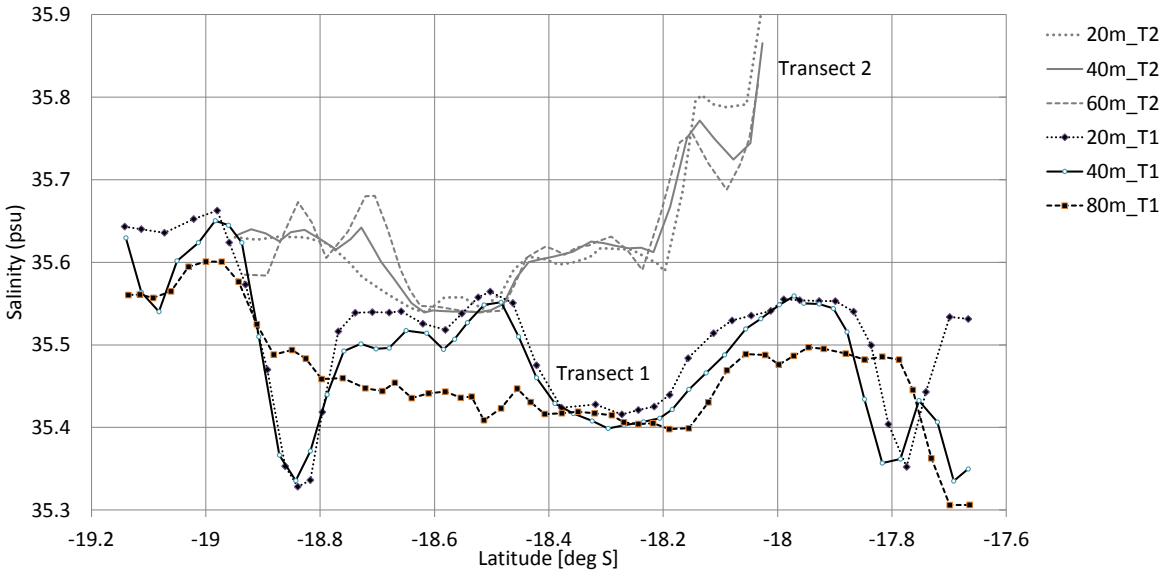

Fig. 5.8: Horizontal latitude vs salinity profiles extracted from three different depths (20,40 and 60/80 m) along each transect.

5.3 Circulation and transport associated with the upwelling filament

Offshore transport through each transect was calculated from the ADCP current measurements by integrating over the cross-sectional area above 500 m depth and across the width of each transect. The results allow a preliminary estimate of transport within the feature. Despite spatial variability in the transport along both transects, offshore transport across transect 1 was found to be 2.98 Sv integrated over 500 m depth and there was a 2.00 Sv onshore transport. In contrast across transect 2 the offshore transport was 3.28 Sv, and 1.81 Sv onshore transport, meaning more water is transported offshore than is retransported back onshore along both transects. Our values were in line with that from [Huyer et al., 1991], who found offshore values between 1.4-4.2 Sv (onshore between 0.2-1.0 Sv) along a 244 km alongshore transect next to the coast of California. In their study the transport, related to geostrophic flow, was also calculated to 500 m depth. Their results further suggested that when the filament was at full strength and still developing, offshore transport was much stronger than the onshore transport. The decaying state of our filament could thus account for the relatively larger onshore transport recorded.

Results from a MOM-4 ecosystem model, representing the same filament described thus far, revealed the large scale regional circulation associated with such a filament. Despite the slight geographic displacement of the filament in the model, the spatial dimensions were found to be similar (Figure 5.9). The current vectors averaged over 20-40 m depth show the strong offshore transport within the cold offshore extension of the upwelling filament. Despite the absence of measured SSH data, both the temperature profile and current measurements from the model support previous results by indicating a dipole like eddy field across the region where the filament is observed [Marchesiello et al., 2003; Sanchez et al., 2008]. There is thus evidence of both cyclonic recirculation onshore as well as anticyclonic offshore transport being related to the feature. Similar to [Sanchez et al., 2008]'s measured and [Marchesiello et al., 2003]'s model results there appears to be a convergence of oceanic water at the equatorward filament edge, where a cyclonic cell is observed to be interacting with the cyclonic circulation related to the core of the filament.

For a three day period from 2-4 October weak south-westerly winds, with a mean speed of 4.45 $m \cdot sec^{-1}$, dominated across the study area, and the corresponding mean Ekman transport for this period was 0.68 (maximum values 1.2 $m^3 \cdot sec^{-1} \cdot m^{-1}$). This means that the offshore transport within the filament (being within the range 10-30 $m^3 \cdot sec^{-1} \cdot m^{-1}$) was more than ten times the Ekman transport providing further evidence for filaments being a major mechanism for the exchange between the coastal and offshore regions. In filaments studied off the coasts of California [Flament et al., 1985; Kosro and Huyer, 1986; Ramp et al., 1991] and north-west Africa [Navarro-Perez and Barton, 1998] the offshore transports

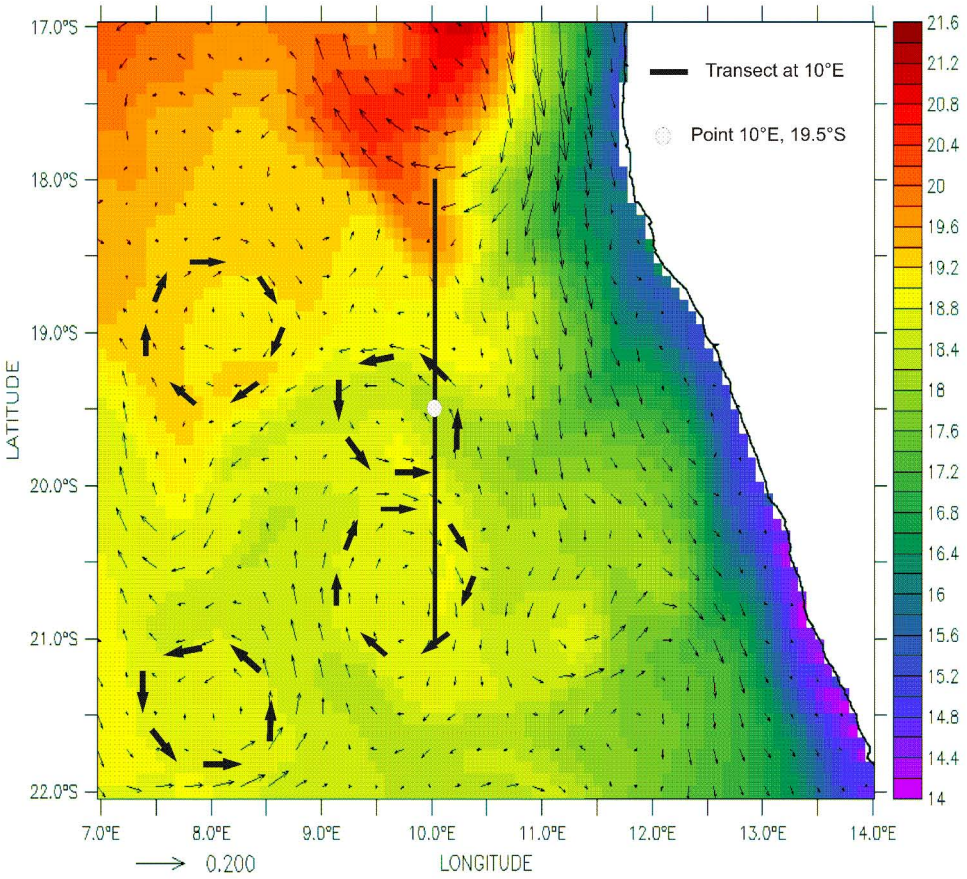

Fig. 5.9: Temperature at 30m depth from MOM-4 model with current vectors (m/s) averaged between 20-40m. The transect presented in Figure 5.12 (black line) and the station presented in Figure 5.13 (white mark) are both shown. The dipole eddies have been marked for clarity.

recorded were also found to be substantially larger than the regional Ekman transport.

5.4 Frontal mixing in the upwelling filament

Measurements from the Microstructure probe (MSS) allowed some insight into the turbulent processes within the filament feature (Figure 5.10). Despite being limited to 5 stations along the 167 km distance of transect 1, low TKE dissipation rates defined the single subsurface core feature observed in this data set at 18.6°S. Intensive mixing was, however, observed at the poleward boundary (18.91°S) of the core from the surface to 70 m depth. In contrast, at the equatorward boundary, strong mixing seemed to be limited to the top 40 m. These observations are similar to previous results which showed enhanced mixing at the frontal zones of a filament, while in the core it tends to be restricted to the upper layers of the water column [Dewey et al., 1987; Barton et al., 2001].

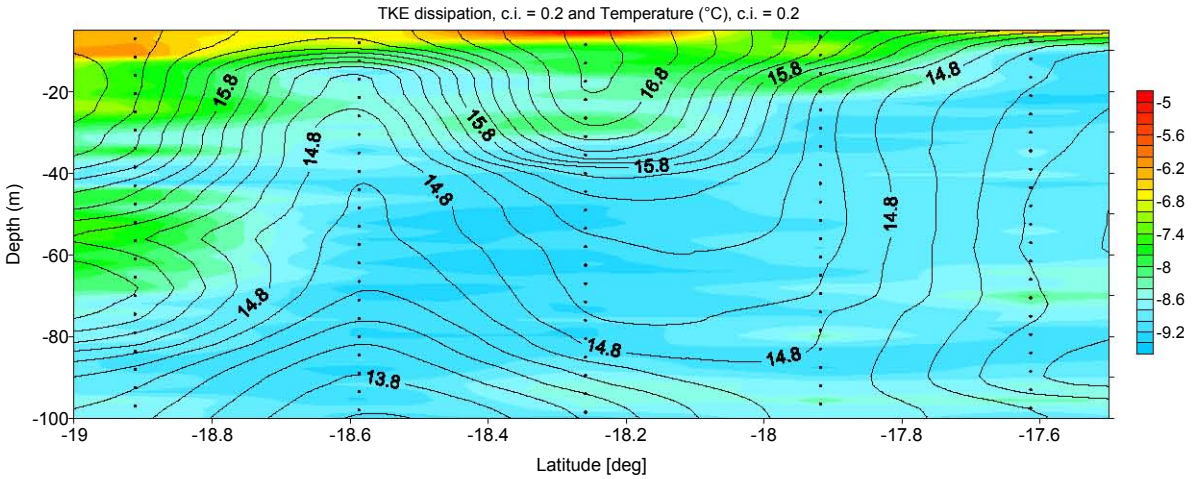

Fig. 5.10: TKE dissipation [log 10 ($W \cdot kg^{-1}$)] along transect 1 (color plot) with isotherms (°C)(black contours). Exact MSS stations are marked by black dotted lines.

5.5 Filament development over time

The subsequent CTD- and xbt-station sampling along approximately the same line as transect 1 allowed a brief look into the scales of change within the filament. Despite the lower spatial resolution of the combined CTD-xbt dataset, all the main filament features were present in the temperature profile of transect 1 (Figure 5.11). At the northern end of the data, no discernable difference can be observed between the two data sets, with this also being the region where sampling was still conducted along the exact same longitudinal line. Further south variations between the profiles can be observed, with only one core visible in the lower resolution data. The temperature between the cores however, remained the same ($<$14.5 °C) between the two profiles. In addition, there was a pronounced surface warming by more than 2 degrees in the upper 20 meters of the CTD-xbt profile. As the velocity profiles above showed though, advection of water masses with different properties through the filament seemed to be a crucial aspect of changes taking place within the filament over time, although no clear conclusions can be made in this regard based on the available measured data presented so far.

A Hovmöller diagram (Figure 5.12) using MOM-4 temperature as well as zonal current data at 30 m depth along a transect at 10°E showed both the evolution of the cold cored filament as well as the associated zonal transport along a transect at 10°E over time. Furthermore, the results of Figure 5.12 are similar to the SST results in section 5.1 in that both show the commencement of filament presence on the 24th of September 2010. While offshore transport dominated the filament core, onshore transport was associated with both the northern and southern boundaries, with the transport observed at the poleward border being stronger and more persistent. In addition, the periods prior and subsequent to the strong

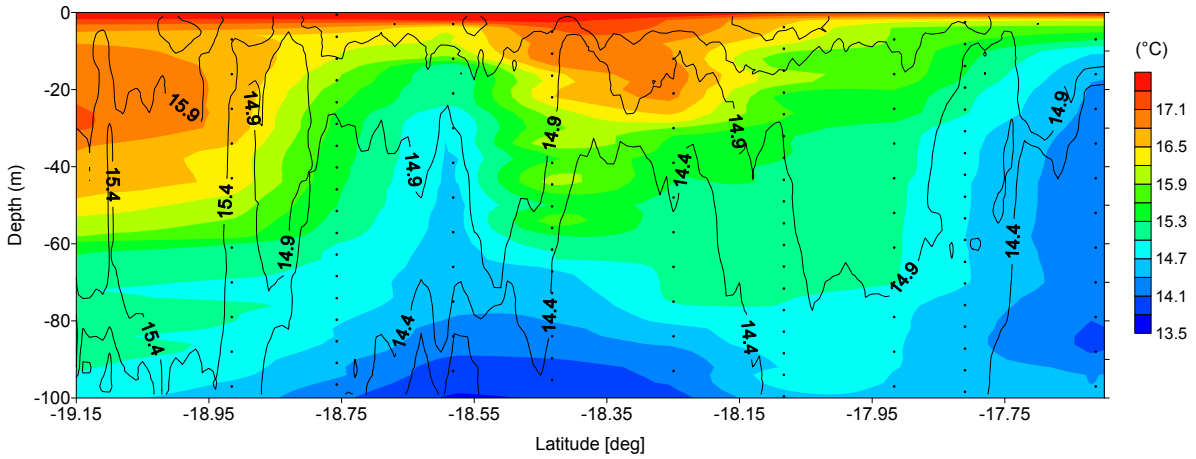

Fig. 5.11: Comparing temperature (°C) profile of the combined CTD-xbt(color plot) with the scanfish profile (black contours) along transect 1. Station locations are indicated as black dotted lines. Approximately 48 hours lapsed between sampling. Data limited to 100 m depth.

temperature signal related to the filament, showed a diminishing onshore transport, with offshore transport dominating these periods across the transect. From both these figures as well as the calculated transport fluxes above it seems that rather than just increasing local offshore transport, the transport associated with the upwelling filament contributes rather significantly to cross-shore exchange by enhancing both on- and off-shore transport locally. In addition the model data reveals an interesting dynamic regarding the development of the filament through the water column and over time as can be seen in Figure 5.13. Here at a point along the centre of the filament core (10°E, 19.5°S) temperature, salinity and density data show that in addition to dissipation of the filament signal from the surface there is also an upward sloping of isopycnals at the base of the feature. The irregularity of change associated with the surface layers of the water column suggests that surface warming alone is not sufficient to explain the sinking of the filament over time. Additionally advection from surrounding water masses, supported by the current data in section 5.2, or the subduction of the feature below a less dense water mass should be considered as this is supported by the density profile in Figure 5.13(c).

5.6 Section summary

The filament described here was observed just offshore of Cape Frio, one of the three preferential upwelling zones where filaments tend to consistently advance far offshore [Van Foreest et al., 1984; Lutjeharms and Stockton, 1987]. Both satellite and ship-based data suggested that the present filament was most likely in a decaying state during sampling. Thus due to the limited area sampled as well as the low temporal resolution, with respect to the

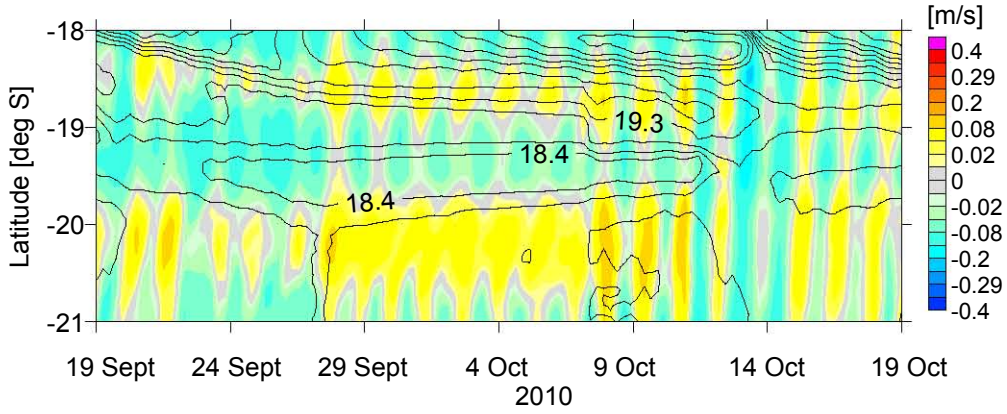

Fig. 5.12: A Hovmöller diagram showing the temperature (°C) contours and corresponding zonal velocity ($m \cdot sec^{-1}$) (color plot) from a MOM-4 model. The filament presence is seen here at 30 m depth between 19 and 20°S, 10°E from the 20th of September to the 14th of September 2010. Zonal current also taken at 30 m depth. For transect orientation relative to filament see Figure 5.9.

decaying time scale of the filament, of our data set, it is difficult to make any concluding statements with regard to the large scale velocity structure of the sampled filament. This study, therefore, does not contribute much to clarify the dominant processes which drive filament development in the northern Benguela. The study does, however, provide much more detail into the mesoscale structure and velocity field in and at the boundaries of the core of a northern Benguela filament. Of real interest was the substantial recirculation observed within the filament, based both on the high resolution hydrographic data, the directly measured currents and the results from a MOM-4 ecosystems model. A strong onshore transport, of warmer water was observed, at the poleward borders of the core to counteract the offshore transport, of colder, fresher water, associated with the core of the feature. In addition, the offshore transport associated with the feature as a whole, being of the order of magnitude of 3 Sv, was found to be substantially larger than the integrated Ekman transport across the study area. Coastal waters were thus clearly being transported offshore by the upwelling filament and the corresponding onshore recirculation allowed for strong frontal mixing with the oceanic waters at the core edges.

The complex circulation dynamics, in combination with both the spatial extent of the feature and the chlorophyll-a distribution across the filament, therefore, again highlighted the potential of these features to play an important role in the across-shelf biological exchange within an ecosystem. More importantly though the evidence suggests that water, which had been modified through its interaction with the surrounding water masses and to a lesser degree the surface, was being transported back onshore within the eddy driven recirculation particularly at the poleward boundary of the filament. This eddy flow field was not dissimilar to that observed by [Marchesiello et al., 2003] and [Sanchez et al., 2008]. Additionally it can be suggested that the filament feature was sinking through the water column, as it was being subducted beneath a less dense water mass over time. This becomes important to

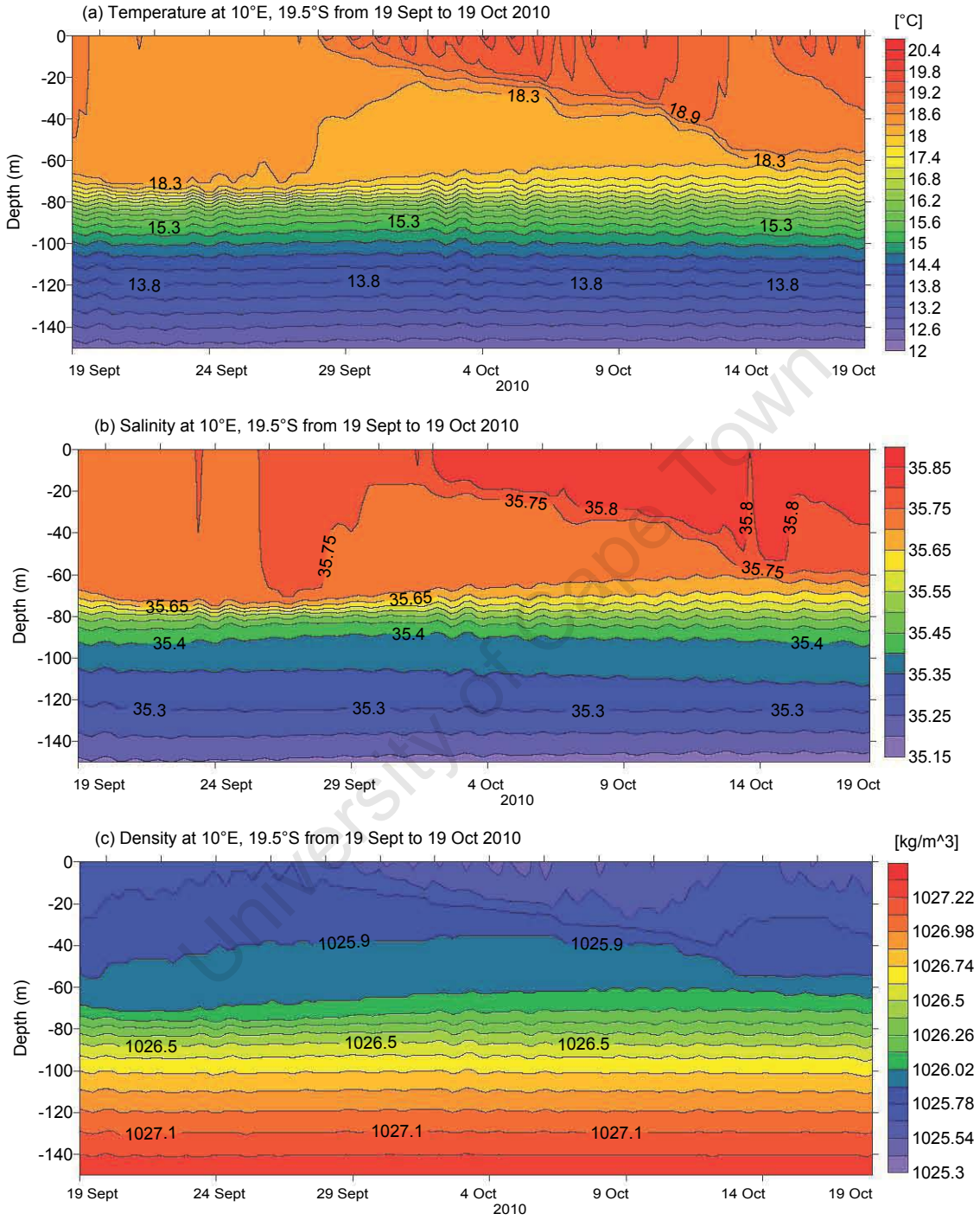

Fig. 5.13: A Hovmöller diagram showing (a) temperature (°C), (b) salinity and (c) density over time at 10°E, 19.5°S centered along filament core in MOM-4 model from 19 September to 19 October 2010 from the surface to 150 m depth. See Figure 5.9 for location of point.

consider with reference to the biological productivity expected to be associated with such a filament. More work however remains to be done in the northern Benguela on the mesoscale processes which drive filament occurrence, development, magnitude, the temporal and spatial scales observed and the energy available for mixing and overturn within these features. Certainly, hydrodynamic or ecosystem models with a higher spatial resolution could provide a unique tool to observe filaments and their dynamics within the Benguela ecosystems. The results presented here however sufficiently show the complex contribution which mesoscale features like upwelling filaments make to local cross-shore circulation and therefore highlight the importance of evaluating local cross-shore exchange with reference to these mesoscale structures and processes.

Chapter 6

Conclusions, limitations and recommendations

The purpose of this research, as stated in section 1.2, was both to quantify where, how much and by what mechanisms water leave or come on to the Namibian shelf as well as to gain a better understanding into the physical dynamics of upwelling filaments within the northern Benguela system and to try and quantify their contribution to the exchange across the shelf edge. The aim was to use data from a MOM-4 regional ecosystem model as well as remote sensing and cruise data for the analyses. The ultimate goal was to provide quantitative information on the contribution of the shelf edge exchange and longshore processes to ecosystem dynamics in the northern Benguela upwelling system. Despite the preceding three chapters being essentially 'stand alone' with section specific results, there is a rational behind their chronology and an association between their content, with Chapter 1 reviewing past research, Chapter 2 outlining the methods and data sources, including a model description, Chapter 3 focusing on preliminary model validation in order to quantify transport fluxes across the northern Benguela shelf in Chapter 4. Finally Chapter 5 is devoted to a case study of an upwelling filament off Cape Frio during October 2010 and the circulation dynamics associated with this feature. Here the results from the individual sections will be summarized, and the main findings as well as the limitations of this research will be highlighted and suggestions will be made for future work.

6.1 Simulating the regional features of the northern Benguela using a MOM-4 ecosystem model

Due to a lack of prior literature dealing with the validation of the MOM-4 regional ecosystem model adjusted for the Benguela, from which data is used in this project, chapter 3 was dedicated to the comparison of measured data from various sources with the output from the MOM-4 ecosystem model described in chapter 2 in order to establish the validity of using the output for the analysis in this project.

The MOM-4 ecosystem model is able to sufficiently simulate regional patterns and features across the northern Benguela region, and therefore provides a unique tool for evaluating both large scale circulation as well as coastal processes. This is invaluable in the context of the critical role the regional circulation plays in the modification of both the shelf conditions as well as water mass properties. The model is able to simulate not only the southward flow of the poleward undercurrent [Nelson, 1989; Shannon, 1995; Monteiro and van der Plas, 2006; Mohrholz et al., 2008; Monteiro et al., 2008], and the equatorward transport of the northern Benguela coastal current [Shannon and Nelson, 1996; Moroshkin et al., 1970; Wedepohl et al., 2000], but also the seasonal variation associated with these features. Furthermore, the main upwelling cells across the northern Benguela, i.e. Lüderitz, Walvis Bay, Namibia, and Cape Frio, are also sufficiently resolved [Hardman-Mountford et al., 2003; Bakun and Nelson, 1991; Shannon and Nelson, 1996] by the model.

Future work remains in improving model performance and particular attention should be paid to possible reasons for the overestimation of both temperature and corresponding salinity in the surface 200 m of the water column. It is recommended that ocean biology-induced heating, the underestimation of the mixed layer depth related to the K-profile Parameterization (KPP) mixing scheme [Large et al., 1994] used by the model as well as the low resolution (1.875° spatial and 6 hourly) of the NCEP temperature data used in forcing the model should be considered in a quest to identify the cause and allow model improvement. In the context of this study, the model deviations were however accepted as reasonable for the purposes of the analyses presented. It could further be of interest to compare results from this MOM-4 model with the ROMS model of [Veitch, 2009; Veitch et al., 2010] in future cooperative work in order to evaluate the strengths and weakness of both approaches.

6.2 Large scale circulation in the northern Benguela and transport across the shelf edge

In an effort to evaluate whether the ventilation of the Namibian shelf is driven primarily by the longshore advection, and only modified by the cross-shore advection, chapter 4 focused on analyzing and quantifying regional transport fluxes and flux budgets along the 300 m deep shelf next to the coast of Namibia. This is important in order to gain a deeper understanding into the role that these processes and possible changes to them may have for oxygen and nutrient availability on the shelf.

The results in this section showed that the simplified cross-shore transport previously suggested [Brüchert et al., 2003; Mohrholz et al., 2008] may not be sufficient for describing the northern Benguela region as a whole. Instead it is shown that if the northern Benguela shelf is divided into four regions, each of these regions exhibit unique meridional and cross-shore dynamics. The four regions chosen were : A) 16°-19°S, including the Cape Frio upwelling cell, B) 19°-22°S, C) 22°-25°S, offshore of Walvis Bay and D) 25°-28°S, which surrounds the Lüderitz upwelling cell. This selection offer an opportunity to investigate the circulation dynamics surrounding the two major upwelling cells (Cape Frio and Lüderitz) and to compare these with the two central regions, where upwelling also occurs but in the form of smaller upwelling cells. The approach also allowed an opportunity to expand on the recent work of [Veitch, 2009; Veitch et al., 2010] by conducting an intensive study into the hydrographic dynamics of the northern Benguela.

Results for the region surrounding the Lüderitz upwelling cell again enhance the view that this region acts as a barrier between the southern and northern Benguela and may inhibit migration of certain species [Agenbag and Shannon, 1988; Hutchings et al., 2009] between the southern and northern Benguela regions. Despite the Lüderitz region showing year round offshore transport, it was found that in summer, as the poleward undercurrent reaches its maximum southward extent somewhere between 25 and 28°S, as previously suggested by [Mohrholz et al., 2008] , this influx from the north promotes the very strong offshore transport across the shelf. In contrast, during winter a strong flux from the south is seen to contribute strongly to the offshore flux. These influences however only form part of the number of forcings (including atmospheric forcings, open ocean circulation and turbulent interactions) shaping the upwelling dynamics associated with the Lüderitz upwelling cell. This result, however, suggests that despite the year round offshore transport across the shelf edge associated with this region, the properties of the water masses being transported offshore and the associated biological processes between summer and winter may be quite distinctive.

The results further show that the dynamics of the region off Cape Frio (defined here as 16-19°S) are much more complicated than the other regions and exhibited high spatial and temporal variability. Whereas there was clearly evidence for strong year round offshore transport in what appear to be distinct narrow jets, there was also evidence for a strong transport of water onto the shelf during summer, perhaps similar to what [Monteiro and van der Plas, 2006] suggested in their work on LOW. The great variability observed is however not entirely surprising as it has already been shown that the Angola-Benguela front migrates seasonally [Boyd et al., 1987] and the different water masses lying in close proximity and the related circulation would also be expected to be highly variable.

Transport across the shelf edge in the two central regions (19-22°S, and 22-25°S) conformed more to the simplified view of cross-shore circulation in the northern Benguela. Here, during summer (DJF) an onshore flux related to strong subsurface compensatory flow was observed, whereas an offshore flux, related to stronger Ekman transport, was observed for both regions during winter, although weaker than at the Lüderitz cell. The qualitative results in particular showed that in the region 19-22°S the subsurface onshore transport across the shelf edge was both stronger and more persistent and therefore that water masses from the deep ocean west of the shelf edge may play a crucial role in the upwelling of this region.

Thus, the results not only support past work which suggest that oxygen poor and nutrient rich SACW (South Atlantic Central Water) will flush the shelf during summer and that during winter oxygen rich and lower nutrient ESACW (East South Atlantic Central Water) will ventilate the shelf [Poole and Tomczak, 1999; Mohrholz et al., 2001; Brüchert et al., 2003; Monteiro and van der Plas, 2006], but they also highlight the unique interplay between the meridional currents in shaping the seasonal and geographic variability in transport across the shelf edge.

These results, however, only provide a mean view of the system based on climatologies from 2000-2008, and thus do not portray the great interannual variability in the circulation of the northern Benguela shelf which has been recorded [Brüchert et al., 2003, 2006; Monteiro and van der Plas, 2006; Hutchings et al., 2009].

6.3 Northern Benguela upwelling filaments

In section 5 the importance of understanding the contribution to the cross-shore exchange from mesoscale features like upwelling filaments is highlighted. This is done through a specific case study of an upwelling filament sampled in the northern Benguela during October

2010. The results provide great insight into the mesoscale structure and velocity field in and at the boundaries of the core of a northern Benguela filament. Of real interest was the substantial recirculation observed within the filament. While strong offshore transport, of colder, fresher water, was found to be associated with the filament core, there was strong onshore transport, of warmer water, observed at the poleward borders of the core. The offshore transport associated with the feature as a whole, being of the order of magnitude of 3 Sv, was found to be substantially larger than the integrated Ekman transport across the region. Coastal waters were thus clearly being transported offshore by the upwelling filament and the corresponding onshore recirculation allowed for strong frontal mixing with the oceanic waters at the core edges.

The complex circulation dynamics, in combination with both the spatial extent of the feature and the chlorophyll-a distribution across the filament, therefore, again highlighted the potential of these features to play an important role in the cross-shelf biological exchange within an ecosystem. More importantly though the evidence suggests that water, which had been modified through its interaction with the surrounding water masses and to a lesser degree the surface, was being transported back onshore within the eddy driven recirculation particularly at the poleward boundary of the filament. This eddy flow field was not dissimilar to that observed by [Marchesiello et al., 2003] and [Sanchez et al., 2008].

This combined work therefore indicates that in addition to the already complex large scale regional circulation across the northern Benguela, and the unique interplay between meridional and cross-shore advection, mesoscale features like upwelling filaments are extremely dynamic with the potential to dramatically shape local ecosystem dynamics on the shelf as well as across the shelf edge and into the open ocean.

6.4 Future research

Several avenues related to the work presented remain open for further exploration in the future.

As already mentioned, these results only provide a mean view of the system based on climatologies from 2000-2008, and do not portray the great interannual variability in the circulation of the northern Benguela shelf. Due to the importance of the Benguela ecosystem for commerce of the surrounding regions, it may be useful to examine the interannual variability in the flux budgets for the system. Furthermore, the results should be expanded to include oxygen and nutrient flux budgets through the four northern Benguela regions as

these are crucial components to the shelf condition of the northern Benguela. With the available data from the MOM-4 model for this region and the period 2000-2012, the scope of possibilities for future work are diverse.

More work also remains to be done in the northern Benguela on the mesoscale processes which drive filament occurrence, development, magnitude, the temporal and spatial scales observed and the energy available for mixing and overturn within these features. Certainly, hydrodynamic or ecosystem models with a higher spatial resolution could provide a unique tool to observe filaments and their dynamics within the Benguela ecosystem.

Bibliography

Agenbag, J. and Shannon, L. (1988). A suggested physical explanation for the existence of a biological boundary at 24°30s in the benguela system. *South African Journal of Marine Science*, 6:119–132.

Andrews, W. and Hutchings, L. (1980). Upwelling in the southern benguela. *Progress in Oceanography*, 9:1:81.

Armi, L. (1978). Some evidence for boundary mixing in the deep ocean. *Journal of Geophysical Research*, 83:1971–1979.

Badenhorst, A. and Boyd, A. (1980). Distribution ecology of the larvae and juveniles of the anchovy engraulis capensis gilchrist in relation to the hydrographic environment off south west africa, 1978-79. *Fisheries Bulletin, Sea Fisheries Institute South Africa*, 13:83–106.

Bailey, G. (1991). Organic carbon flux and the development of oxygen defficiency of the modern benguela continental shelf south of 22°s: spatial and temporal variability. *Geological Society Special Publication*, 58:171–183.

Bakun, A. (1993). *Large marine ecosystems - stress mitigation and sustainability.*, chapter The California Current, Benguela Current and Southwestern Atlantic shelf ecosystems: a comparitive approach to identify factors regulating biomass yields., pages 199–221. American Association for the Advance Science, Washington, DC.

Bakun, A. and Nelson, C. (1991). The seasonal cycle of wind-stress curl in subtropical eastern boundary current regions. *Journal of Physical Oceanography*, 21:1815–1834.

Barange, M. and Pillar, S. C. (1992). Cross-shelf circulation, zonation and maintenance mechanisms of the euphausiids nyctiphanes capensis and euphausia hanseni in the northern benguela upwelling system. *Continental Shelf Research*, 12 (9):1027–1042.

Barton, E., Inall, M., Sherwin, T., and Torres, R. (2001). Vertical structure, turbulent mixing and fluxes during lagrangian observations of an upwelling filament system off northwest iberia. *Progress in Oceanography*, 51:249–267.

Biscaye, P., Flagg, C., and Falkowski, P. (1994). The shelf edge exchange processes experiment, seep-ii: an introduction to hypotheses, result and conclusions. *Deep Sea research II*, 41:231–252.

Boyd, A. (1987). *The oceanographiy of the Namibian shelf.* PhD thesis, University of Cape Town, South Africa.

Boyd, A., de Sousa Neto, L., Barlow, R., da Silva, A., Wedeinge, J., Monteiro, P., Currie, B., Hutchings, L., Bartholomae, C., Peard, K., Verheye, H., Kreiner, A., Gibbons, M., and Roux, J. (2006). Final report submitted to isap for benefit project. In *BENEFIT project reports*.

Boyd, A., Salat, J., and Maso, M. (1987). The seasonal intrusion of relatively saline water on the shelf off northern and central namibia. *South African Journal of Marine Science*, 5:107–120.

Brüchert, V., Currie, B., Peard, K., Lass, U., Endler, R., Dübecke, A., Julies, E., Leipe, T., and Zitzman, S. (2006). *Past and present water column anoxia*, chapter Biogeochemical and physical control of shelf anoxia and water column hydrogen sulphide in the Benguela coastal upwelling system, pages 161–193. Springer, New York.

Brüchert, V., Jorgensen, B., Neumann, K., Riechmann, D., Schlösser, M., and Schulz, H. (2003). Regulation of bacterial sulfate reduction and hydrogen sulfide fluxes in the central namibian coastal upwelling zone. *Geochimica et Cosmochimica Acta*, 67:4505–4518.

Brink, K. (1983). The near-surface dynamics of coastal upwelling. *Progress in Oceanography*, 12:223–257.

Brink, K., Beardsley, R., Niiler, P., Abbott, M., Huyer, A., Ramp, S., Stanton, T., and Stuart, D. (1991). Statistical properties of near-surface flow in the california coastal transition zone. *Journal of Geophysical Research*, 96:14637–14647.

Brink, K. and Cowles, T.J., . (1991). The coastal transition zone program. *Journal of Geophysical Research*, 96:14637–14647.

Buchholz, F. (2010). Report of cruisereport of cruise d356 rrs discovery 10 september (walvis bay) to 13 october 2010 (cape town). *Cruise Report D356 RRS Discovery*, 356:1–20.

Capet, X., Colas, F., Penven, P., Marchesiello, P., and McWilliams, J. (2008). *Ocean Modeling in an Eddying Regime, Vol 177*, chapter Eddies in eastern boundary subtropical upwelling systems., page pp. AGU, Washington, D.C.

Chapman, P. and Shannon, L. (1985). *Oceanography and Marine Biology, an anual review.*, chapter The Benguela ecosystem 2. Chemistry and related processes., pages 183–251. Aberdeen University Press.

Chapman, P. and Shannon, L. (1987). Seasonality in the oxygen minimum layers at the extremities of the benguela system. *South African Journal of Marine Science*, 5:85–94.

Chavez, F., Strutton, P., Friedrich, G., Feely, R., Feldman, G., Foley, D., and McPhaden, M. (1999). Biological and chemical response of the equatorial pacific ocean to the 1997-98 el nino. *Science*, 286:2126–2131.

Chavez, F., P., Strutton, P., and McPhaden, M. (1998). Biological-physical coupling in the central equatorial pacific during the onset of the 1997-98 el nino. *Geop*, 25(19):3543–3546.

Chereskin, T., Morris, M., Niiler, P., Kosro, P., Smith, R., Ramp, S., Collins, C., and Musgrave, D. (2000). Spatial and temporal characteristics of the mesoscale circulation of the california current from eddy-resolving moored and shipboard measurements. *Journal of Geophysical Research*, 105:1245–1269.

Clarke, A. (1989). *Poleward flows along Eastern Ocean Boundaries*, chapter Theoretical understanding of eastern ocean boundary poleward undercurrents., pages 110–130. Springer, Berlin.

Colberg, F. and Reason, C. (2006). A model study of the angola benguela frontal zone: Sensitivity to atmospheric forcing. *Geophysical Research Letters*, 33:pp.

Cole, J. (1997). *The surface dynamics of the northern Benguela upwelling system and its relationship to patterns of Clupeoid production.* PhD thesis, University of Warwick, UK.

Conkright, M., Locarnini, R., Garcia, H., O'Brien, T., Boyer, T., Stephens, C., and Antonov, J. (2002). World ocean atlas 2001: Objective analyses and data statistics. *Technical Report National Oceanographic Data Centre*, 2001:pp.

Copenhagen, W. (1953). The periodic mortality of fish in the walvis region: a phenomenan within the benguela current. *Investigational Report - Division of Fisheries, South Africa*, 14:35.

Currie, R. (1953). Upwelling in the benguela current. *Nature*, 171:497–500.

Davis, R. (1985). Drifter observations of coastal surface currents during code: The method and descriptive view. *Journal of Geophysical Research*, 90 (C3):4741–4755.

De Dekker, A. (1969). Notes on oxygen-depleted subsurface current off the west coast of south africa. *Division of Sea Fisheries Investigative Report, Cape Town.*, 84:1–31.

Dengler, A. (1985). Relationship between physical and biological processes at an upwelling front off peru, 15°s. *Journal of Geophysical Research*, 32:1301–1315.

Dewey, R., Grawford, W., Gargett, A., and Oakey, N. (1987). A microstructure instrument for profiling oceanic turbulence in coastal bottom boundary layers. *Journal of Atmosphere and Ocean Technology*, 4:288–297.

Duncombe Rae, C. (2005). A demonstration of the hydrographic partition of the benguela upwelling ecosystem at 26°40's. *African Journal of Marine Science*, 27(3):617–628.

Duncombe Rae, C., Shillington, F., Agenbag, J., Tauton-Clark, J., and Gründlingh, M. (1992). An agulhas ring in the south atlantic ocean and its interaction with the benguela upwelling frontal system. *Deep Sea research*, 100 (C12):10604–10620.

Emery, W., Lee, W., and Maagard, L. (1984). Geographical and seasonal distribution of brunt-väisälä frequency and rossby radii in the north pacific and north atlantic. *Journal of Physical Oceanography*, 14:294–317.

Fennel, W. (1988). Analytical theory of the steady state coastal ocean and equatorial ocean. *Journal of Physical Oceanography*, 18:834–850.

Fennel, W., Junker, T., Schmidt, M., and Mohrholz, V. (2012a). Response of the benguela upwelling system to spatial variation in wind stress. *Continental shelf research*, 45:65–77.

Fennel, W., Junker, T., Schmidt, M., and Mohrholz, V. (2012b). Response of the benguela upwelling system to spatial variations in the wind stress. *Continental Shelf Research*, 45:65–77.

Field, J. and Shillington, F. (2006). *The Sea*, chapter Variability of the Benguela Current System, pages 833–861. Harvard University Press, Boston.

Flament, P., Armi, L., and Washbrun, L. (1985). The evolving structure of an upwelling filament. *Journal of Geophysical Research*, 90 (C6):11765–11778.

Garzoli, S., Gordon, A., Kamenkovich, V., Pillsbury, D., and Duncombe Rae, C. (1996). Variability and sources of the south eastern atlantic circulation. *Journal of Marine Research*, 54:1039–1071.

Giraudeau, J., Monteiro, P., and Nikodemus, K. (1993). Distribution and malformation of living coccolithosphores in the northern benguela upwelling system off nambia. *Marine Micropaleontology*, 22:93–110.

Gordon, A., Bosley, K., and Aikman, F. (1995). Tropical atlantic water within the benguela upwelling system at 27°s. *Deep Sea research*, 42:1–12.

Griffies, S. (2004). *Fundamentals of ocean climate models*. Princeton University Press.

Grobler, C. and Noli-Peard, K. (1997). Jasus lalandii fishery in post independence namibia: monitoring population trends and stock recovery in relation to a variable environment. *Journal of Marine and Freshwater Research*, 48:1015–1022.

Hagen, E., Feistel, R., Agenbag, J., and Ohde, T. (2001). Seasonal and interannual changes in intense benguela upwelling (1982-1999). *Oceanologica Acta*, 24 (6):557–568.

Hardman-Mountford, N., Richardson, A., Agenbag, J., Hagen, E., N. L., Shillington, F., and Villacastin, C. (2003). Ocean climate of the south east atlantic observed from satellite data and wind models. *Progress in Oceanography*, 59:181–221.

Hart, T. J. and Currie, R. I. (1960). The benguela current. *Discovery Report*, 31:123–298.

Haynes, R., Barton, E., and Pilling, I. (1993). Development, persistence and variability of upwelling filaments off the atlantic coast of the iberian peninsula. *Journal of Geophysical Research*, 96 (C12):22681–22692.

Heaps, N. (1980). A mechanism for local upwelling along the european continental slope. *Oceanologica Acta*, 3:449.

Hutchings, L., van der Lingen, C., Shannon, L., Crawford, R., Verheye, H., Bartholomae, C., van der Plas, A., Louw, D., Kreiner, A., Ostrowski, M., Fidel, Q., Barlow, R., Lamot, T., Coetzee, J., Shillington, F., Veitch, J., Currie, J., and Monteiro, P. (2009). The benguela current: An ecosystem of four components. *Progress in Oceanography*, 83:15–32.

Huthnance, J. (1981). Waves and currents near the continental shelf edge. *Progress in Oceanography*, 10:193–226.

Huthnance, J. (1995). Circulation, exchange and water masses at the ocean margin: the role of physical processes at the shelf edge. *Progress in Oceanography*, 35:353–431.

Huyer, A., Kosro, P., Fleischbein, J., Ramp, S., Stanton, T., Washburn, L., Chavez, F., Cowles, T., Pierce, S., and Smith, R. (1991). Currents and water masses of the coastal transition zone off northern california, june to august 1988. *Journal of Geophysical Research*, 96(C8):22681–22692.

Ikeda, M. and Emery, W. (1984). Satellite observations and modeling of meanders in the california current system off oregon and northern california. *Journal of Physical Oceanography*, 14:1434–1450.

Jackett, D., McDougall, T., Feistel, R., Wright, D., and Griffies, S. (2006). Algorithms for density, potential temperature, conservative temperature, and freezing temperature of seawater. *Journal of Atmosphere and Ocean Technology*, 23:1709–1728.

John, H.-C., Mohrholz, V., Lutjeharms, J., Weeks, S., Cloete, R., Kreiner, A., and da Silva Neto, D. (2004). Oceanographic and faunistic structures across an angola current intrusion into northern namibian waters. *Journal of Marine Science*, 46:1–22.

John, H.-C., Zelck, C., and Erasmi, W. (2000). Poleward transport of equatorial fish larvae in the atlantic eastern boundary current system. *Archive of Fisheries and Marine Research*, 48 (1):61–88.

Johnson, J. and Manja, B. (1980). Unsteady currents over a continental shelf. *Tellus*, 32:482.

Johnson, J. and Nurser, A. (1983). A model of secondary upwelling over the shelf break. *Geophysical and Astrophysical Fluid Dynamics*, 23:301–320.

Junker, T. (2011). Saisonale variabilität von vertikalen transportprozessen in der ostsee. Master's thesis, Universität Rostock.

Jury, M. (1988). Case studies of the response and spatial distribution of wind-driven upwelling off the coast of africa: 29-34° south. *Continental Shelf Research*, 8(11):1257–1271.

Jury, M., Kamstra, F., and Tauton-Clark, J. (1985). Diurnal wind cycles and upwelling off the northern portion of the cape peninsula in summer. *South African Journal of Marine Science*, 3:33–42.

Knauer, G. (1987). Ocean margins in global ocean flux studies. *U.S. global ocean flux study planning report*, 6:245.

Kosro, P. and Huyer, A. (1986). Ctd and velocity surveys of seaward jets off northern california, july 1981 and 1982. *Journal of Geophysical Research*, 91(C6):7680–7690.

Kostianoy, A. and Zatsepin, A. (1996). The west african coastal upwelling filaments and cross-frontal water exchange conditioned by them. *Journal of Marine Systems*, 7:349–359.

Large, W., McWilliams, J., and Doney, S. (1994). Oceanic vertical mixing: A review and a model with a nonlocal boundary parameterization. *Reviews of geophysics*, 32:363–403.

Large, W. G., Danabasoglu, G., Doney, S., and McWilliams, J. C. (1997). Sensitivity to surface forcing and boundary layer mixing in a global ocean model: Annual-mean climatology. *Journal of Physical Oceanography*, 27:2418–2447.

Large, W. G. and Pond, S. (1981). Open ocean momentum flux measurements in moderate to strong winds. *Journal of Physical Oceanography*, 11:324–336.

Lutjeharms, J. and Meeuwis, J. (1987). The extent and variability of south-east atlantic upwelling. *South African Journal of Marine Science*, 5:51–62.

Lutjeharms, J., Shillington, F., and Duncombe Rae, M. (1991). Observations of extreme upwelling filaments in the southeast atlantic ocean. *Science*, 253(5021):774–776.

Lutjeharms, J. and Stockton, P. (1987). Kinematics of the upwelling front off southern africa. in the benguela and comparable ecosystems. *South African Journal of Marine Science*, 5:35–49.

Mackenzie, F. (1991). *Ocean margin processes in global change*, chapter What is the importance of ocean margin processes in global change?, pages 433–454. John Wiley, Chichester.

Marchesiello, P., McWilliams, J., and Shchepetkin, A. (2003). Equilibrium structure and dynamics of the california current system. *Journal of Physical Oceanography*, 33:753–783.

McCreary, J. and Kundu, P. (1985). Western boundary circulation driven by an alongshore wind: with application to the somali current system. *Journal of Marine Research*, 43:493–516.

Meeuwis, J. and Lutjeharms, J. R. E. (1990). Surface thermal characteristics of the angola-benguela front. *South African Journal of Marine Science*, 9:261–280.

Mied, R., McWilliams, J., and Lindemann, G. (1991). The generation and evolution of mushroomlike vortices. *Journal of Physical Oceanography*, 21:489–510.

Mohrholz, V., Bartholomae, C., van der Plas, A., and Lass, H. (2008). The seasonal variability of the northern benguela undercurrent and its relation to the oxygen budget on the shelf. *Continental Shelf Research*, 28:424–441.

Mohrholz, V., Schmidt, M., and Lutjeharms, J. (2001). The hydrography and dynamics of the angola-benguela frontal zone and environment in april 1999. *South African Journal of Marine Science*, 97:199–208.

Monteiro, P. (1996). *The oceanography, the biogeochemistry and the fluxes of carbon dioxide in the Benguela upwelling system.* PhD thesis, University of Cape Town.

Monteiro, P. and van der Plas, A. (2006). Low oxygen water (low) variability in the benguela system: Key processes and forcing scales relevant to forecasting. *Large Marine Ecosystems*, 14:91–109.

Monteiro, P., van der Plas, A., Melice, J.-L., and Florencie, P. (2008). Interannual hypoxia variability in a coastal upwelling system: Ocean-shelf exchange, climate and ecosystem-state implications. *Deep-Sea Research I*, 55:434–450.

Monteiro, P., van der Plas, A., Mohrholz, V., Mabille, E., Pascall, A., and Joubert, W. (2006). Variability of natural hypoxia and methane in a coastal upwelling system: oceanic physics or shelf biology? *Geophysical Research Letters*, 33:L16614.

Mooers, C. and Robinson, A. (1984). Turbulent jets and eddies in the california current and inferred cross-shore transports. *Science*, 223:51–53.

Moroshkin, K., Bunov, V., and Bulatov, R. (1970). Water circulation in the eastern south atlantic ocean. *Oceanology*, 10:27–34.

Navarro-Perez, E. and Barton, E. (1998). The physical structure of an upwelling filament off the north-west african coast during august 1993. *South African Journal of Marine Science*, 19:61–73.

Nelson, G. (1989). *Poleward flows along eastern ocean boundaries.*, chapter Poleward motion in the Benguela area., pages 110–130. Springer, New York.

Nelson, G., Boyd, A., Agenbag, J., and Duncombe Rae, C. (1998). An upwelling filament north west of cape town, south africa. *South African Journal of Marine Science*, 19:75–88.

Nelson, G. and Hutchings, L. (1983). The benguela upwelling area. *Progress in Oceanography*, 12 (3):333–356.

NOAA (1988). Data announcement 88-mgg-02, digital relief of the surface of the earth. *Technical report of NOAA*, 1988:pp.

O'Toole, M. (1980). Seasonal distribution of temperature and salinity in the surface waters off south west africa, 1972-1974. *Investigational Report South Africa Sea Fisheries Institute*, 121:1–25.

Pacanowski, R. and Griffies, S. (2000). Mom 3.0 manual. *Technical Report Geophysical Fluid Dynamics Laboratory*, 1:xx–xx.

Parrish, R., Bakun, A., Husby, D., and Nelson, C. (1983). *Proceedings of the Expert Consultation to Examine Changes in Abundance and Species Composition of Neritic Fish Resources, San Jose, Costa Rica, April 1982.*, chapter Comparitive climatology of selected environmental processes in relation to eastern boundary current pelagic fish reproduction., pages 731–777. F.A.O. Fisheries Reports.

Penven, P., Echevin, V., Pasapera, J., Colas, F., and Tam, J. (2005). Average circulation, seasonal cycle, and mesoscale dynamics of the peru current system: A modeling approach. *Journal of Geophysical Research*, 110:C10021.

Pillar, S., Maloney, C., Payne, A., and Shillington, F. (1998). Benguela dynamics. *South African Journal of Marine Science*, 19:512.

Pitcher, G., Brown, P., and Mitchell-Innes, B. (1992). Spatio-temporal variability of phytoplankton in the southern benguela upwelling system. *South African Journal of Marine Science*, 12:439–456.

Pollock, D. and Shannon, L. (1987). Responses of rock-lobster populations in the benguela ecosystem to environmental change - a hypothesis. *So*, 5:85–94.

Poole, R. and Tomczak, M. (1999). Optimum multiparameter analysis of the water mass structure in the atlantic ocean thermocline. *Deep Sea research*, 46:1895–1921.

Ramp, S., Jessen, P., Brink, K., Niiler, P., Daggett, F., and Best, J. (1991). The physical structure of cold filaments near point arena, california during june 1987. *Journal of Geophysical Research*, 96(C8):14859–14883.

Reynolds, R., Smith, T., Liu, C., Chelton, D., Casey, K., and Schlax, M. (2007). Daily high-resolution-blended analyses for sea surface temperature. *Journal of Climate*, 20:5473–5496.

Rienecker, M., Moores, C., Hagan, D., and Robinson, A. (1985). A cool anomaly off northern california: An investigation using ir imagery and in situ data. *Journal of Geophysical Research*, 90:4807–4818.

Saha, S. et al. (2010). The ncep climate forecast system reanalysis. *Bulletin of the American Meteorological Society*, 91 (8):1015–1057.

Salat, J., Maso, M., and Boyd, A. J. (1992). Water mass distribution and geostrophic circulation off nambia during april 1986. *Continental Shelf Research*, 12:355–366.

Sanchez, R., Relvas, P., Martinho, A., and Miller, P. (2008). Physical description of an upwelling filament west of cape st. vincent in late october 2004. *Journal of Geophysical Research*, 113:C07044.

Schmidt, M. and Eggert, A. (2012). A regional 3d coupled ecosystem model of the benguela upwelling system. *Marine Science Reports IOW*, 87:1–62.

SeaBird Electronics, I. (2013). Sbe user's manual. *Manual SBE*, 17:1–73.

Shannon, L. (1966). Hydrology of the south and east coasts of south africa. *Investigational Report - Division of Fisheries, South Africa*, 58:1–22.

Shannon, L. (1985). The benguela ecosystem, i., evolution of the benguela, physical features and processes. *Oceanography and Marine Biology*, 23:105–182.

Shannon, L. (1995). The benguela current ecosystem: Physical environmental and atmospheric impact: Climate variability and change. *Benguela Report*, 1995:5–13.

Shannon, L. and Agenbag, J. (1987). Some aspects of the physical oceanography of the boundary zone between the benguela and angola current systems. *Collection of Scientific Papers International Commisions for the South East Atlantic Fisheries*, 1987:249–261.

Shannon, L., Agenbag, J., and Buys, M. (1987). Large- and mesoscale features of the angola-benguela front. *So*, 5:11:34.

Shannon, L. and Nelson, G. (1996). *The South Atlantic: Present and past circulation.*, chapter The Benguela: large scale features and processes and system variability., pages 163–210. Springer, Berlin.

Shannon, L., Nelson, G., and Jury, M. (1981). *Coastal and Estuarine sciences. I. Coastal upwelling*, chapter Hydrological and meteorological aspects of upwelling in the southern Benguela Current., pages 146–159. American Geophysical Union, Washington DC.

Shannon, V. (2006). *Benguela: Predicting a Large Marine Ecosystem*, chapter A plan comes together, pages 3–10. Elsevier.

Shillington, F., Hutchings, L., Probyn, T., Waldron, H., and Peterson, W. (1992). Filaments and the benguela frontal zone: offshore advection or recirculating loops? *South African Journal of Marine Science*, 12:207–218.

Shillington, F., Peterson, W., Hutchings, L., Probyn, A., Waldron, H., and Agenbag, J. (1990). A cool upwelling filament off namibia, southwest africa: preliminary measurements of physical and biological features. *Deep-Sea Research*, 37(11):1753–1772.

Shillington, F., Reason, C., Duncombe Rae, C., Florencie, P., and Penven, P. (2006). Large scale physical variability of the benguela current large marine ecosystem (bclme). *Large Marine Ecosystems*, 14:49–70.

Siesser, W., Scrutton, R., and Simpson, E. (1974). *The geology of Continental Margins.*, chapter Atlantic and Indian Ocean margins of Southern Africa, pages 641–654. Springer, New York.

Simpson, J., Edelsten, D., Edwards, A., Morris, N., and Ten, P. (1979). The islay front: physical structure and phytoplankton distribution. *Estuarine Coastal Marine Science*, 9:713–726.

Sivkov, V. (1994). *The influence of currents on the concentration and dispersion of suspended matter (on the example of the selected regions of the North Atlantic).* PhD thesis, P.P. Shirshov Institute Oceanology, Kaliningrad, Russia.

Sobarzo, M. and Figueroa, D. (2001). The physical structure of a cold filament in a chilean upwelling zone (peninsula de mejillones, chile, 23°s). *Deep-Sea Research I*, 48:2699–2726.

Stander, G. (1964). The pilchard of south west africa (sardinops ocellata). the benguela current off south west africa. *Investigative reports - Marine Research Laboratory of South West Africa*, 11:1–42.

Strutton, P. and Chavez, F. (2004). Biological heating in the equatorial pacific: Observed variability and potential for real-time calculation. *Journal of Climate*, 17:1097–1109.

Swenson, M., Niiler, P., Brink, K., and Abbott, M. (1992). Drifter observations of a cold filament off point arena, california, in july 1988. *Journal of Geophysical Research*, 97(C3):3593–3610.

Thomas, A. and Strub, P. (1989). Interannual variability in phytoplankton pigment distribution during the spring transition along the west coast of north america. *Journal of Geophysical Research*, 94(C12):18095–18117.

Tomalin, B. (1993). Migration of spiny rock-lobsters, jasus lalandii, at lüderitz: environmental causes and effects on the fishery and benthic ecology. Master's thesis, University of Cape Town.

Traganza, E., Conrad, J., and Breaker, L. (1981). *Coastal Upwelling, Coastal Estuarine Science vol. 1*, chapter Satellite observations of a cyclonic upwelling system and giant plume in the California current., pages 228–241. AGU, Washington, D.C.

Traganza, E., Nestor, D., and McDonald, A. (1980). Satellite observations of a nutrient upwelling off the coast of california. *Journal of Geophysical Research*, 85:4104–4106.

Tyson, P. (1986). *Climate Change and Variability in Southern Africa.* Oxford University Press, Cape Town., South Africa.

Tyson, P. and Preston-Whyte, R. (2000). *The weather and climate of southern Africa.* Oxford University Press, Cape Town., South Africa.

Van Camp, L., Nykjaer, L., Mittelstaedt, E., and Schlittenhardt, P. (1991). Upwelling and boundary circulation off northwest africa as depicted by infrared and visible satellite observations. *Progress in Oceanography*, 26(4):357–402.

van der Lingen, C., Freon, P., Hutchings, L., Roy, C., Bailey, G., Bartholomae, C., Cockcroft, A., Field, K., Peard, K., and van der Plas, A. (2006). Forecasting shelf processes of relevance to living marine resources in the bclme. *Large Marine Ecosystems*, 14:309–347.

Van Foreest, D., Shillington, F., and Legeckis, R. (1984). Large scale, stationary, frontal features in the benguela current system. *Continental Shelf Research*, 3(4):465–474.

Veitch, J. (2009). *Equilibrium dynamics of the Benguela system: a numerical model approach.* PhD thesis, University of Cape Town, South Africa.

Veitch, J., Penven, P., and Shillington, F. (2010). Modeling equilibrium dynamics of the benguela current system. *Journal of Physical Oceanography*, 40:1942–1964.

Walsh, J., Biscaye, P., and Csanady, G. (1988). The 1983-1984 shelf edge exchange processes (seep) i experiment: hypotheses and highlights. *Continental Shelf Research*, 8:435–456.

Washburn, L., Kadko, D., Jones, B., Hayward, T., Kosro, P., Stanton, T., Ramp, S., and Cowles, T. (1991). Water mass subduction and the transport of phytoplankton in a coastal upwelling system. *Journal of Geophysical Research*, 96(C8):14637–14647.

Wedepohl, P., Lutjeharms, J., and Meeuwis, J. (2000). Surface drift in the south-east atlantic ocean. *South African Journal of Marine Science*, 22:71–79.

Weeks, S., Barlow, R., Roy, C., and Shillington, F. (2006). Remotely sensed variability of temperature and chlorophyll in the southern benguela: upwelling frequency and phytoplankton response. *African Journal of Marine Science*, 28:3–4.

Zhang, R.-H. and Busalacchi, A. (2009). Ocean biology-induced climate feedback effects on interannual variability in the tropical pacific: A missing process in the ncep cfs. *Science and technology infusion climate bulletin*, Nov 2009:1–9.